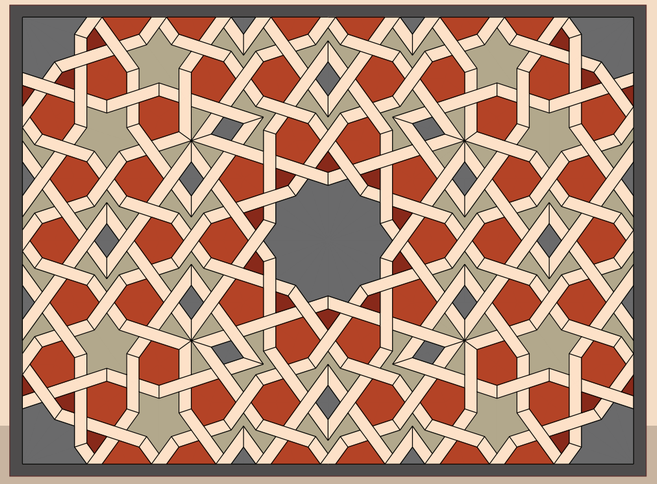

Research Journal of Mathematics and Technology, Volume 13, Number 2, 2024

Research Journal of Mathematics & Technology

ISSN 2163-0380

Vlume 13, Number 2, 2024

Research Journal of Mathematics & Technology

Volume 13, Number 2

ISSN 2163-0380

December 2024

RJMT Editorial Board

Web site: http://rjmt.mathandtech.org/
Published by:

Mathematics and Technology, LLC
PO Box 215
Welcome, NC27374-0215, USA

Foreword

We hope that you, as friends and colleagues, your families, and your loved ones are all in good health and good spirits.

The Research Journal of Mathematics and Technology (RJMT) is a printed forum for the publication of selected papers from the Electronic Journal of Mathematics and Technology (eJMT: http://ejmt.mathandtech.org/). One of eJMT's goals is to publish peer-reviewed papers demonstrating how "technology" can be utilized to make mathematics and its applications fun (F), accessible (A), challenging (C) and theoretical (T).

This special issue contains papers from five selected papers from the Scopus-indexed Electronic Proceedings of ATCM 2023, which was held in Pattaya, Thailand. As you read these five papers you will see discussions of different areas of mathematics using various technologies. We hope these innovative ways of exploring mathematics will be beneficial to you and your students. As you do so, we encourage you to write about your experiences for future issues of eJMT. Instructions for preparing and submitting papers to eJMT can be found online at https://ejmt.mathandtech.org/SubmissionGuidelines.html.

As this edition of RJMT is being prepared, the 29th ATCM (Asian Technology Conference in Mathematics: https://atcm.mathandtech.org/) is going to be held in hybrid format from December 8-11, 2024, which is to be in Yogyakarta, Indonesia. Thank you all for your continued support of eJMT, RJMT, and ATCM.

Mirosław Majewski
Guest Editor

Wei-Ch Yang
Editor-in-chief

TABLE OF CONTENTS

Uniform Convergence on Iterations generated by Special Convex Combinations of Parametric Equations

Wei-Chi YANG
wyang@radford.edu
Department of Mathematics
and Statistics
Radford University
Radford, VA 24142
USA

Abstract

This is an expansion and modification of the paper from [6]. We discuss the convergence of locus in the paper [5], which originated from a practice problem for the Chinese college entrance exam. Next, we extended some results in [6] from 2D to 3D. We are interested in the limit of a recursive sequence of loci that is built on a special convex combination of vectors involving curves or surfaces. We shall see many interesting graphs of uniform convergence of sequences generated by parametric curves and surfaces, which we hope to inspire many applications in computer graphics, and other related disciplines.

1 Introduction and Motivation

In [5], the problem is to find the locus that is determined by two fixed vectors using bisection theorem. In this paper, we discuss the proposed question of what will happen when we iterate the locus sequentially, and would like to find the limit of such locus. In short, we shall see a continuous deformation of an initial shape into a target shape, which is an interesting subject in computer graphics. We shall see the limit of a recursive sequence of convex combinations of vectors that involve curves or surfaces.

Original College Entrance Practice Problem: *Given a unit circle centered at* $(0,0)$ *and a fixed point at* $A=(2,0)$*. Let* Q *be a moving point on the unit circle* C*. Find the locus* M *which is the intersection between the angle bisector* QOA *and line segment* QA*.*

It is an easy exercise to verify that the locus of point M is a circle, which we leave as an exercise for the readers. Moreover, it is natural to imagine when DGS and CAS tools are available for students in a classroom as a project to explore, they may quickly pose 'what if' scenarios. We briefly state the following Exploratory Activity has been discussed in [4] and [5]. We then extend it to what we will focus on in this paper.

Exploratory Activity ([4] and [5])**:** Given an ellipse C: $[x(t), y(t)] = [a\cos(t), b\sin(t)], t \in [0, 2\pi]$, and a fixed point $A = (p, q) \notin C$. Let Q be a moving point on the ellipse (shown in green in Figure 1). Find the locus of the point M which is the intersection between the bisector QOA and line segment QA.

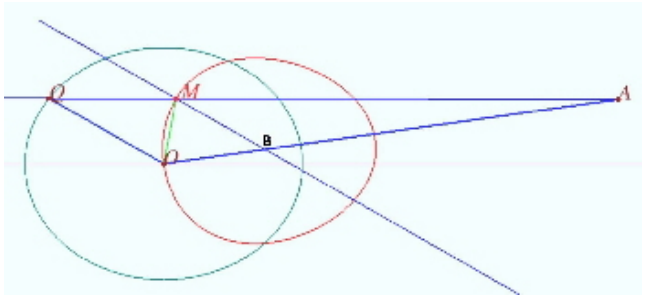

Figure 1. Locus, bisection and an ellipse

We derived that

$$\overrightarrow{OM} = \frac{OQ}{OA + OQ}\overrightarrow{OA} + \frac{OA}{OA + OQ}\overrightarrow{OQ}, \tag{1}$$

where $OQ = \left\|\overrightarrow{OQ}\right\| = \sqrt{a^2\cos^2 t + b^2\sin^2 t}$ and $OA = \left\|\overrightarrow{OA}\right\| = \sqrt{p^2 + q^2}$. We see that the parametric equation for the locus $M(t)$ can be plotted directly from Eq. (1) (see the red curve in Figure 1 above) with the help of a computational tool. It should cause no confusion throughout the paper that when $t \in [0, 2\pi]$, we often use $\overrightarrow{OM}$ to denote the vector $\overrightarrow{OM(t)}$, OQ stands for the magnitude of $\left\|\overrightarrow{OQ(t)}\right\|$ when $Q(t)$ is a parametric curve, and OA stands for the magnitude of $\left\|\overrightarrow{OA}\right\|$ if A is simply a point.

It is natural to extend our exploration and ask what would happen to the plot of

$$\overrightarrow{OM_{n+1}} = \begin{bmatrix} x_{n+1}(t) \\ y_{n+1}(t) \end{bmatrix} = \frac{OQ_n}{OA + OQ_n}\overrightarrow{OA} + \frac{OA}{OA + OQ_n}\overrightarrow{OQ_n}, \tag{2}$$

when $n \to \infty$, where $\overrightarrow{OQ_n} = \overrightarrow{OM_n}, OQ_n = OM_n = \sqrt{x_n(t)^2 + y_n(t)^2}, n \in \mathbb{Z}^+$, and $OA = \sqrt{p^2 + q^2}$. Consequently, consider the following extension with extra weights of coefficients r and s as follows: We therefore, consider the following scenario with extra weights of coefficients r and s as follows:

Theorem 1 *Given a non-zero closed curve C: $[x(t), y(t)]$, and a non-zero fixed point $A = (p, q) \notin C$. Let Q be a moving point on C. For $r, s > 0$, and $\overrightarrow{OM_1} = \frac{s\cdot OQ}{r\cdot OA + s\cdot OQ}\overrightarrow{OA} + \frac{r\cdot OA}{r\cdot OA + s\cdot OQ}\overrightarrow{OQ}$, if we write the Eq. (2) as*

$$\overrightarrow{OM_{n+1}} = \begin{bmatrix} x_{n+1}(t) \\ y_{n+1}(t) \end{bmatrix} = \frac{s\cdot OQ_n}{r\cdot OA + s\cdot OQ_n}\overrightarrow{OA} + \frac{r\cdot OA}{r\cdot OA + s\cdot OQ_n}\overrightarrow{OQ_n}. \tag{3}$$

Then $\overrightarrow{OM_{n+1}}$ converges for some $t \in [0, 2\pi]$ when $n \to \infty$ if and only if either $OQ_n = \sqrt{x_n^2(t) + y_n^2(t) + z_n^2(t)} \to 0$ or $\overrightarrow{OM_n(t)} \to \overrightarrow{OA}$ for some $t \in [0, 2\pi]$ when $n \to \infty$.

Proof: First, if $\overrightarrow{OM_{n+1}}$ converges for some $t \in [0, 2\pi]$ when $n \to \infty$, then $\overrightarrow{M_nM_{n+1}} = \overrightarrow{OM_{n+1}} - \overrightarrow{OM_n} \to 0$ for some $t \in [0, 2\pi]$ when $n \to \infty$. Moreover, since

$$\begin{aligned}
\overrightarrow{M_nM_{n+1}} &= \overrightarrow{OM_{n+1}} - \overrightarrow{OM_n} \\
&= \frac{s \cdot OQ_n}{r \cdot OA + s \cdot OQ_n}\overrightarrow{OA} + \frac{r \cdot OA}{r \cdot OA + s \cdot OQ_n}\overrightarrow{OM_n} - \overrightarrow{OM_n} \\
&= \frac{s \cdot OQ_n}{r \cdot OA + s \cdot OQ_n}\overrightarrow{OA} + \overrightarrow{OM_n}\left(\frac{r \cdot OA}{r \cdot OA + s \cdot OQ_n} - 1\right) \\
&= \frac{s \cdot OQ_n}{r \cdot OA + s \cdot OQ_n}\overrightarrow{OA} + \overrightarrow{OM_n}\left(\frac{-s \cdot OQ_n}{r \cdot OA + s \cdot OQ_n}\right). \\
&= \frac{s \cdot OQ_n}{r \cdot OA + s \cdot OQ_n}\left(\overrightarrow{OA} - \overrightarrow{OM_n}\right). \qquad (4)
\end{aligned}$$

Hence, $\overrightarrow{OM_{n+1}} = \begin{bmatrix} x_{n+1}(t) \\ y_{n+1}(t) \end{bmatrix}$ converges for some $t \in [0, 2\pi]$ if either $OQ_n = \sqrt{x_n^2(t) + y_n^2(t) + z_n^2(t)} \to 0$ or $\overrightarrow{OM_n(t)} \to \overrightarrow{OA}$ for some $t \in [0, 2\pi]$ when $n \to \infty$. The other direction is clear. ■

We describe a special convex combination of vectors in the vector space $\mathbb{R}^n$ below.

Definition 2 *Given a finite number of vectors $v_1, v_2, ... v_n$ in $\mathbb{R}^n$, a conical combination of these vectors is vector of the form*

$$\alpha_1 v_1 + \alpha_2 v_2 + ...\alpha_n v_n,$$

where $\alpha_i > 0, i = 1, 2, ...n$. A set of conical combination of vectors is called a ***convex combination*** *[2] if in addition the coefficient satisfying the following condition*

$$\sum_{i=1}^{n} \alpha_i = 1.$$

In this paper, we shall discuss a special weighted convex combination of vectors that involve a recursive sequence. For example, if

$$\begin{aligned}
\overrightarrow{OM_{n+1}(t)} &= \begin{bmatrix} x_{n+1}(t) \\ y_{n+1}(t) \end{bmatrix} = \frac{\alpha_1}{\alpha_1 + \alpha_2 + \alpha_3}v_1 + \frac{\alpha_2}{\alpha_1 + \alpha_2 + \alpha_3}v_2 \\
&+ \frac{\alpha_3}{\alpha_1 + \alpha_2 + \alpha_3}\overrightarrow{OM_n(t)}, \qquad (5)
\end{aligned}$$

then α_1, α_2 and α_3 are positive real numbers. Using the scaling techniques, without loss of generality, we assume α_1, α_2 and α_3 are real numbers in $(0, 1)$. We shall see in later proofs that the coefficient α_3 is irrelevant to the convergence of $\lim_{n\to\infty} \overrightarrow{OM_{n+1}(t)}$.

2 2D iterations

2.1 One curve and one fixed vector

For the rest of the paper, we assume the fixed point A is not on the original curve C. In view of the Theorem (1), we further extend the knowledge of uniform convergence of sequences of

functions, which students learn in Advanced Calculus. We begin with the domain $D = [0, 2\pi]$, and $\{M_n : D \to \mathbb{R}^2\}$ being a sequence of functions, and note that since the metric space $\mathbb{R}^2$ is complete, which means that every uniformly Cauchy sequence M_n is convergent. We consider the following:

Definition 3 *Suppose $D = [0, 2\pi]$, and $\{M_n : D \to \mathbb{R}^2\}$ is a sequence of functions. If we write $M_n(t) = [x_n(t), y_n(t)]$, with $t \in [0, 2\pi]$, $\{M_n(t))$ is said to* ***converge uniformly*** *to $M^*(t) = [p(t), q(t)]$ if $\forall \epsilon > 0$, $\exists$ a positive integer $N = N(\epsilon)$ (i.e. N depends only on ϵ in this case) such that the Euclidean distance between two points, $M_n(t)$ and $M^*(t)$, $\|M_n(t) - M^*(t)\|$ or $\|M_n(t) M^*(t)\|$, is arbitrarily small:*

$$\|M_n(t) - M^*(t)\| = \|M_n(t) M^*(t)\| = \sqrt{(x_n(t) - p(t))^2 + (y_n(t) - q(t))^2} < \epsilon.$$

Similarly, the sequence $\{M_n(t))$ is said to ***converge uniformly*** *to a point $A = (p, q)$ if $\forall \epsilon > 0$, $\exists$ a positive integer $N = N(\epsilon)$ such that $\|M_n(t) A\|$ is arbitrarily small. In other words,*

$$\|M_n(t) A\| = \sqrt{(x_n(t) - p)^2 + (y_n(t) - q)^2} < \epsilon$$

for all $n \geq N$ and all $t \in [0, 2\pi]$. Intuitively, there exists a positive integer N, such that the parametric curves $M_n(t)$ will shrink to the point A for all $n \geq N$ and all $t \in [0, 2\pi]$.

Definition 4 *Suppose $D = [0, 2\pi]$, and $\{M_n : D \to \mathbb{R}^2\}$ is a sequence of functions. If we write $M_n(t) = [x_n(t), y_n(t)]$, with $t \in [0, 2\pi]$, $\{M_n(t))$ is said to be uniformly Cauchy if for every $\varepsilon > 0$, there exists a positive integer N such that the inequality*

$$\|M_n(t) M_m(t)\| < \varepsilon$$

holds whenever $m \geq N$, $n \geq N$, and for all $t \in D$. We take it for granted in this paper that the sequence $\{M_n : D \to \mathbb{R}^2\}$ converges uniformly to another M on D if and only if, the sequence $\{M_n)$ is uniformly Cauchy.

Remarks:

1. We remark that definitions in (3) and in (4) can be extended to $\mathbb{R}^n$.
2. We remind readers to distinguish the difference between uniform convergence versus pointwise convergence.
3. Recall our original bisection problem (1) is such that $\frac{M_1A}{M_1Q_0} = \frac{AB}{OB} = \frac{AB}{M_1B} = \frac{OA}{OQ_0} = k_1(t)$, where the convergence in the case of (2) is a homothety (see [3]). We may denote the following:
$$\frac{M_nA}{M_nM_{n-1}} = k_n(t) \left(= \frac{OA}{OM_{n-1}} \right), \tag{6}$$
where $n = 1, 2, ...$, and $M_0 = Q$, which is a point on the given curve C.

4. On one hand, we usually prove how a sequence of parametric curves $\{M_n(t)\}_{n=1}^{\infty}$ converge uniformly directly in this paper. On the other hand, we note that $\{M_n(t)\}$ is a sequence from $D=[0,2\pi]$ to $\mathbb{R}^2$, and since $\mathbb{R}^2$ is a complete metric space, if one can show that $\{M_n(t)\}$ is a uniformly Cauchy sequence, then $\{M_n(t)\}$ is uniformly convergent. Instead of proving that $\{M_n(t)\}$ is a uniformly Cauchy sequence theoretically in this paper, with the help of a CAS, we often demonstrate that the graph of square distance function $f_n(t)=\sup\left(\|M_n(t)-M_{n-1}(t)\|\right)^2$ or $g_n(t)=\sup\left(\|M_n(t)-A\|\right)^2$, for all $t\in D=[0,2\pi]$, is decreasing to 0 uniformly, and use such observation to conjecture that $\{M_n(t)\}_{n=1}^{\infty}$ converges uniformly.

The next observation is natural:

Theorem 5 *Let C be a given simple closed curve $[x_0(t),y_0(t)]$, $A=(p_1,q_1)\notin C$. For $r,s\in(0,1)$ and $r\neq s$, we let*

$$\overrightarrow{OM_1}=\begin{bmatrix}x_1(t)\\ y_1(t)\end{bmatrix}=\frac{s\cdot OQ}{r\cdot OA+s\cdot OQ}\overrightarrow{OA}+\frac{r\cdot OA}{r\cdot OA+s\cdot OQ}\overrightarrow{OQ},$$

where Q is a moving point on C. Now for $n\in\mathbb{Z}^+$, we consider

$$\overrightarrow{OM_{n+1}}=\begin{bmatrix}x_{n+1}(t)\\ y_{n+1}(t)\end{bmatrix}=\frac{s\cdot OQ_n}{r\cdot OA+s\cdot OQ_n}\overrightarrow{OA}+\frac{r\cdot OA}{r\cdot OA+s\cdot OQ_n}\overrightarrow{OQ_n},\tag{7}$$

where Q_n is a moving point on $(x_n(t),y_n(t))$, and $\overrightarrow{OQ_n(t)}=\overrightarrow{OM_n(t)}$. Then $\overrightarrow{OM_n(t)}\to\overrightarrow{OA}$ uniformly as $n\to\infty$ for all $t\in[0,2\pi]$, $\overrightarrow{M_{n-1}(t)M_n(t)}$ converges uniformly to 0 for all $t\in[0,2\pi]$. Consequently, $\{M_n(t)\}_{n=1}^{\infty}$ converges to A uniformly.

Proof: First, if $r=s$ and $r,s\in(0,1)$, we refer to Theorem (1) for discussion. Now, for $r,s\in(0,1)$ and $r\neq s$,

$$\overrightarrow{OM_1}=\begin{bmatrix}x_1(t)\\ y_1(t)\end{bmatrix}=\frac{s\cdot OQ}{r\cdot OA+s\cdot OQ}\overrightarrow{OA}+\frac{r\cdot OA}{r\cdot OA+s\cdot OQ}\overrightarrow{OQ},$$

we first observe that $M_n=Q_n=(x_n(t),y_n(t))$ for $n\geq 1$, and

$$\begin{aligned}\overrightarrow{OM_2} &= \begin{bmatrix}x_2(t)\\ y_2(t)\end{bmatrix}=\frac{s\cdot OQ_1}{r\cdot OA+s\cdot OQ_1}\overrightarrow{OA}+\frac{r\cdot OA}{r\cdot OA+s\cdot OQ_1}\begin{bmatrix}x_1(t)\\ y_1(t)\end{bmatrix}\\ &= \frac{s\cdot OQ_1}{r\cdot OA+s\cdot OQ_1}\overrightarrow{OA}+\frac{r\cdot OA}{r\cdot OA+s\cdot OQ_1}\left(\frac{s\cdot OQ}{r\cdot OA+s\cdot OQ}\overrightarrow{OA}+\frac{r\cdot OA}{r\cdot OA+s\cdot OQ}\overrightarrow{OQ}\right)\\ &= \overrightarrow{OA}\left(\frac{(rs)\left[(OA)(OQ)+(OA)OQ_1\right]+s^2(OQ)(OQ_1)}{(r\cdot OA+s\cdot OQ_1)(r\cdot OA+s\cdot OQ)}\right)\\ &\quad +\overrightarrow{OQ}\left(\frac{r^2\cdot(OA)^2}{(r\cdot OA+s\cdot OQ_1)(r\cdot OA+s\cdot OQ)}\right).\end{aligned}$$

By induction, we see

$$\begin{aligned}\overrightarrow{OM_{n+1}} &= \overrightarrow{OA}\left(\frac{(r\cdot OA+s\cdot OQ_n)\cdots(r\cdot OA+s\cdot OQ_1)(r\cdot OA+s\cdot OQ)-r^n\cdot(OA)^n}{(r\cdot OA+s\cdot OQ_n)\cdots(r\cdot OA+s\cdot OQ_1)(r\cdot OA+s\cdot OQ)}\right)\\ &\quad +\overrightarrow{OQ_n}\left(\frac{r^n\cdot(OA)^n}{(r\cdot OA+s\cdot OQ_n)\cdots(r\cdot OA+s\cdot OQ_1)(r\cdot OA+s\cdot OQ)}\right)\end{aligned}\tag{8}$$

Since $0 < r < 1$,

$$\frac{r^n \cdot (OA)^n}{(r \cdot OA + s \cdot OQ_n) \cdots (r \cdot OA + s \cdot OQ_1)(r \cdot OA + s \cdot OQ)} \to 0.$$

Furthermore, since $\overrightarrow{OM_{n+1}} = a\overrightarrow{OA} + b\overrightarrow{OQ_n}$, where a and b are coefficients of $\overrightarrow{OA}$ and $\overrightarrow{OQ_n}$ respectively as seen in Eq. (8) with $a, b \in (0,1)$ and $a+b=1$, this implies that $\overrightarrow{OM_{n+1}(t)} \to \overrightarrow{OA}$ as $n \to \infty$ for all $t \in [0, 2\pi]$. Since three points, $M_{n-1}(t)$, $M_n(t)$ and A are collinear, and $M_n(t)$ is in the interior of $M_{n-1}(t)$ and A, we see $\overrightarrow{M_{n-1}(t)M_n(t)}$ converges uniformly to 0 for all $t \in [0, 2\pi]$, which can be shown that $\overrightarrow{M_n(t)}$ is uniformly Cauchy, and hence $\{M_n(t)\}_{n=1}^{\infty}$ converges to A uniformly. ■

We remark that the uniform convergence of $\{M_n(t)\}_{n=1}^{\infty}$ to the point A does not depend on the curve C.

Example 6 *We consider the curve C of $[a\cos(t), b\sin t]$, $A = (p_1, q_1) \notin C$, For the convex combination of r and s, we let*

$$\begin{bmatrix} x_1(t) \\ y_1(t) \end{bmatrix} = \frac{s \cdot OQ}{r \cdot OA + s \cdot OQ} \begin{bmatrix} p_1 \\ q_1 \end{bmatrix} + \frac{r \cdot OA}{r \cdot OA + s \cdot OQ} \begin{bmatrix} x_0(t) \\ y_0(t) \end{bmatrix},$$

and

$$\overrightarrow{OM_{n+1}} = \begin{bmatrix} x_{n+1}(t) \\ y_{n+1}(t) \end{bmatrix} = \frac{s \cdot OQ_n}{r \cdot OA + s \cdot OQ_n}\overrightarrow{OA} + \frac{r \cdot OA}{r \cdot OA + s \cdot OQ_n}\overrightarrow{OQ_n}.$$

If we choose $a = 5, b = 4$, and convex combination for $r = \frac{1}{3}, s = \frac{2}{3}$, $A = (3, 2)$, then $\{M_n(t)\}_{n=1}^{\infty}$ converges to A uniformly. (See Figure 2)

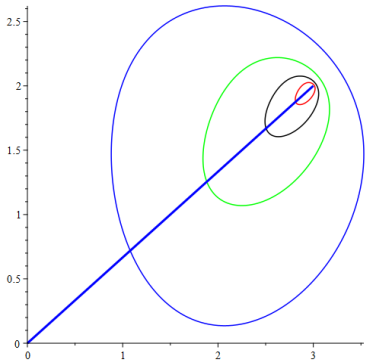

Figure 2. Uniform converges to a point.

Exercises: (1) If we use $r = s$ in Example (6), then we leave it to the readers to verify that $g_n(t) = (\|M_n(t) - A\|)^2$ does not converge uniformly to 0. In fact, the maximum value of $g_n(t)$ is the distance $(OA)^2$ at some $t \in (0, 2\pi)$. (2) If we replace C by $[a\sin t, b\sin t\cos t]$, $a = 5, b = 4$, $r = \frac{1}{3}, s = \frac{2}{3}$, $A = (3, 2)$ in Example (6), then we may conjecture that $\{M_n(t)\}_{n=1}^{\infty}$ does not converge to A uniformly by observing the graph of $f_n(t) = \|M_n(t) - M_{n-1}(t)\|$ does not converge uniformly to 0.

2.2 One curve and two fixed vectors

We consider convex combinations of three vectors below: Let C be a given closed curve $[x_0(t), y_0(t)]$, $A = (p_1, q_1)$ and $B = (p_2, q_2)$ be two distinct points not lying on C. If Q is a moving point on C, and r_1, r_2, and r_3 are real numbers in $(0, 1)$. For $n \in \mathbb{Z}^+ \cup \{0\}$, we consider

$$\begin{aligned}\overrightarrow{OM_{n+1}} &= \begin{bmatrix} x_{n+1}(t) \\ y_{n+1}(t) \end{bmatrix} = \frac{r_1 \cdot OQ_n}{r_1 OQ_n + r_2 OA + r_3 OB}\overrightarrow{OA} + \frac{r_2 \cdot OA}{r_1 OQ_n + r_2 OA + r_3 OB}\overrightarrow{OB} \\ &+ \frac{r_3 \cdot OB}{r_1 OQ_n + r_2 OA + r_3 OB}\overrightarrow{OM_n},\end{aligned}$$

where $M_0(t) = Q(t) \in C$, and $M_n(t) = Q_n(t)$ is a moving point on $(x_n(t), y_n(t))$. We are interested in $\lim_{n\to\infty} \overrightarrow{OM_{n+1}}$.

2.3 Generating sequence of shrinking curves due to convex combinations

Since the plot of the sequence $\overrightarrow{OM_{n+1}}$ in (9), where r_1, r_2, and r_3 are distinct real numbers in $(0, 1)$, is a convex combinations of vectors $\overrightarrow{OA}, \overrightarrow{OB}$ and $\overrightarrow{OM_n}$, the plot of $[x_{n+1}(t), y_{n+1}(t)]$ is generated by the following steps:

1. Connect three points of $M_n = (x_n(t), y_n(t))$, A and B to form the triangle $\triangle M_n AB$.
2. We view the point M_n as the convex combination of three points A, B and M_{n-1}, for $n \in \mathbb{Z}^+$, where $M_0 = Q$, which is a point on the curve C. Since r_1, r_2, and $r_3 \in (0, 1)$, the point $M_n(t)$ belongs to the interior of the triangle $\triangle M_{n-1}AB$ for each $t \in [0, 2\pi]$, and $n \in \mathbb{Z}^+$, see [2].
3. We shall see later in the proof of the Theorem (8) that the coefficient r_3 will not affect the final plot of $\overrightarrow{OM_n}$ when $n \to \infty$.
4. The convergence of $\overrightarrow{OM_n}$ will only depend on $\overrightarrow{OA}$ and $\overrightarrow{OB}$, and will not depend on the curve C.

Example 7 *We use closed curve C to be $[a \sin u, b \sin u \cos u]$, $a = 5, b = 4$, $A = (3, 4)$, $B = (2, 5)$, $r_1 = \frac{1}{2}, r_2 = \frac{1}{3}$, and $r_3 = \frac{1}{6}$ for demonstrating how $[x_2(t), y_2(t)]$ is generated from $[x_1(t), y_1(t)]$. The graphs of $[x_1(t), y_1(t)]$ and $[x_2(t), y_2(t)]$ can be seen in black and purple respectively in Figure 3 (d) respectively.*

- Figure 3(a) shows when $t = 0$,the plot of $[x_2(t), y_2(t)]$ has not been generated yet.
- Figure 3(b) shows when $t \in [0, 0.9106]$, the plot of $[x_2(t), y_2(t)]$ is being generated in this interval and will be in the interior of $\triangle M_1 AB$ for each corresponding t.
- Figure 3(c) shows when $t \in [0, 3.1871]$, the plot of $[x_2(t), y_2(t)]$ is being generated in this interval and will be in the interior of $\triangle M_1 AB$ for each corresponding t, and finally, Figure

4(d) shows when $t \in [0, 2\pi]$, the plot of $[x_2(t), y_2(t)]$ is smaller than that of $[x_1(t), y_1(t)]$.

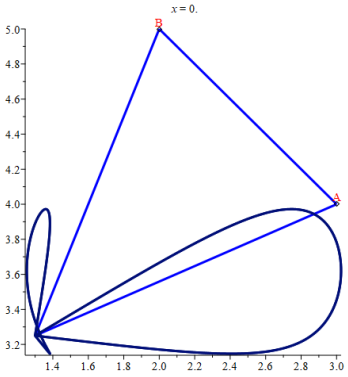

Figure 3(a), $t = 0$.

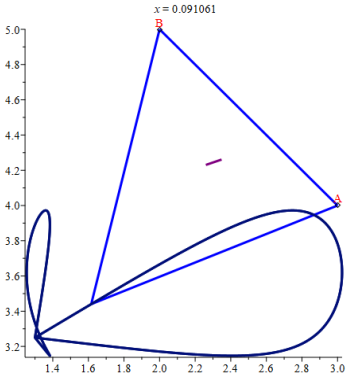

Figure 3(b), $t \in [0, 0.9106]$.

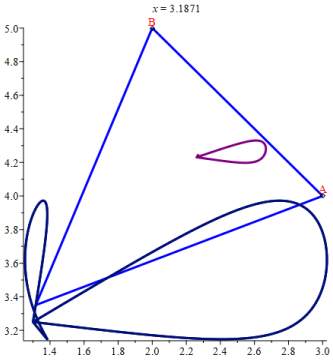

Figure 3(c), $t \in [0, 3.1871]$.

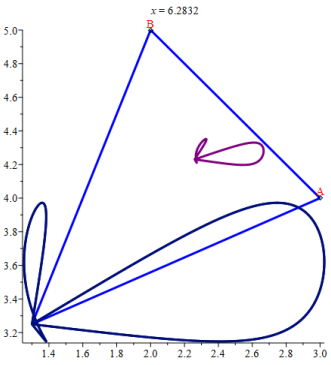

Figure 3(d), $t \in [0, 2\pi]$.

Theorem 8 *Let C be a given closed curve $[x_0(t), y_0(t)]$, $A = (p_1, q_1)$ and $B = (p_2, q_2)$ be two non-zero distinct points not lying on C. If Q is a moving point on C, and r_1, r_2, and r_3 are positive real numbers in $(0, 1)$, we let*

$$\overrightarrow{OM_1} = \begin{bmatrix} x_1(t) \\ y_1(t) \end{bmatrix} = \frac{r_1 \cdot OQ}{r_1 OQ + r_2 OA + r_3 OB}\overrightarrow{OA} + \frac{r_2 \cdot OA}{r_1 OQ + r_2 OA + r_3 OB}\overrightarrow{OB} + \frac{r_3 \cdot OB}{r_1 OQ + r_2 OA + r_3 OB}\overrightarrow{OQ}.$$

We further consider

$$\overrightarrow{OM_{n+1}} = \begin{bmatrix} x_{n+1}(t) \\ y_{n+1}(t) \end{bmatrix} = \frac{r_1 \cdot OQ_n}{r_1 OQ_n + r_2 OA + r_3 OB}\overrightarrow{OA} + \frac{r_2 \cdot OA}{r_1 OQ_n + r_2 OA + r_3 OB}\overrightarrow{OB} + \frac{r_3 \cdot OB}{r_1 OQ_n + r_2 OA + r_3 OB}\begin{bmatrix} x_n(t) \\ y_n(t) \end{bmatrix}, \tag{9}$$

where Q_n is a moving point on $(x_n(t), y_n(t))$. Then $\{M_n(t)\}_{n=1}^{\infty}$ converges uniformly to a point D, ***which lies on the line segment*** *$\overline{AB}$. Consequently, $\overrightarrow{M_{n-1}(t)M_n(t)}$ converges uniformly to 0 for all $t \in [0, 2\pi]$. We remark that the coefficient $r_3 \in (0,1)$ will not affect the location of the convergence $\{M_n(t)\}_{n=1}^{\infty}$.*

Proof: First, we observe

$$\begin{aligned}
\overrightarrow{OM_2} &= \begin{bmatrix} x_2(t) \\ y_2(t) \end{bmatrix} = \frac{r_1 \cdot OQ_1}{r_1 OQ_1 + r_2 OA + r_3 OB}\overrightarrow{OA} + \frac{r_2 \cdot OA}{r_1 OQ_1 + r_2 OA + r_3 OB}\overrightarrow{OB} \\
&\quad + \frac{r_3 \cdot OB}{r_1 OQ_1 + r_2 OA + r_3 OB}\left(\begin{array}{c} \frac{r_1 \cdot OQ}{r_1 OQ + r_2 OA + r_3 OB}\overrightarrow{OA} + \frac{r_2 \cdot OA}{r_1 OQ + r_2 OA + r_3 OB}\overrightarrow{OB} \\ + \frac{r_3 \cdot OB}{r_1 OQ + r_2 OA + r_3 OB}\overrightarrow{OQ} \end{array} \right) \\
&= \overrightarrow{OA}\left(\left\|\overrightarrow{OA}\right\|\right) + \overrightarrow{OB}\left(\left\|\overrightarrow{OB}\right\|\right) + \overrightarrow{OQ}\left(\frac{r_3^2 (OB)^2}{(r_1 OQ_1 + r_2 OA + r_3 OB)(r_1 OQ + r_2 OA + r_3 OB)}\right),
\end{aligned}$$

It follows from induction that

$$\begin{aligned}
\overrightarrow{OM_{n+1}} &= \overrightarrow{OA}\left(\left\|\overrightarrow{OA}\right\|\right) + \overrightarrow{OB}\left(\left\|\overrightarrow{OB}\right\|\right) \\
&\quad + \overrightarrow{OQ}\left(\frac{r_3^n (OB)^n}{(r_1 OQ_n + r_2 OA + r_3 OB)\cdots(r_1 OQ_1 + r_2 OA + r_3 OB)(r_1 OQ + r_2 OA + r_3 OB)}\right).
\end{aligned}$$

Since $0 < r_3 < 1$, we see $r_3^n (OB)^n \to 0$, and

$$\overrightarrow{OM_{n+1}} \to m\overrightarrow{OA} + (1-m)\overrightarrow{OB},$$

when $n \to \infty$, where $m = \left\|\overrightarrow{OA}\right\|$, and $1 - m = \left\|\overrightarrow{OB}\right\|$. Let $D = m\overrightarrow{OA} + (1-m)\overrightarrow{OB}$, then $D \in \overline{AB}$, and $\overrightarrow{OM_{n+1}}$ converges uniformly to $\overrightarrow{OD}$. Hence $\overrightarrow{OM_{n+1}}$ converges uniformly to $\overrightarrow{OD}$, where $D \in \overline{AB}$. In view of the observations from section (2.3), we see $\{M_n(t)\}_{n=1}^{\infty}$ converges uniformly to the point D, which lies on the line segment $\overline{AB}$. Moreover, it is clear that $\overrightarrow{M_{n-1}(t)M_n(t)} = \overrightarrow{OM_n} - \overrightarrow{OM_{n-1}}$ converges uniformly to 0 for all $t \in [0, 2\pi]$, ■

Computationally, we assume $\begin{bmatrix} x_{n+1}(t) \\ y_{n+1}(t) \end{bmatrix} \to F = \begin{bmatrix} p \\ q \end{bmatrix}$, then the norm of the vector, $\left\|\begin{bmatrix} x_{n+1}(t) \\ y_{n+1}(t) \end{bmatrix}\right\|$, converges to $\|F\| = \sqrt{p^2 + q^2}$, and we have

$$\left(1 - \frac{r_3 OB}{r_1\|F\| + r_2 OA + r_3 OB}\right)\begin{bmatrix} p \\ q \end{bmatrix} = \frac{r_1\|F\|}{r_2 OA + r_3 OB + r_1\|F\|}\overrightarrow{OA} + \frac{r_2 OA}{r_2 OA + r_3 OB + r_1\|F\|}\overrightarrow{OB}$$

$$\begin{aligned}
\begin{bmatrix} p \\ q \end{bmatrix} &= \left(\frac{1}{\left(\frac{r_1\|F\| + r_2 OA}{r_1\|F\| + r_2 OA + r_3 OB}\right)}\right)\left(\frac{r_1\|F\|}{r_2 OA + r_3 OB + r_1\|F\|}\overrightarrow{OA} + \frac{r_2 OA}{r_2 OA + r_3 OB + r_1\|F\|}\overrightarrow{OB}\right) \\
&= \left(\frac{r_1\|F\|}{r_1\|F\| + r_2 OA}\right)\overrightarrow{OA} + \left(\frac{r_2 OA}{r_1\|F\| + r_2 OA}\right)\overrightarrow{OB} \\
&= m\overrightarrow{OA} + (1-m)\overrightarrow{OB}, \qquad (10)
\end{aligned}$$

where $m = \frac{r_1\|F\|}{r_1\|F\|+r_2OA}$. To find the point F, it amounts to solve two equations in (10) for two variables p and q in terms of t; however, due to too many parameters that are involved, we are unable to express the solutions p and q in explicit form. Instead, we do the followings:

1. If r_1, r_2, and r_3 are real numbers in $(0, 1)$, we substitute the solutions p and q obtained (10) into the line equation $\overleftrightarrow{AB}$, we get the following equation from Maple after setting **the length of computations** to be 20,000 lines:

$$\frac{(q-q_2)\,p_1 + (q_1-q)\,p_2 - p\,(q_1-q_2)}{p_1-p_2} = 0$$

$$\begin{aligned} \Longrightarrow \quad & \frac{qp_1 - pq_1 + pq_2 - qp_2 - p_1q_2 + p_2q_1}{p_1-p_2} = 0, \\ \Rightarrow \quad & \frac{q(p_1-p_2) - p(q_1-q_2) - p_1q_2 + p_2q_1}{p_1-p_2} = 0. \end{aligned} \tag{11}$$

2. Assume $p_1 \neq p_2$ we deduce the numerator of (11) be to the following:

$$\begin{aligned} q(p_1-p_2) - p(q_1-q_2) - p_1q_2 + p_2q_1 &= 0, \\ \frac{q(p_1-p_2) - p(q_1-q_2) - p_1q_2 + p_2q_1}{p_1-p_2} &= 0, \\ q - p\left(\frac{q_1-q_2}{p_1-p_2}\right) - \frac{p_1q_2 - p_2q_1}{p_1-p_2} &= 0. \end{aligned}$$

On the one hand, we see $F = (p, q)$ lies on the line of

$$y = \left(\frac{q_1-q_2}{p_1-p_2}\right)x + \frac{p_1q_2 - p_2q_1}{p_1-p_2}. \tag{12}$$

On the other hand, we note that the line $\overleftrightarrow{AB}$ is with the slope $\frac{q_1-q_2}{p_1-p_2}$ and passes through the point (p_1, q_1) :

$$\begin{aligned} y - q_1 &= \left(\frac{q_1-q_2}{p_1-p_2}\right)(x-p_1) \\ y &= q_1 + \left(\frac{q_1-q_2}{p_1-p_2}\right)(x-p_1) \\ &= \left(\frac{q_1-q_2}{p_1-p_2}\right)x + \frac{p_1q_2 - q_1p_2}{p_1-p_2}. \end{aligned} \tag{13}$$

We see (12) coincides with (13) and hence F lie on line segment $\overline{AB}$. We remark that when solving p and q symbolically if r_1, r_2 and r_3 are also considered to be variables, it is not possible to express using p and q due to too many unknowns when using [1], but numerical computations do show that the point (p, q) lie on the line segment AB. We use the following Example for demonstration.

Example 9 *We consider the closed curve* C_1 *with the parametric equation,* $[x_0(t), y_0(t)] = [\cos u(a - \cos(bu)) + 1, \sin u(a - \cos bu))]$, $A = (p_1, q_1)$, $B = (p_2, q_2)$, *and* Q *is a moving point on* C_1. *We let* r_1, r_2, *and* r_3 *be three distinct real numbers in* $(0, 1)$, *and*

$$\overrightarrow{OM_{n+1}} = \begin{bmatrix} x_{n+1}(t) \\ y_{n+1}(t) \end{bmatrix} = \frac{r_1 \cdot OQ_n}{r_1 OQ_n + r_2 OA + r_3 OB}\overrightarrow{OA} + \frac{r_2 \cdot OA}{r_1 OQ_n + r_2 OA + r_3 OB}\overrightarrow{OB} + \frac{r_3 \cdot OB}{r_1 OQ_n + r_2 OA + r_3 OB} \begin{bmatrix} x_n(t) \\ y_n(t) \end{bmatrix}.$$

If we pick $a = 5, b = 4$, $p_1 = 3, q_1 = 4, p_2 = 2, q_2 = 5$, and $r_1 = \frac{1}{2}, r_2 = \frac{1}{3}$, and $r_3 = \frac{1}{6}$. Then we see

$$\lim_{n\to\infty} \{M_n(t)\}_{n=1}^{\infty} = (2.60516252, 4.39483748),$$

see Figure 4(a) below for the convergence. In view of (10), we note that the convergence does not depend on the value of r_3.We also remark that convergence to the point $(2.60516252, 4.39483748)$ is irrespective to the curve C_1 we pick. For example, if we replace C_2 by $[a \sin u, b \sin u \cos u]$, and use the same a, b, point A, and point B, we shall get the same convergence for $\lim_{n\to\infty} \{M_n(t)\}_{n=1}^{\infty} = (2.60516252, 4.39483748)$, (see Figure 4(b)). Similarly is true if we replace C_3 by $\left[4a \cos u (\sin u)^2 \cos u, 4a \cos\right.$ see (Figure 4(c)).

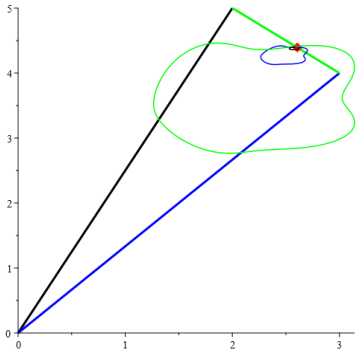

Figure 4(a). Convergence for C_1.

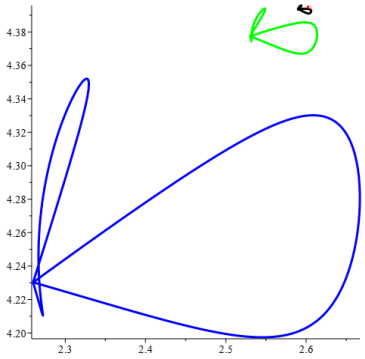

Figure 4(b). Convergence for C_2.

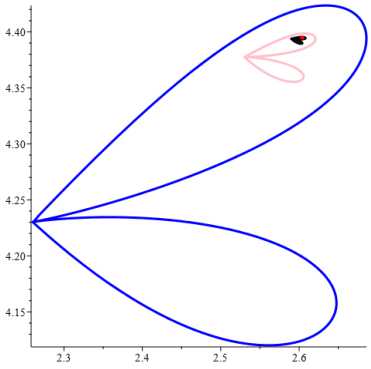

Figure 4(c). Convergence for C_3.

2.4 Uniform convergence using geometric constructions

In view of the Theorem (8) and observation from section (2.3), C is a non-zero closed curve, A and B are two non-zero distinct fixed points, not lying on C, and $M_n(t)$ is in the interior of the triangle of $\triangle M_{n-1}(t)\, AB$ for each $t \in [0, 2\pi]$. We see the distance between $M_n(t) = [x_n(t), y_n(t)]$ and $M_{n-1}(t) = [x_{n-1}(t), y_{n-1}(t)]$ is decreasing and converges to 0 when $n \to \infty$, for all $t \in [0, 2\pi]$. In other words, the square distance function

$$f_n(t) = (x_n(t) - x_{n-1}(t))^2 + (y_n(t) - y_{n-1}(t))^2$$

converges to 0 uniformly. Consequently, we see $\{M_n(t)\}_{n=1}^{\infty}$ converges to a point lying on the line segment $\overline{AB}$. In other words, if the graphs of $f_n(t)$ does not converges to 0 uniformly, then $\overrightarrow{OM_{n+1}}$ does not converge uniformly.

Suppose we adopt the Example in the section (2.3), we depict the pair functions $\{f_3(t), f_4(t)\}$ and $\{f_4(t), f_5(t)\}$ in the following Figures 5(a) and 5(b) with red and blue colors respectively:

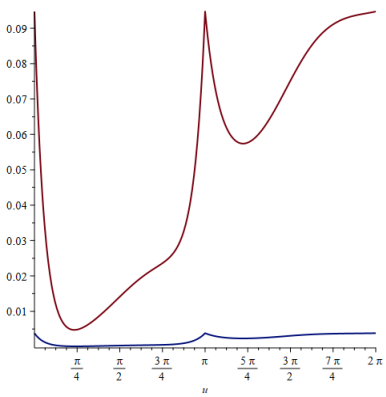

Figures 5(a). Plots of $\{f_3(t), f_4(t)\}$.

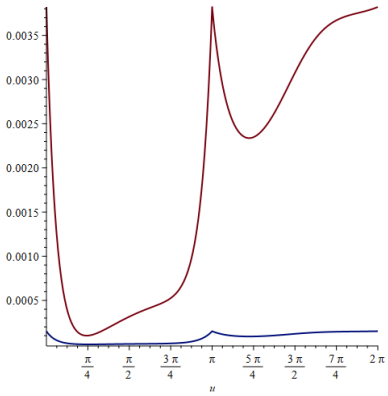

Figures 5(b). Plots of $\{f_4(t), f_5(t)\}$

In view of the plot of $f_5(t)$ (the blue in Figure 5(b)), we can see that if we pick $\epsilon = 0.0005$, for $n \geq 5$, $f_n(t) \to 0$ uniformly for all $t \in [0, 2\pi]$. In view of the Example (9), the speed of the uniform convergence of $\lim_{n\to\infty} \{M_n(t)\}_{n=1}^{\infty} = (2.60516252, 4.39483748)$ is rather fast.

2.5 Iterations on one curve, and two vectors on two respective curves

Now, we consider the plots of convex combinations of three vectors, one vector is iterated one curve, and two vectors are on two respective curves.

Theorem 10 *Let C be a given non-zero closed curve $[x_0(t), y_0(t)]$, D and E be two additional distinct closed curves of $[d_1(t), d_2(t)]$ and $[e_1(t), e_2(t)]$ respectively. Furthermore, we let Q be a moving point on C. If r_1, r_2, and r_3 are real numbers in $(0, 1)$, we let*

$$\begin{aligned} OQ &= \sqrt{x_0(t)^2 + y_0(t)^2}, \\ OE &= \sqrt{e_1(t)^2 + e_2(t)^2}, \\ OD &= \sqrt{d_1(t)^2 + d_2(t)^2}, \end{aligned}$$

and

$$\begin{aligned} \overrightarrow{OM_1} &= \begin{bmatrix} x_1(t) \\ y_1(t) \end{bmatrix} = \frac{r_1 \cdot OQ}{r_1 OQ + r_2 OE + r_3 OD}\overrightarrow{OE} + \frac{r_2 \cdot OE}{r_1 OQ + r_2 OE + r_3 OD}\overrightarrow{OD} \\ &\quad + \frac{r_3 \cdot OD}{r_1 OQ + r_2 OE + r_3 OD}\overrightarrow{OQ}. \end{aligned}$$

In addition, for $n \in \mathbb{Z}^+$, we consider

$$\begin{aligned} \overrightarrow{OM_{n+1}} &= \begin{bmatrix} x_{n+1}(t) \\ y_{n+1}(t) \end{bmatrix} = \frac{r_1 \cdot OQ_n}{r_1 OQ_n + r_2 OE + r_3 OD}\overrightarrow{OE} + \frac{r_2 \cdot OE}{r_1 OQ_n + r_2 OE + r_3 OD}\overrightarrow{OD} \\ &\quad + \frac{r_3 \cdot OD}{r_1 OQ_n + r_2 OE + r_3 OD} \begin{bmatrix} x_n(t) \\ y_n(t) \end{bmatrix}, \end{aligned} \tag{14}$$

where Q_n is a moving point on $(x_n(t), y_n(t))$, for $n = 0, 1, ...$ If $\{M_n(t)\}_{n=1}^{\infty}$ converges, then $\{M_n(t)\}_{n=1}^{\infty}$ converges uniformly to the curve $F(t)$, which satisfies the solutions (15) and (16) for $t \in [0, 2\pi]$. Furthermore, the real solutions of the parametric curve is a subset of $\lim_{n\to\infty}\{M_n(t)\}_{n=1}^{\infty}$. We remark that the coefficient $r_3 \in (0,1)$ will not affect where $\{M_n(t)\}_{n=1}^{\infty}$ will converge to.

Remark: Unlike the Theorem (8), where we make use of a decreasing sequence of closed convex sets, in this Theorem (10), we have two moving points on the curves D and E respectively. We may not have a decreasing sequence of closed convex sets, therefore, the assumption of $\{M_n(t)\}_{n=1}^{\infty}$ being convergent is needed. We shall explore ways of relaxing this condition in future paper.

Proof: We assume $\begin{bmatrix} x_{n+1}(t) \\ y_{n+1}(t) \end{bmatrix}$ converges to a real solution of $\begin{bmatrix} p(t) \\ q(t) \end{bmatrix}$, where $t \in [0, 2\pi]$. We see

$$\begin{bmatrix} p(t) \\ q(t) \end{bmatrix}\left(1 - \frac{r_3 \cdot OD}{r_1\sqrt{p(t)^2 + q(t)^2} + r_2 OE + r_3 OD}\right)$$

$$= \frac{r_1\sqrt{p(t)^2 + q(t)^2}}{r_1\sqrt{p(t)^2 + q(t)^2} + r_2 OE + r_3 OD}\overrightarrow{OE} + \frac{r_2 \cdot OE}{r_1\sqrt{p(t)^2 + q(t)^2} + r_2 OE + r_3 OD}\overrightarrow{OD}.$$

$$\begin{bmatrix} p(t) \\ q(t) \end{bmatrix}\frac{r_1\sqrt{p(t)^2 + q(t)^2} + r_2 OE}{r_1\sqrt{p(t)^2 + q(t)^2} + r_2 OE + r_3 OD}$$

$$= \begin{pmatrix} \frac{r_1\sqrt{p(t)^2+q(t)^2}}{r_1\sqrt{p(t)^2+q(t)^2}+r_2OE+r_3OD}\begin{pmatrix} e_1(t) \\ e_2(t) \end{pmatrix} \\ +\frac{r_2OE}{r_1\sqrt{p(t)^2+q(t)^2}+r_2OE+r_3OD}\begin{pmatrix} d_1(t) \\ d_2(t) \end{pmatrix} \end{pmatrix}$$

It amounts to find the real solutions for $p(t)$ and $q(t)$ from the two equations (15) and (16) in terms of t, when r_1, r_2, r_3 are given.

$$\begin{bmatrix} p(t) \\ q(t) \end{bmatrix} = \frac{r_1\sqrt{p(t)^2 + q(t)^2}}{r_1\sqrt{p(t)^2 + q(t)^2} + r_2\sqrt{e_1(t)^2 + e_2(t)^2}}\begin{pmatrix} e_1(t) \\ e_2(t) \end{pmatrix} \quad (15)$$

$$+\frac{r_2\sqrt{e_1(t)^2 + e_2(t)^2}}{r_1\sqrt{p(t)^2 + q(t)^2} + r_2\sqrt{e_1(t)^2 + e_2(t)^2}}\begin{pmatrix} d_1(t) \\ d_2(t) \end{pmatrix}. \blacksquare \quad (16)$$

In the next Example, we shall see how the graphs of the square distance functions can be used as a conjecture if the convergence of $\{M_n(t)\}_{n=1}^{\infty}$ is uniform. Secondly, we will see how the real solutions from solving for $p(t)$ and $q(t)$ computationally from the two equations (15) and (16) can serve as partial solution for the parametric curve $F(t) = \begin{bmatrix} p(t) \\ q(t) \end{bmatrix}$ under the uniform convergence of $\lim_{n\to\infty}\{M_n(t)\}_{n=1}^{\infty}$.

Example 11 *Let C be the given ellipse curve $[x_0(t), y_0(t)] = [a\cos t, b\sin t]$, D be the closed curve of*

$$[d_1(t), d_2(t)] = [(\sin 2t + 2)\cos t, (\sin 2t + 2)\sin t],$$

and E be the closed curve of

$$[(a - \cos(bt)\cos t + 1, (a - \cos(bt)\sin t].$$

Let Q be a moving point on C. We are interested in the plot of $\lim_{n\to\infty} M_n(t)$, see (14), when $n \to \infty$.

1. We consider $r_1 = \frac{1}{2}, r_2 = \frac{1}{3}, r_3 = \frac{1}{6}, a = 5, b = 3$. In addition, it is also worth noting that the square distance function

$$f_n(t) = (x_n(t) - x_{n-1}(t))^2 + (y_n(t) - y_{n-1}(t))^2$$

converges to 0 rather quickly in this case. We depict the pair functions $\{f_4(t), f_5(t)\}$ and $f_5(t)$ in the following Figures 6(a) and 6(b) respectively. Consequently, we may use these observations to conjecture that the convergence of $\{M_n(t)\}_{n=1}^{\infty}$ is uniform.

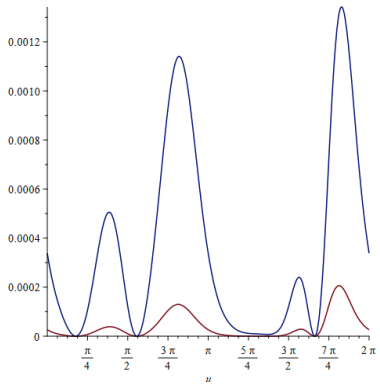

Figure 6(a). Plots of $\{f_4(t), f_5(t)\}$.

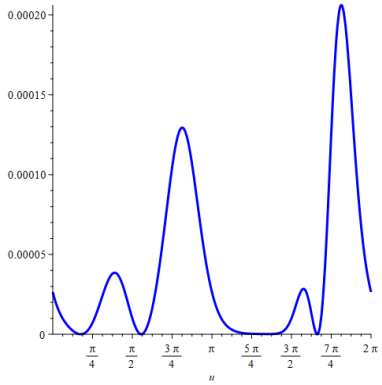

Figure 6(b). Plot of $f_5(t)$.

2. If we plot the real solutions of the branch 1, out of four branches when solving two equations (15) and (16), it coincides 'almost' exactly with that of $M_5(t) = \begin{bmatrix} x_5(t) \\ y_5(t) \end{bmatrix}$, see Figure 7 below, which we cannot tell them apart. See Supplementary Electronic Material

[S1].

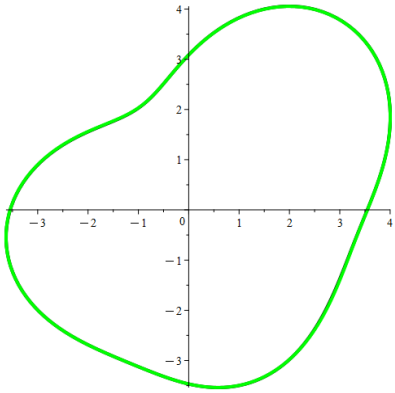

Figure 7. Graph of $M_5(t)$.

Exercise: We invite readers to explore that the plot of the curve $\lim_{n\to\infty} M_n(t)$, see (10), is invariant with the choice of curve $C = [x_0(t), y_0(t)]$.

3 Uniform Convergence of an Iterated Sequence in R^3

3.1 The limit of a uniform convergence is of rank one

We should call a point, a curve and a surface in R^3 to be of rank 1, rank 2 and rank 3 respectively. We shall discuss how the limit of a uniform convergence of an iterated sequence that will result in a point, a curve and a surface in R^3.

Theorem 12 *Let S be a given closed surface $[x_0(u_1,u_2), y_0(u_1,u_2), z_0(u_1,u_2)]$, and the point $A = (p_1, q_1, w_1)$ is fixed and is not on the surface S. For r_1 and r_2 being two distinct real numbers in $(0,1)$, we let*

$$\overrightarrow{OM_1} = \begin{bmatrix} x_1(u_1,u_2) \\ y_1(u_1,u_2) \\ z_1(u_1,u_2) \end{bmatrix} = \frac{r_1 \cdot OQ}{r_1 OQ + r_2 OA}\overrightarrow{OA} + \frac{r_2 \cdot OA}{r_1 OQ + r_2 OA}\overrightarrow{OQ},$$

where Q is a moving point on S, and the locus M_1 is described in $(x_1(u_1,u_2), y_1(u_1,u_2), z_1(u_1,u_2))$. Now for $n \in \mathbb{Z}^+$, we consider

$$\overrightarrow{OM_{n+1}} = \begin{bmatrix} x_{n+1}(u_1,u_2) \\ y_{n+1}(u_1,u_2) \\ z_{n+1}(u_1,u_2) \end{bmatrix} = \frac{r_1 \cdot OQ_n}{r_1 OQ_n + r_2 OA}\overrightarrow{OA} + \frac{r_2 \cdot OA}{r_1 OQ_n + r_2 OA} \begin{bmatrix} x_n(u_1,u_2) \\ y_n(u_1,u_2) \\ z_n(u_1,u_2) \end{bmatrix},$$

where Q_n is a moving point on $[x_n(u_1,u_2), y_n(u_1,u_2), z_n(u_1,u_2)]$. Then $\overrightarrow{OM_n(u_1,u_2)} \to \overrightarrow{OA}$ as $n \to \infty$ uniformly, $\overrightarrow{M_n(u_1,u_2)\, M_{n-1}(u_1,u_2)}$ converges uniformly to 0, and $\{M_n(u_1,u_2)\}_{n=1}^{\infty}$ converges uniformly to the point A for all for all $(u_1,u_2) \in [0,2\pi] \times [0,2\pi]$.

Proof: The convergence of $\{M_n(u_1,u_2)\}_{n=1}^{\infty}$ follows directly from the corresponding 2D Theorem (5), which we omit here. ■

Example 13 *Let S be the given closed surface*

$$[x_0(u_1,u_2), y_0(u_1,u_2), z_0(u_1,u_2)] = [5\cos(u_1)\sin(u_2), 4\sin(u_1)\sin(u_2), 3\cos(u_2)],$$

and the point $A=(1,2,3)$ be fixed. For r_1 and $r_2 \in (0,1)$, and

$$\overrightarrow{OM_{n+1}} = \begin{bmatrix} x_{n+1}(u_1,u_2) \\ y_{n+1}(u_1,u_2) \\ z_{n+1}(u_1,u_2) \end{bmatrix} = \frac{r_1 \cdot OQ_n}{r_1 OQ_n + r_2 OA}\overrightarrow{OA} + \frac{r_2 \cdot OA}{r_1 OQ_n + r_2 OA}\begin{bmatrix} x_n(u_1,u_2) \\ y_n(u_1,u_2) \\ z_n(u_1,u_2) \end{bmatrix}.$$

Then $\{M_n(u_1,u_2)\}_{n=1}^{\infty}$ converges uniformly to the point A.

We depict the convergence for $r_1 = \frac{1}{3}$ and $r_2 = \frac{2}{3}$, and the plots of $\left\{\overrightarrow{OM_2}, \overrightarrow{OM_3}, \overrightarrow{OM_4}, \overrightarrow{OM_5}\right\}$ and the point $A=(1,2,3)$ in Figure 8:

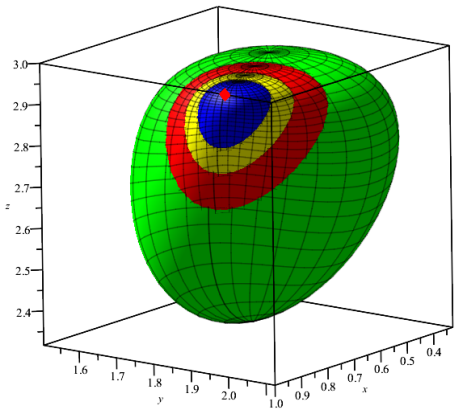

Figure 8. 3D convergence to a point.

It is natural to observe that the uniform convergence of $\{M_n(u_1,u_2)\}_{n=1}^{\infty}$ to the point A will be invariant when starting with difference surfaces, which we demonstrate this using difference closed surfaces next.

Example 14 *If we replace S to be the closed surface of $S_2 = [\cos(u_1)\sin(u_2), \sin(u_1)\cos(u_2), \cos(u_2)+1]$, and the point $A=(1,2,3)$ be fixed. Furthermore, we pick $r_1 = \frac{1}{3}$, and $r_2 = \frac{2}{3}$, we depict the nested plots of $\{M_2(u_1,u_2), M_3(u_1,u_2), M_4(u_1,u_2), M_5(u_1,u_2)\}$ and the point $A=(1,2,3)$ below on Figure 9(a). The plot of $M_5(u_1,u_2)$ and the point A (shown in red) is depicted in the Figure 9(b). We also plot the Figure 8 together with Figure 9(a) in Figure 9(c) below, which*

we can see both sequences of closed surfaces converge to the same point A.

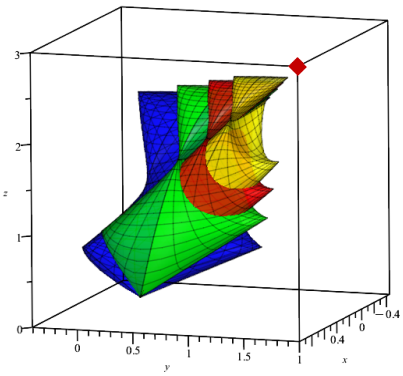

Figure 9(a). Sequence of surfaces converge to the point A.

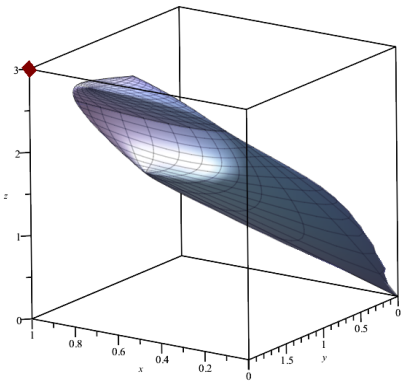

Figure 9(b). The plots of $M_5(u_1, u_2)$ and A.

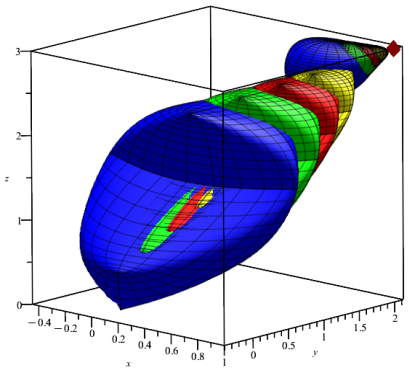

Figure 9(c). Convergences do not depend on the original surface C.

Exercise: If we use the same point A, and same coefficients $r_1 = \frac{1}{3}$ and $r_2 = \frac{2}{3}$, but use the surface S_3 of $\begin{bmatrix} 2\cos(u_1)\sin(u_1)\cos(u_1)\sin(u_2)+1 \\ 2\cos(u_1)\sin(u_1)\sin(u_1)\sin(u_2)+2 \\ 2\cos(u_1)\sin(u_1)\cos(u_2)-3 \end{bmatrix}$ as expected, we should see another sequence of surfaces converge uniformly to the same point A (shown in red in Figure 10).

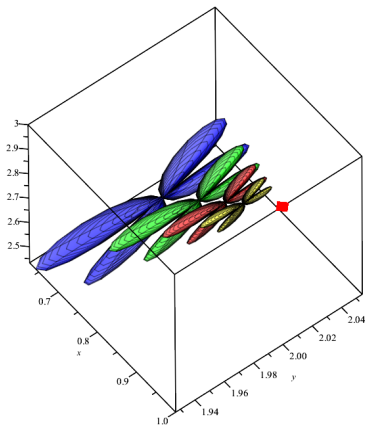

Figure 10. Convergence of S_3 and A.

3.2 The limit of a uniform convergence is of rank two

Now we consider the locus of two moving vectors and with two fixed vectors in $\mathbb{R}^3$.

Theorem 15 *Let C be a given closed non-zero surface $[x_0(u,v), y_0(u,v), z_0(u,v)]$, $A = (p_1, q_1, w_1)$, $B = (p_2, q_2, w_2)$ be two distinct points. Let D be the space curve lying on the surface of $(x_2(u,v), y_2(u,v), z_2(u,v))$*

when either u_1 or u_2 being kept as a constant. Suppose $v = v_0$, for r_1, r_2, r_3 and $r_4 \in (0,1)$, we let

$$\begin{aligned}\overrightarrow{OM_1} &= \begin{bmatrix} x_1(u,v) \\ y_1(u,v) \\ z_1(u,v) \end{bmatrix} = \frac{r_1 \cdot OQ}{r_2OA + r_3OB + r_1OQ + r_4OD}\overrightarrow{OA} + \frac{r_2 \cdot OA}{r_2OA + r_3OB + r_1OQ + r_4OD}\overrightarrow{OB} \\ &+ \frac{r_3 \cdot OB}{r_2OA + r_3OB + r_1OQ + r_4OD}\overrightarrow{OD\,(u,v_0)} + \frac{r_4 \cdot OC}{r_2OA + r_3OB + r_1OQ + r_4OD}\overrightarrow{OQ},\end{aligned}$$

where Q is a moving point on C, and the locus M_1 is described in $(x_1(u,v), y_1(u,v), z_1(u,v))$. Now for $n \in \mathbb{Z}^+$, if

$$\begin{aligned}\overrightarrow{OM_n} &= \begin{bmatrix} x_n(u,v) \\ y_n(u,v) \\ z_n(u,v) \end{bmatrix} \\ &= \frac{r_1 \cdot OQ_n}{r_2OA + r_3OB + r_1OQ_n + r_4OD}\overrightarrow{OA} + \frac{r_2 \cdot OA}{r_2OA + r_3OB + r_1OQ_n + r_4OD}\overrightarrow{OB} \\ &+ \frac{r_3 \cdot OB}{r_2OA + r_3OB + r_1OQ_n + r_4OD}\overrightarrow{OD\,(u,v_0)} \\ &+ \frac{r_4 \cdot OC}{r_2OA + r_3OB + r_1OQ_n + r_4OD}\begin{bmatrix} x_{n-1}(u,v) \\ y_{n-1}(u,v) \\ z_{n-1}(u,v) \end{bmatrix}, \qquad (17)\end{aligned}$$

where Q_n is a moving point on $[x_n(u,v), y_n(u,v), z_n(u,v)]$. If $\overrightarrow{M_n\,(u,v)}$ converges, then $\overrightarrow{M_n\,(u,v)}$ converges uniformly to a space curve spanned by $\overrightarrow{OA}$, $\overrightarrow{OB}$, and $\overrightarrow{OD\,(u,v_0)}$, where $u \in [0, 2\pi]$.

Proof: The proof is standard which we omit here.

Now we consider a 3D Locus of three moving vectors and one fixed vector as follows, which we leave the proof to the readers.

3.3 The limit of a uniform convergence is of full rank

Now, we consider a scenario when the limit of a uniform convergence $\{M_n\,(u,v)\}$ is another two variables 3D surface.

Theorem 16 *Let C be a given closed non-zero surface $[x_0(u,v), y_0(u,v), z_0\,(u,v)]$. Let D, E and F be three distinct surfaces of $(x_2(u,v), y_2(u,v), z_2(u,v))$, $(x_3(u,v), y_3(u,v), z_3(u,v))$, and $(x_4(u,v), y_4(u,v), z_4(u,v))$ respectively. For r_1, r_2, r_3 and $r_4 \in (0,1)$, we let*

$$\begin{aligned}\overrightarrow{OM_1} &= \begin{bmatrix} x_1(u,v) \\ y_1(u,v) \\ z_1(u,v) \end{bmatrix} = \frac{r_1 \cdot OQ}{r_2OF + r_3OE + r_1OQ + r_4OD}\overrightarrow{OF\,(u,v)} \\ &+ \frac{r_2 \cdot OF}{r_2OF + r_3OE + r_1OQ + r_4OD}\overrightarrow{OE\,(u,v)} \\ &+ \frac{r_3 \cdot OE}{r_2OF + r_3OE + r_1OQ + r_4OD}\overrightarrow{OD\,(u,v)} \\ &+ \frac{r_4 \cdot OD}{r_2OF + r_3OE + r_1OQ + r_4OD}\overrightarrow{OQ},\end{aligned}$$

where Q is a moving point on C, and the locus M_1 is described in $(x_1(u,v), y_1(u,v), z_1(u,v))$. Now for $n \in \mathbb{Z}^+$, if

$$\begin{aligned}
\overrightarrow{OM_n} &= \begin{bmatrix} x_n(u,v) \\ y_n(u,v) \\ z_n(u,v) \end{bmatrix} \\
&= \frac{r_1 \cdot OQ_n}{r_2OF + r_3OE + r_1OQ_n + r_4OD}\overrightarrow{OF\,(u,v)} + \frac{r_2 \cdot OF}{r_2OF + r_3OE + r_1OQ_n + r_4OD}\overrightarrow{OE\,(u,v)} \\
&\quad + \frac{r_3 \cdot OE}{r_2OF + r_3OE + r_1OQ_n + r_4OD}\overrightarrow{OD\,(u,v)} \\
&\quad + \frac{r_4 \cdot OD}{r_2OF + r_3OE + r_1OQ_n + r_4OD}\begin{bmatrix} x_{n-1}(u,v) \\ y_{n-1}(u,v) \\ z_{n-1}(u,v) \end{bmatrix},
\end{aligned}$$

where Q_n is a moving point on $[x_n(u,v), y_n(u,v), z_n(u,v)]$, and if $\overrightarrow{M_n\,(u,v)}$ converges, then $\overrightarrow{M_n\,(u,v)}$ converges uniformly to the surface that is generated by $\overrightarrow{OD\,(u,v)}, \overrightarrow{OE\,(u,v)}$ and $\overrightarrow{OF\,(u,v)}$, where $u \in [0, 2\pi]$, and $v \in [0, \pi]$.

Proof: We assume $\begin{bmatrix} x_{n+1}(u,v) \\ y_{n+1}(u,v) \\ z_{n+1}(u,v) \end{bmatrix} \to F^* = \begin{bmatrix} p\,(u,v) \\ q\,(u,v) \\ w\,(u,v) \end{bmatrix}$, we denote it as $\begin{bmatrix} p \\ q \\ w \end{bmatrix}$ in brevity, then the norm of the vector, $\left\| \begin{bmatrix} x_{n+1}(u,v) \\ y_{n+1}(u,v) \\ z_{n+1}(u,v) \end{bmatrix} \right\|$, converges to $\|F^*\| = \sqrt{p^2+q^2+w^2}$, and we have

$$\begin{aligned}
&\left(1 - \frac{r_4 \cdot OD}{r_2OF + r_3OE + r_1\|F^*\| + r_4OD}\right)\begin{bmatrix} p \\ q \\ w \end{bmatrix} \\
&= \frac{r_1\|F\|}{r_2OF + r_3OE + r_1\|F^*\| + r_4OD}\overrightarrow{OF} \\
&\quad + \frac{r_2OF}{r_2OF + r_3OE + r_1\|F^*\| + r_4OD}\overrightarrow{OE} \\
&\quad + \frac{r_3 \cdot OE}{r_2OF + r_3OE + r_1\|F^*\| + r_4OD}\overrightarrow{OD}
\end{aligned}$$

$$\begin{aligned}
&\begin{bmatrix} p \\ q \\ w \end{bmatrix} \\
&= \left(\frac{r_2OF + r_3OE + r_1\|F^*\| + r_4OD}{r_2OF + r_3OE + r_1\|F^*\|}\right)\left(\begin{array}{c} \frac{r_1\|F^*\|}{r_2OF+r_3OE+r_1\|F^*\|+r_4OD}\overrightarrow{OF} \\ +\frac{r_2OF}{r_2OF+r_3OE+r_1\|F^*\|+r_4OD}\overrightarrow{OE} + \frac{r_3 \cdot OE}{r_2OF+r_3OE+r_1\|F^*\|+r_4OD}\overrightarrow{OD} \end{array}\right) \\
&= \left(\frac{r_1\|F^*\|}{r_2OF + r_3OE + r_1\|F^*\|}\right)\overrightarrow{OF} + \left(\frac{r_2OF}{r_2OF + r_3OE + r_1\|F^*\|}\right)\overrightarrow{OE} \\
&\quad + \left(\frac{r_3 \cdot OE}{r_2OF + r_3OE + r_1\|F^*\|}\right)\overrightarrow{OD}. \qquad (18)
\end{aligned}$$

4 Conclusions

We first remark that there are many other areas that readers can extend from this paper. For example, we assumed that in several places that the sequence $\overrightarrow{M_n(u,v)}$ converges first before we state the conclusions, one can make use of Cauchy Criterion for uniform convergence to search for sufficient conditions for a sequence $\overrightarrow{M_n(u,v)}$ being convergent. In addition, we can extend the plots of convex combinations to the plots of conical combinations both in 2D and 3D. Finally, one can talk about the applications of the uniform convergence of sequences of parametric equations, and infinite series of parametric equations. Nevertheless, in this paper, we have seen some interesting graphics that resulted from sequence of convex combinations of vectors in 2D and 3D. Also, readers should have gained some insights how we can comprehend a complex concept of uniform convergence of sequences of parametric curves or surfaces. As a reminder, we indeed extended a simple college exam practice problem on locus into various interesting exploratory activities, both in 2D and 3D settings. Consequently, these exploratory activities have led to many interesting areas of computer graphics by integrating mathematical knowledge in Multivariable Calculus, Advanced Calculus, and Linear Algebra. We thus propose that a math curriculum should include proper components of exploration with the help of technological tools, especially where real life applications can be found.

It is common sense that teaching to a test can never promote creative thinking skills, it could even lose potential students who might pursue mathematics related fields in the future. We know that addressing the importance and timely adoption of technological tools in teaching, learning and research can never be wrong. Access to technological tools has motivated us to rethink how mathematics can and should be presented more interestingly and also how mathematics can be made a more cross disciplinary subject. There is no doubt that evolving technological tools have helped learners to discover mathematics and to become aware of its applications.

5 Acknowledgements

Author would like to express sincere thanks to Harald Pleym of Norway for writing sequence of plots using Maple [1].

6 Supplementary Electronic Materials

[S1] A Maple file for Example 10:

$$https://atcm.mathandtech.org/EP2023/invited/22003/ATCM2023.mw$$

References

[1] Maple: A product of Maplesoft, see http://maplesoft.com/.

[2] Convex combination: https://en.wikipedia.org/wiki/Convex_combination.

[3] https://en.wikipedia.org/wiki/Homothety

[4] Yang, W.-C. Locus, Parametric Equations and Innovative Use of Technological Tools (pp. page 120-133). Proceedings of the 21st ATCM, the electronic copy can be found at this URL: https://atcm.mathandtech.org/EP2016/invited/4052016_21300.pdf, ISBN:978-0-9821164-9-4 (hard copy), ISSN 1940-4204 (online version), Mathematics and Technology LLC.

[5] Yang, W.-C. From Static Locus Problems to Exploring Mathematics with Technological Tools (pp. page 67-88). The Electronic Journal of Mathematics and Technology, Volume 11, Number 2, ISSN 1933-2823, Mathematics and Technology LLC.

[6] Yang, W.-C. Graphs of Uniform Convengence on Iteration of Loci generated by Special Convex Combinations of Curves and Surfaces, the Electronnic Proceedings of the 28th Asian Technology Conference in Mathematics (ATCM 2023), ISSN 1940-4204, soft copy can be obtained from http://atcm.mathandtech.org/EP2023/invited/22003.pdf, Mathematics and Technology LLC.

Geometry, 3D models and Virtual Reality to explain the mathematics of andalusian monumental heritage

José L. Rodríguez[1], *Álvaro Martínez-Sevilla*[2], *Sergio Alonso*[3]
[1] jlrodri@ual.es, Department of Mathematics, University of Almería, Spain
[2] asevilla@ugr.es, DaSCI Research Institute, University of Granada, Spain
[3] zerjioi@ugr.es, Software Engineering Department,
University of Granada, Spain

Abstract

In this paper we address the construction of virtual reality scenarios for the NeoTrie VR software, to make some 3D models of architectural objects manageable anywhere. Students will be able to see the pieces (muqarnas, vaults and arches and towers) in a 3D model, manipulate and assemble them, to understand their spatial arrangement. They will also be able to use Neotrie tools to build and thus better assimilate the underlying geometric structures.

1 Introduction

Islamic architecture in Andalusia has provided us with some of the most beautiful architectural objects and intricate geometry. All of these objects have very useful characteristics in the teaching of mathematics, but some are also especially suitable for understanding geometric processes in 3D [7], [8]. This is the case of the muqarnas domes, where hundreds, and sometimes thousands, of pieces are added to form a complex dome given by the union of the pieces. We also deal with crossed ribbed vaults, made for the first time in Córdoba, and which allow the construction of domes with interlocking arches. Finally, some architectures, such as that of the Torre del Oro in Seville, a separate tower that gave welcome along the Guadalquivir river in Seville, are especially suitable for construction in 3D. We will detail these constructions in Section 2.

However, 3D tools are necessary to transfer and understand these concepts with students. Our main goal in this article is to explain the process of designing and creating various virtual reality scenarios with interactive activities.

The chosen tool for this task is NeoTrie VR (briefly, Neotrie) [1], a multiplayer virtual reality software, developed by Virtual Dor (spin-off of the University of Almería), which allow users to create, manipulate and interact with geometric objects and 3D models in general, of different

[1] `https://www2.ual.es/neotrie/`

types. Before thinking about its implementation in virtual reality, the 3D models (Section 3) were designed for 3D printing to perform manipulative workshops [9].

Recent implementations by the developers team of Neotrie (see [11, 5]) have allowed to generate new scenarios, with friendlier interfaces, menus and new functions, such as arcs creation.

Students can play and learn together the VR scenarios, thanks to the multiplayer mode, which is being improved in the forthcoming Neotrie version 4.7.0. Hence, they will be able to see and interact with the pieces in virtual reality collaboratively, manipulate and assemble them, to understand their spatial arrangement. The VR scenes will also include interactive step-by-step activities to understand the architectural structures by building them themselves using the dynamic geometry tools provided by the software (see Section 4).

These interactive activities can be better carried out simultaneously with the manipulative workshop with the printed pieces, usually in the same room that hosts the exhibition Paseo *Matemático Al-Ándalus*, as it was done the University of Almería in October 2022, the Instituto Cervantes of Fez in May 2023, and more recently in the Casa Árabe of Cordoba in May 2024.

2 Mathematical description

2.1 Muqarnas mathematical construction

The muqarnas vaults are among the most complex 3D objects in decoration in islamic architecture. They are formed from the aggregation of simpler pieces [4, 6, 12]. Muqarnas are marvelous geometric art creations that challenge our spatial understanding by their capacity of interrelation.

To create them we start from 4 basic prisms, with sections based on $\sqrt{2}$ that fit together (Figure 1a). These prisms are called *conza*, *medio cuadrado* (half square), *dumbaque* and *jaira* (Figure 1b). Other singular pieces such as the *estrella* (star) or the *almendrilla* (little almond) are also added to these. The star usually forms centers with radial symmetry (total or local) around it.

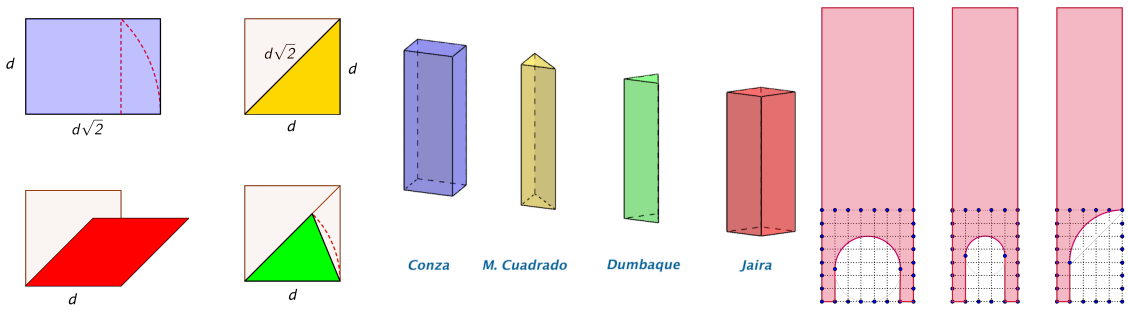

(a) Muqarnas prisms plan. (b) Muqarnas prisms. (c) Convex cutting of a conza.

Figure 1: Geometry of muqarnas.

The final pieces or *adarajas* are made by producing some concave cuts of these basic prisms, at one end, in one or both directions. The cuts are based on integer divisions of 7 and 5 (1/7

is very close to $\sqrt{2}$). At the ends of a piece there remain elongated parts of 1/7 of the length or width of the piece, or square, 1/7 x 1/7 size of section. These pins, called *patillas*, are where the small arcs of the cut ends. In Figure 1c we show the *conza* piece with the corresponding cuts.

When the prisms are assembled they form, in plan, a tessellation of a rectangular or polygonal area (see Figure 2a). There are innumerable ways to cover such a space with these prisms, which together with the creativity of the craftsmen, gave rise to a great multitude of possible designs. But all of them maintain properties of radial symmetry around the stars and axial symmetries in the basic axes of the polygon we are dealing with.

After a layer is added around a central piece, new layers are added at lower levels, thus forming level contour lines. A muqarnas dome can have up to dozens of layers at different levels. The patillas or pins are joined together making clusters. This arrangement, together with the concave cuts, makes the whole look very pleasing to the eye. It is a dome structure reminiscent of stalactites in a cave. It is said that the muqarnas domes are inspired by these natural formations (Figure 2c).

In this work we have modeled the central part of the *Puerta del Lagarto* ceiling (XII A.D.), a door in the main mosque of Seville (Spain), over which the present cathedral was built. The original ceiling is the first and simplest built in Andalusia. It has 255 pieces arranged in 7 different levels. (Figure 2b)

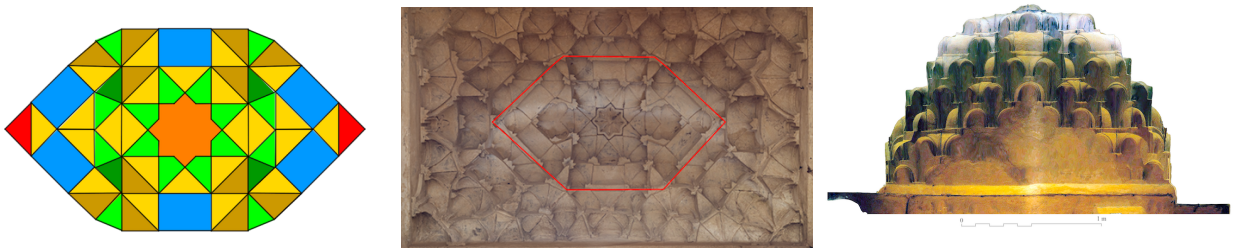

(a) Muqarnas vault plan. (b) Picture from bottom. (c) Photogrammetric model showing dome-like structure.

Figure 2: Muqarna vault of *Puerta del Lagarto*.

2.2 The intricate ribbed domes

Another of the pieces that we use in VR scenarios are ribbed domes. These are vaults formed by interlaced arches that cross each other. In the Mosque of Córdoba (VIII A.D.) these domes were tested in a pioneering way. There we can find three different ribbed dome types, although all of them are formed by 8 arches [2].

The first type has 4 crossing points, and in each of them 3 arches of different lengths and curvature cross simultaneously. Although geometrically it is the simplest to construct, it nevertheless has practical problems in its execution, due to the resulting complex crossings. The second type has 8 crossing points, with two overlapping arcs at each point, and where all arcs are equal. It forms in its projection, on a plane parallel to the ground, a stellate polygon *[8/2]* (Schläfli symbol for stellate polygons). It is the most colorful dome and the one that leaves more space in the center, and yet it was not the most replicated in history [3].

This honor goes to the third type of dome, which although geometrically more complicated, it is easier to execute due to the greater number of crossings, which makes the crossing pieces easier to design. It also has 8 equal arcs, but each arc crosses with the 4 consecutive arcs, if these are arranged circularly. It forms, in its projection on a plane, a stellated polygon of type *[8/3]*. In Figure 3 we show the geometrical structure of the three domes. In Figure 4 we show the photogrammetric view of the three types of domes in the Mosque of Córdoba, and in Figure 5 the 3D models for each one of these types.

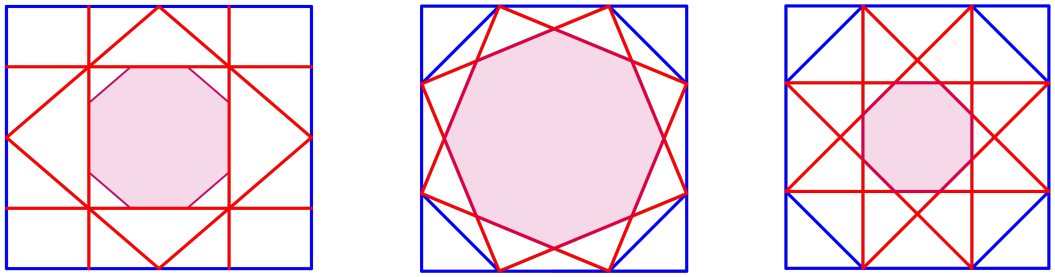

Figure 3: The geometry of the 3 ribbed domes. All with 8 arches, but with 4, 8 and 12 crossing number, respectively: lattice + diamond, and stars [8/2] and [8/3]

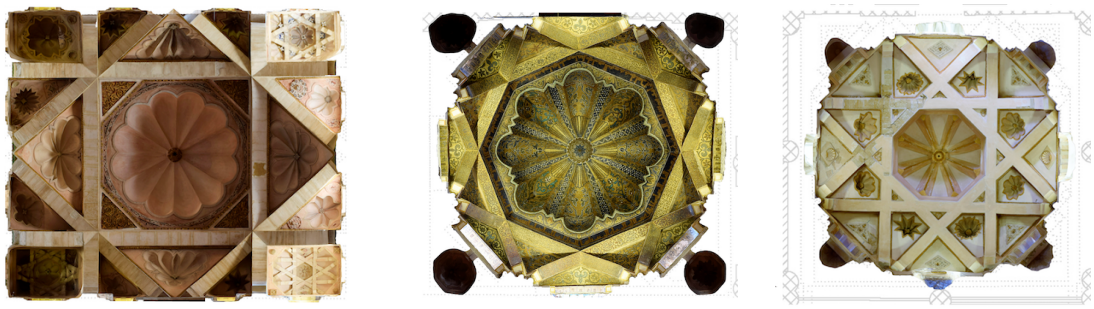

Figure 4: Photogrammetric view of the 3 types of ribbed domes. From left to right: Villaviciosa chapel, Maqsura and lateral Maqsura domes.

Figure 5: Rendering of the 3 types of ribbed domes in a 3D view.

2.3 The geometry of The Throne Hall

In the third VR scenario we deal with one of the most majestic and beautiful spaces of the Alhambra: the Throne Hall, or Comares Tower. It is the prototype of what has been called *qubba*, in Islamic architecture, formed by a prism with a square base and a splendid wooden roof with 8,017 pieces that resemble a vault of stars. In fact, its symbolic interpretation is that of the 7 heavens of Islamic cosmogony.

This number 7 plays an important role in the geometry of the dome. Therefore, it is not surprising that it is built with a trough-shaped dome, which geometrically corresponds to a truncated and stepped pyramid, whose sections are half of a regular tetradecagon, and then, they have 7 sides. We can geometrically construct the dome using two regular 7-sided semipolygons, resulting from cutting a regular 14-sided one in half. See Figure 6a.

This construction fully corresponds to the design of the dome, as can be seen in Figure 6b. In light blue, a regular 14-sided polygon is represented, built on the side delimited by the two light blue points above. In red you can see how the real construction is barely distinguishable from the geometric one, overlapping exactly on several sides. The angles of inclination of the sides of the dome also coincide, with less than one degree differences between them. This represents not only evidence of the previous geometric design, but also great construction mastery for the 14th century.

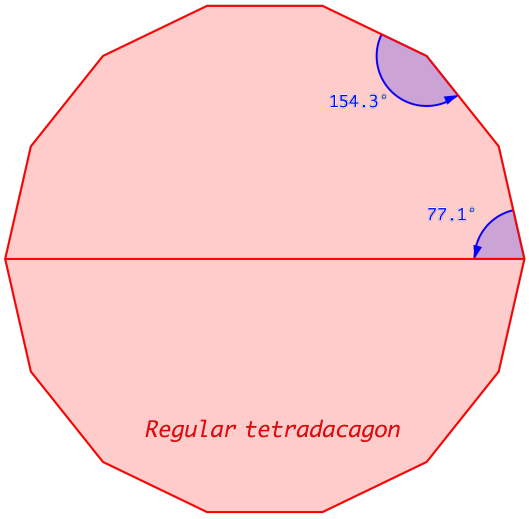

(a) Regular 14-gon and their angles

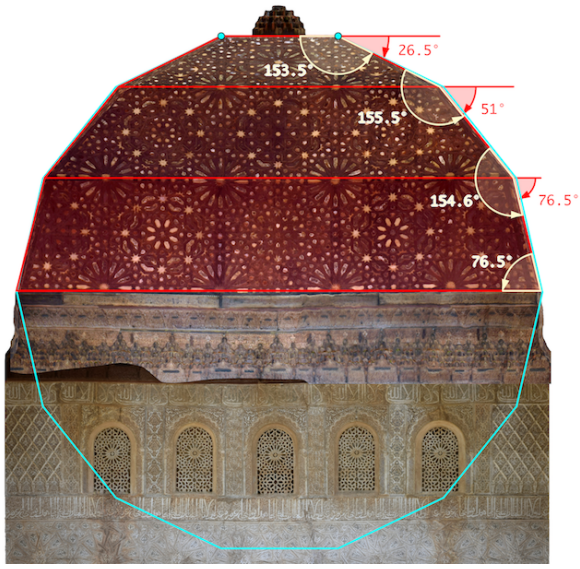

(b) The Throne dome: geometry with superimposed regular 14-gon.

Figure 6: The regular 14-gon and the dome geometry.

To geometrically construct the dome and address an intuitive and accessible didactic procedure in the VR scenario, we proceed as follows:
1st. We cross orthogonally on the upper side, parallel to the ground, these two semipolygons.
2nd. This will result in a first face delimited by the 4 vertices of the sides that intersect in the

center. This will be the upper face, parallel to the ground, which will contain the stars of the seventh heaven, and will delimit the width of the central niche (see Figure 7a).
3rd. Then we pass 4 planes through each of its edges that contain the next side of the base semipolygon. We cut the planes with a line orthogonal to the face of the semipolygon and contained in it, and each plane with their adjacent ones. These will leave us with 4 more faces. This procedure is equivalent to projecting the corresponding sides of the semipolygon, by sliding them throught the straight line that defines each of the 4 sides of the first face.
4th. We continue this procedure for the two remaining sides of the semipolygon on each side, which will give us 2 more faces per side of the room. This way we will fill the 13 resulting faces (3 for each side of the qubba, plus the common central one).

In Figure 7a the main body of the qubba appears, given by a cube with 3 zones delimiting the niches (lower part), plasterwork (central part) and the five windows area (upper part). Above it, a frieze of wooden muqarnas gives way to the dome, which contains 3 trapezoidal faces on each side and the upper closing face. The projection of the grid of unit size (side by side of the semipolygon) is also shown in Figure 7a by dashed light blue lines.

Also, in Figure 7b we obtain $\sqrt{2}$ and golden ratios for the central and lateral niches. We will construct these ratios in the corresponding scenario using the usual geometric method.

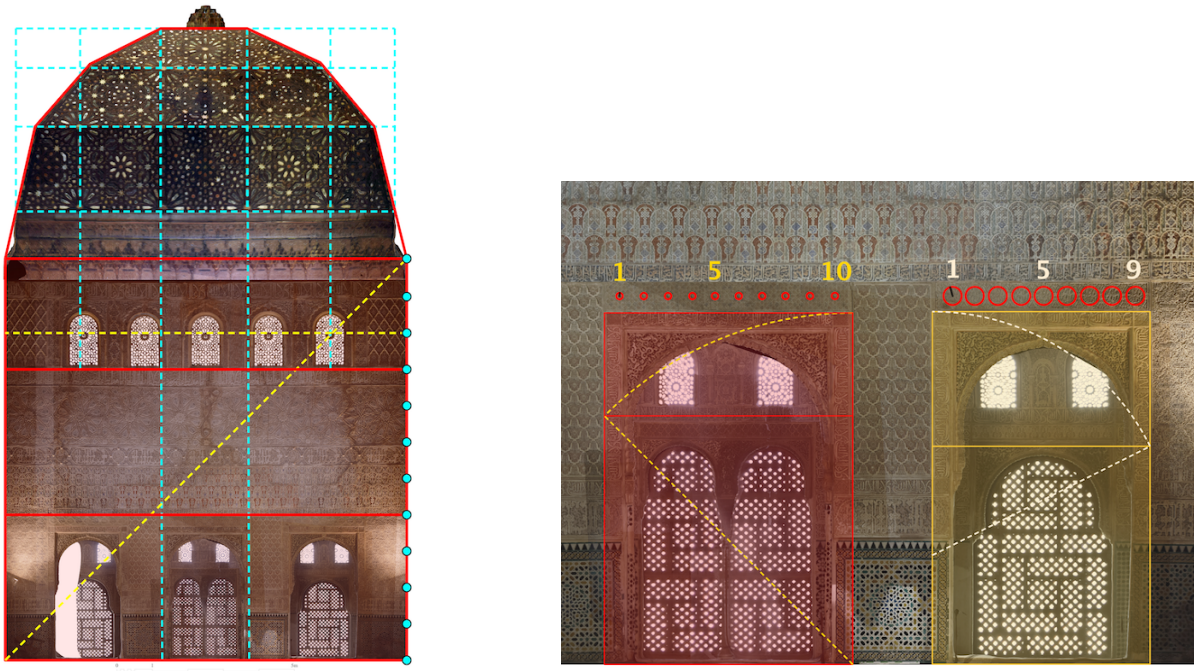

(a) The Throne Hall full section. Cube and dome geometry.

(b) Ratios in the niches of the Throne Hall.

Figure 7: The geometry of The Throne Hall.

2.4 The double prisms of Torre del Oro.

In the fourth stage we address the construction of the *Torre del Oro* in Seville. It is an interesting prismatic tower for the manipulation of prisms and simple 3D constructions. It is the only dodecagonal tower in the medieval islamic world (dodecagonal regular prism).

In it, an external dodecagon (whose diametrical section is $\sqrt{2}$, surrounds a hexagonal prism that contains a spiral staircase inside. The construction of this tower in its spatial form allows us to understand the processes of duplication from a hexagon to a dodecagon and to manipulate them spatially.

3 3D models

Prior to the development of the virtual reality scenarios we modeled all the pieces in order to 3D print them. Those 3D prints have been used to not only ensure that the proportions of the pieces are correct but also to guarantee that they will fit correctly together. Moreover, the pieces have also been used in different workshops with students and the general public where we noticed the interest of the participants in the manipulation of these objects to fully understand their geometrical properties and relations [9]. The modeling have been done using FreeCAD (`https://www.freecad.org`), a free parametric modeler which is quite suitable for this kind of pieces that are well described by its geometrical properties.

For the muqarnas scenario we selected the central part of the muqarnas ceiling of the *Puerta del Lagarto* in the Cathedral of Seville. That section contains 8 different pieces (Figure 8a). All of them part from a simple prism extruded from a rectangle, a star-shaped polygon or a triangle. Then some parts of the prism are cutted out by means of the application of boolean operators with some other basic volumetric parts (cylinders, spheres, cubes...). For example, in Figure 9 one of the muqarnas is constructed from a prism of rectangular base to which a cylinder and another rectangular prism have been substracted. In addition to the muqarnas themselves, a layered box was also designed to help participants to mount the muqarnas ceiling replica that are attached to it by means of some neodymium magnets. In Figure 8b we show the 3D printed muqarnas being used in a practical workshop.

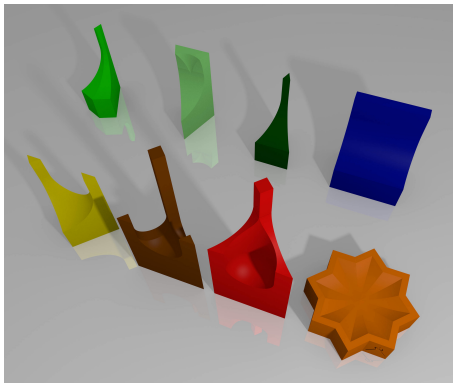

(a) The modeled muqarnas of the central part of the ceiling in the *Puerta del Lagarto*

(b) The 3D printed muqarnas used in a workshop with high-school students.

Figure 8: The muqarnas and their assembly in a workshop.

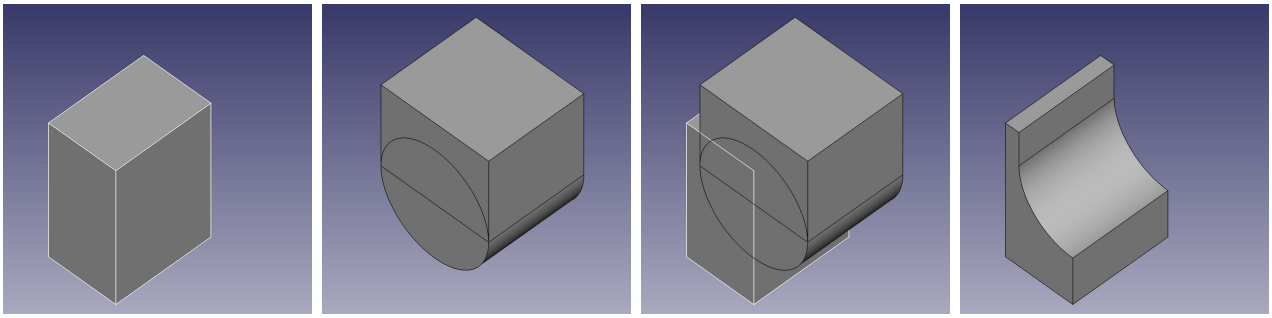

Figure 9: Geometrical modeling of one of the muqarnas.

For the crossed ribbed vaults scenario we wanted to model the arches in such a way that 8 pieces of a single model of an arch allow the construction of the ribbed vault. To do so we started with a simple extruded piece from a 2D model of the shape of the arch and then applied different boolean operators to make some cuts and additions in the intersection points of the arches that allow the interlocking of the adjacent arches (Figure 10).

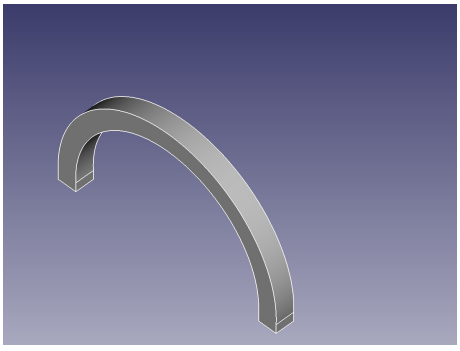

(a) The initial extruded arch from a 2D shape.

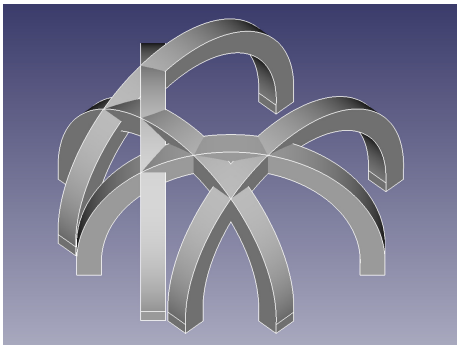

(b) The adjacent arches on the vault.

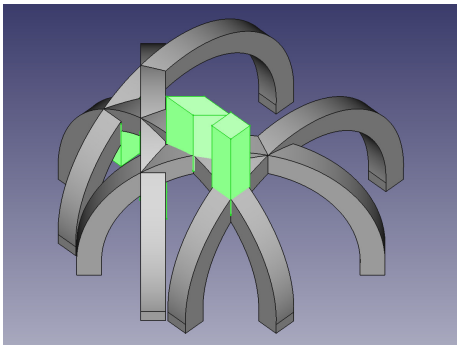

(c) Some prisms are added or subtracted to produce some cuts

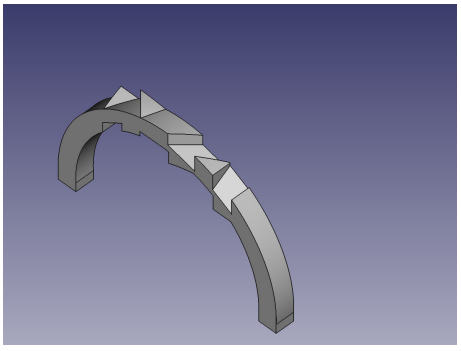

(d) Final model of the arch.

Figure 10: Modeling an arch for the crossed ribbed vaults scenario.

In addition to the arches themselves we have also modelled the domes that rest over the arches. This last piece is used in the workshop once the participants have been able to engage all the arches (Figure 11).

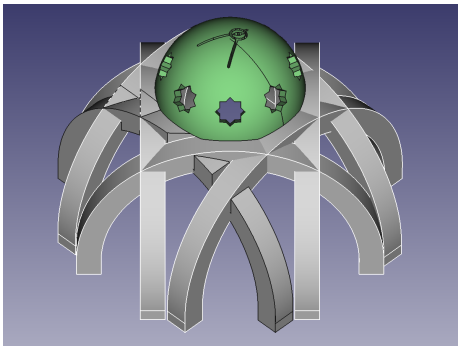

Figure 11: Complete model with interlocked arches and upper dome. Picture of the 3D printed model.

4 The VR scenarios

Once in the game, there is a box *Paseo Matemático al-Ándalus* to access the activities of this project. Each scenario contain pictures in this article, short explanations and instructions, the described 3D models (STL format) to assemble, and some interactive activity to work on the geometry associated with the corresponding architectural structures.

The first attempt is usually started with simpler exercises for the user, in which the patterns and organization of the architectural elements are recognized in broad strokes. Later, in a math workshop led by the teacher, students deepen and assimilate the necessary concepts to better understand the geometric structures. To this end, the teacher presents more complex exercises using dynamic geometry tools, such as the compass or perpendiculars and parallels, to build simple models of these pieces and STL structures.

By carrying out these activities the students between the ages of 12 and 16 years work on perpendicularity and parallelism in space, the notions of straight prisms with regular bases, practice and learn about different proportions, build circles and arcs in space, spheres, cylinders and cones, and find a way to scale the figures to obtain models of real sizes.

4.1 Muqarnas

The first scenario (Figure 12) is devoted to muqarnas. Here the player must make copies of the pieces and place them on the virtual ceiling following the pattern indicated on a template (Figures 12b). One can also construct the prisms that generate the muqarnas, by using the compass, perpendicular and parallel tools, and then extruding. However, the software does not yet allow to make spherical or cylindrical cuts on the prisms, which would allow to obtain each of the muqarnas.

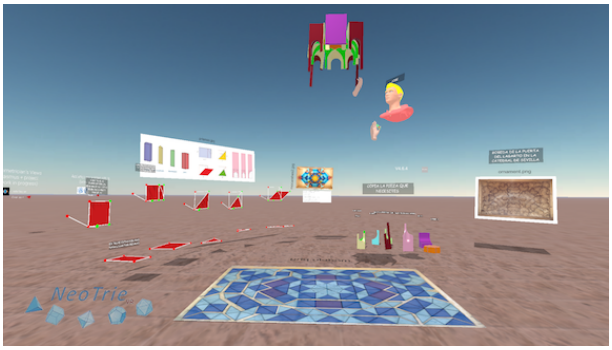

(a) General view.

(b) Cloning a piece with the copy seal tool.

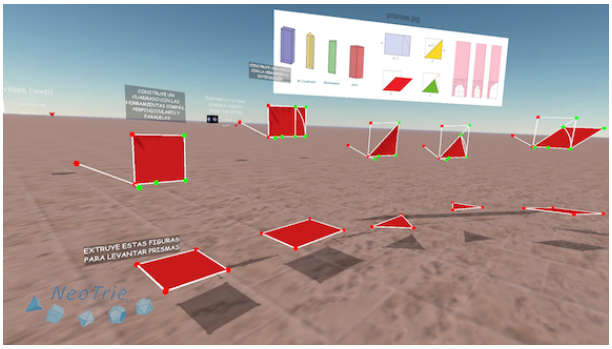

(c) Build the basis of prisms for muqarnas.

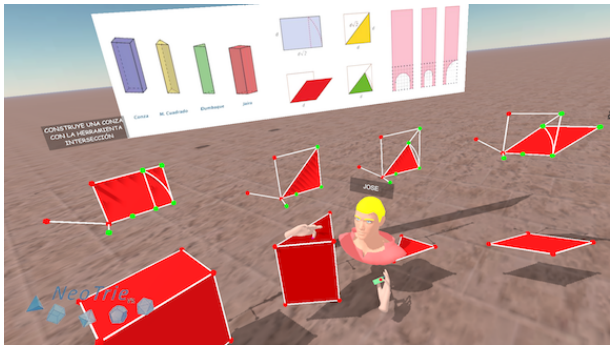

(d) Extrude the polygons to get the prisms.

Figure 12: VR scenario for muqarnas dome.

4.2 Vaults and arches

The second scenario (Figure 14) contains the 3 vaults described in Section 2. The player observes the geometrical bases of each vault and makes copies of the arches and put them in place (Figure 14b). Then, one can further propose to students to build the base figure of the dome or to build the missing circled arcs with the compass tool or to build a Carpanel arc.

We would like to point out that the implementation of arcs in space has required the use of shadders in Unity. This has been implemented by Hernandez in the compass tool (see[5, Section 5.2]), which already used the case of a circle passing through 3 points and the circle, giving 4 points, the 4th fixing the normal direction to the circle (Figure 13).

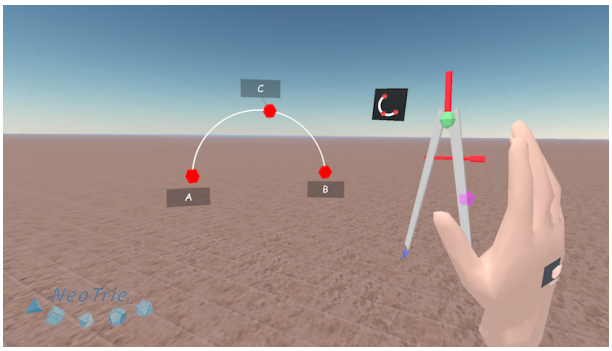

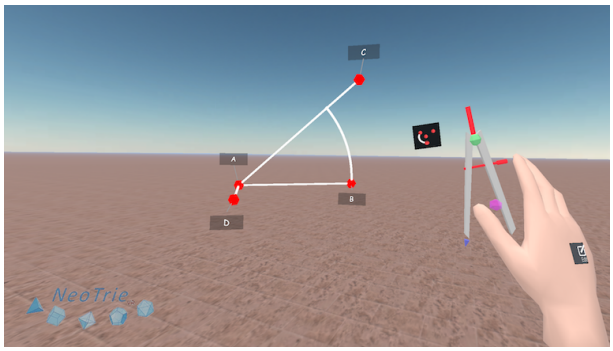

Figure 13: Arc by touching A, B, and C; Oriented arc by touching A, B, C, D.

It is also possible to dispense with the fourth point and use the normal obtained by the cross product of two vectors formed by the first 3 points.

The real domes consist of carpanel arches. In the scene the user can see one to try to reproduce it (see Figure 14d). The difficulty in constructing these arcs in space is that we need auxiliary perpendicular directions that indicate the plane where the arc is located, As we have seen in Figure 13.

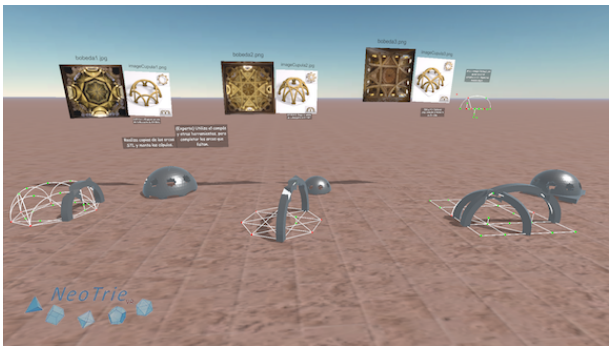

(a) General view.

(b) Assembling a dome.

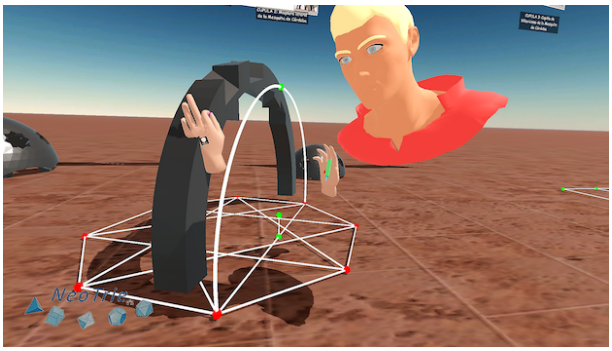

(c) Make the base figure, the circled arcs and place the STL objects correctly.

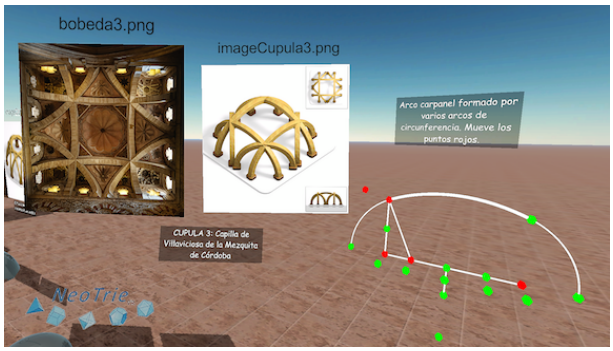

(d) Build a dynamic Carpanel arc with the compass, perpendicular and parallel tools.

Figure 14: VR scenario for vaults and arches.

4.3 Torre de Comares

In the third scenario (Figure 16) we used our photogrammetric images to assemble a full-scale model of the throne hall. It is completed with a step-by-step construction of a simple model of its dome, based on the regular tetradecagon adjustment described in section 2.3.

Therefore, students are asked to build a regular tetradecagon in Neotrie. For this, they have to calculate first the angle between two adjacent edges of the regular tetradecagon, that is $180 - 360/14 \simeq 154.2857$, and make the entire tetradecagon with the corresponding tool. Then unlink dependencies of the green points and make a copy to get the regular tetradecagon (see Figure 15).

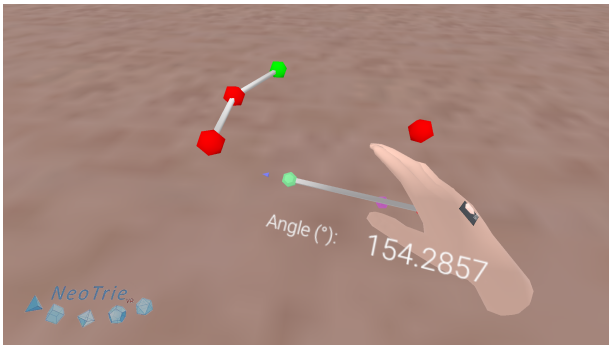

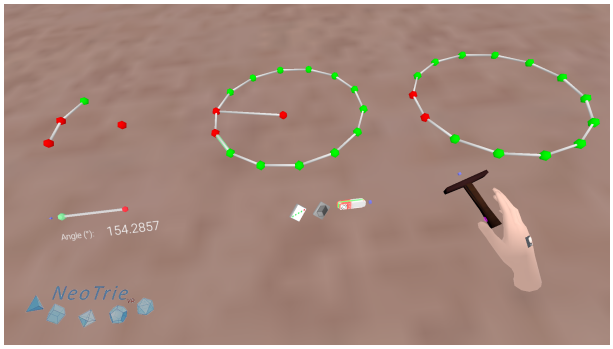

Figure 15: Touch two points of an edge, and a third point to fix the plane containing the angle. Remove dependencies and copy the figure.

The next step is to use two half parts of the 14-gon to form the axis of the dome (Figure 16b), by rotating them, creating middle points and joining them appropriately. Then, by intersecting parallels, one finds the sided edges of the dome (Figure 16c). Finally, one completes the faces to get a small model of the dome (Figure 16d).

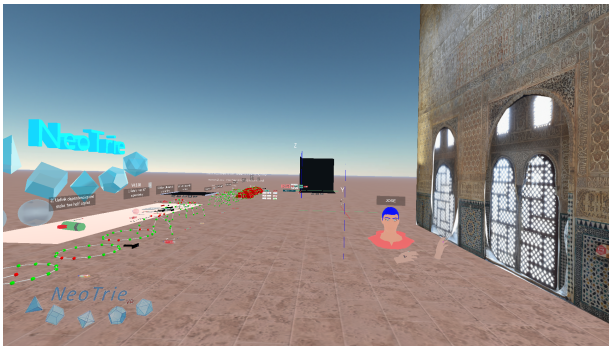

(a) General view.

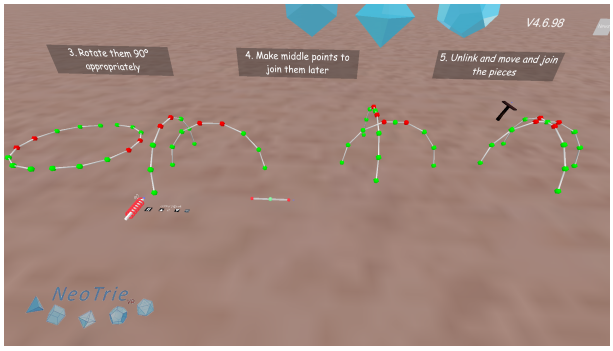

(b) Building the axis of the dome.

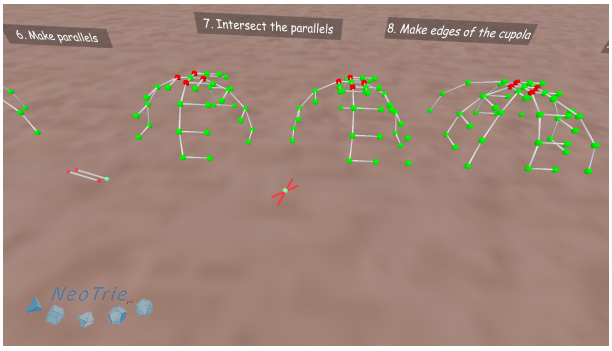

(c) Making the crossing intersecting edges.

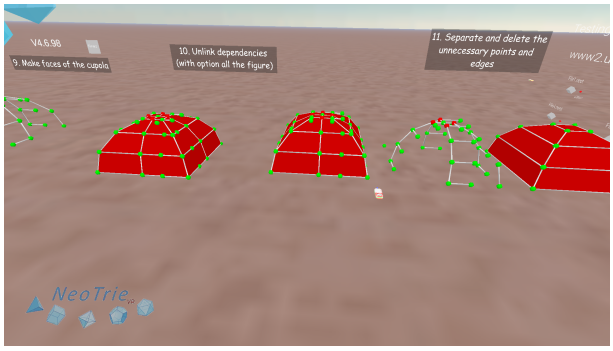

(d) Making the faces and unlink dependencies.

Figure 16: VR construction of a model of the Comares dome.

Students can then get a real scaled copy of the dome. For that, they need first to find the real size of the square base of the tower (11 meters) and measure the length of the base of the small dome (44,9 cm), then get the change of scale as $1100/44{,}9 \simeq 24{,}5$ (Figure 17a), make the scaled copy and put it at the top of the tower (Figure 17b). Furthermore, they can check with the Tape tool that the height of the tower is about 18 meters.

Inside the tower, we in Figure 7b, the points of two interactive rectangles can be moved to find the proportions of two niches of real size (Figure 17c). They can also adjust semicircular arcs passing through 3 points and locate the center (Figure 17d).

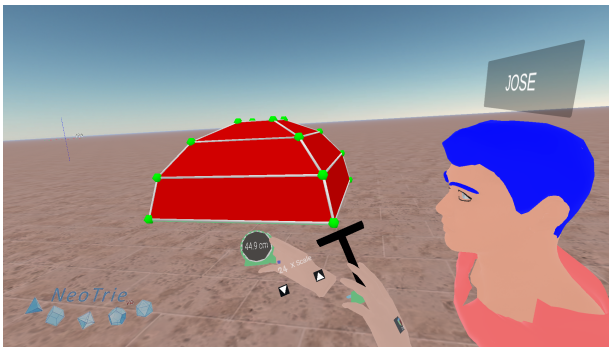

(a) Scaling the dome to get a base of side 11 meters.

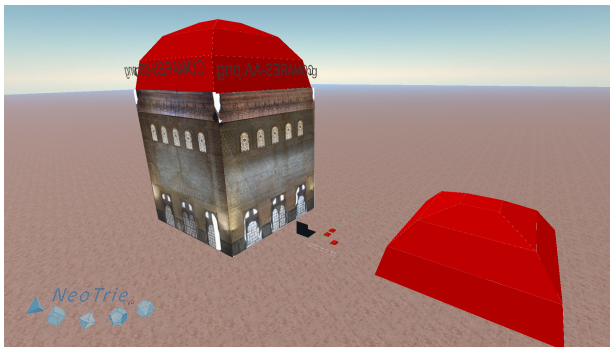

(b) Tower mounted with scaled photos and the dome.

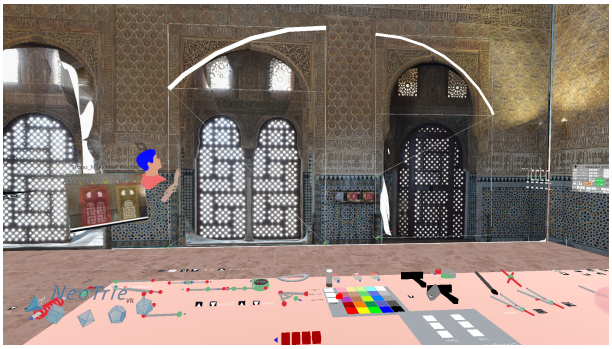

(c) Adjusting a $\sqrt{2}$ ratio and golden ratio rectangles on niches.

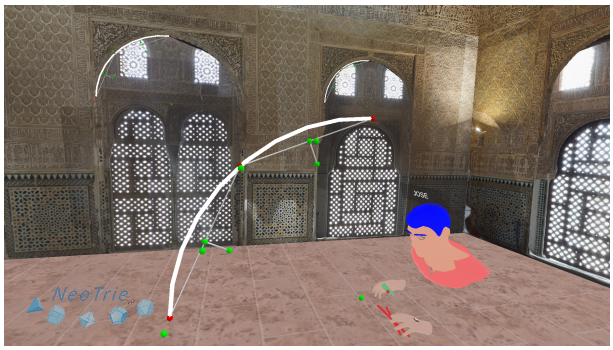

(d) Construction of an arc and its center. Adjustment to the arches of the niches.

Figure 17: VR model of the tower of Comares with interactive activities.

4.4 Torre del Oro

In the fourth scenario (Figure 18) the player can build a simple model of the *Torre del Oro* step by step. Starting with regular polygons (1 hexagon, 6 squares and 6 equilateral triangles), he must use the magnet tool to form the polygonal base of the tower (Figure 18b). Then, lift the prism with the perpendicular, parallel and compass tools, to finish by extruding the inner hexagon. This process can be seen step by step in the video `https://youtu.be/2BkjtrMByNo`. Further exercises could be (see Figures 18c and 18d) to add more geometric elements at the top of the tower: sphere, cylinder, cone, to use the scale copy seal tool to get a model of the tower with real measures and to build a spiral staircase in the interior of the hexagonal prism.

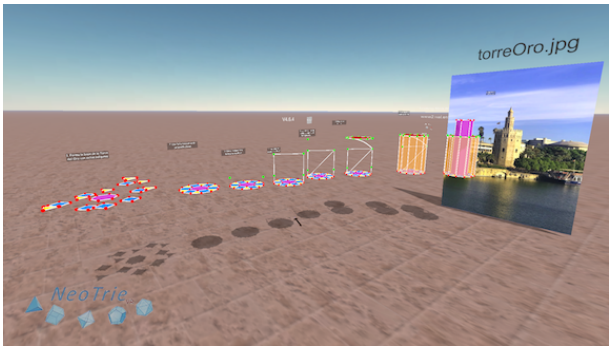

(a) General view.

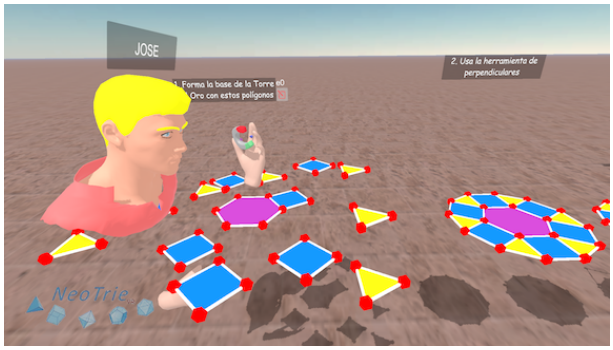

(b) Assembling the base of the tower.

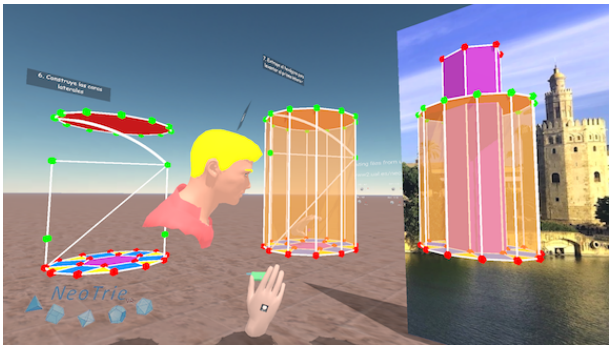

(c) Last steps of the construction.

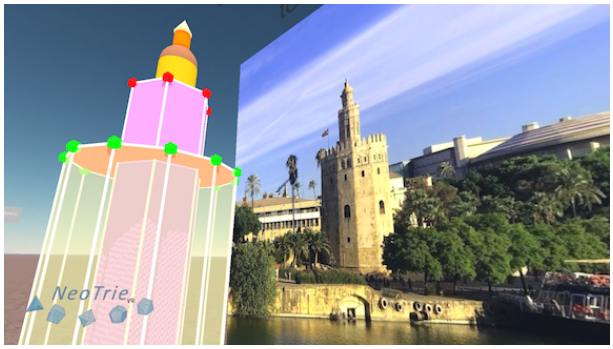

(d) Adding more elements to the top.

Figure 18: VR scenario for the Torre del Oro.

5 Conclusion

In this paper we have described a motivating learning situation that combines history, art and geometry, with the help of new technologies (3D printing and virtual reality). Students can learn by building by themselves various structures involving important geometry concepts: scaling, proportions, parallelism, perpendicularity, intersections, symmetries, projections, tessellations, spatial curves and surfaces, etc. They have the incentive of being able to build them in real size, in an interactive and totally immersive way.

We conclude that the power of VR, together with the challenge of its assembly and the admiration aroused by its composition make NeoTrie VR, along with these scenarios, an ideal tool for teaching mathematics together with art and technology, giving rise to a STEAM workshop.

6 Acknowledgements

The 1st author was partially supported by the ERDF (European Regional Development Fund) research project from the FEDER-Andalusian Regional Government grant UAL2020 -SEJ - B2086, and by the Spanish Ministry of Science and Innovation grant PID2020-117971GB-C22. The 2nd and 3rd authors were partially supported by the FECYT (Spanish Foundation for Science and Technology) FCT-19-14359. We would also like to thank the Descubre Foundation for their permission to use Figures 2, 4 and 7.

References

[1] Cromwell, Peter R. (1997) Polyhedra. Cambridge University Press, Cambridge. ISBN 0-521-66405-5.

[2] Fuentes, P. (2019) The Islamic Crossed-Arch Vaults in the Mosque of Córdoba, Nexus Network Journal 21, 441–463. DOI 10.1007/s00004-018-0403-y.

[3] Fuentes P. and Huerta, S. (2010) Islamic domes of crossed-arches: Origin, geometry and structural behavior. Arch' 10. 6th International Conference on Arch Bridges, Fuzhou (China), 346-353.

[4] Gokmen, S., Basik, A., Aykin, Y. and Alacam, S. (2022) Computational Modeling and Analysis of Seljukid Muqarnas in Kayseri, Journal on Computing and Cultural Heritage, Vol. 15 (2), Article No.: 27, DOI 10.1145/3477399.

[5] Hernández, R. (2023) New implementations in Neotrie VR: Mathitems, Final project of mathematics degree, University of Almería.

[6] Kazempour, H. (2016) The Evolution of Muqarnas in Iran, Supreme Century.

[7] Martínez-Sevilla, A. (Coord.) (2017) Paseos Matemáticos por Granada: un estudio entre Arte, Ciencia e Historia, Ed. Universidad de Granada, Granada.

[8] Martínez-Sevilla, A. (2017) Artistic Heritage meets GeoGebra. GeoGebra Global Gathering, GGG'17, Linz (Austria).

[9] Martínez-Sevilla, A. and Alonso, S. (2023) 3D printing and laser cutting of architectural heritage for use in mathematics education, The Electronic Journal of Mathematics and Technology, vol. 17, 3, 147-164.

[10] Rodriguez, J.L., Martinez-Sevilla, A. and Alonso, S. (2023) Virtual reality to study geometrical aspects of architectural heritage. Proceedings of the 28th Asian Technology Conference in Mathematics. Thailand, 2023. 380-389.

[11] Rodríguez, J.L., Hernández, R., Cangas D. (2022). Nueva versión de Neotrie VR para el dispositivo de realidad virtual Meta Quest, Actas de las 20ª JAEM, Valencia.

[12] Sakkal, M. (1982) Geometry of Muqarnas In Islamic Architecture, PhD. Thesis, University of Washington.

A Maplet for Analyzing Progressive Casino Game Betting Systems

D. Cole Payne
paynedc33@gmail.com
Department of Mathematical Sciences
Appalachian State University
Boone, North Carolina, USA 28608

Richard E. Klima
klimare@appstate.edu
Department of Mathematical Sciences
Appalachian State University
Boone, North Carolina, USA 28608

Neil P. Sigmon
npsigmon@radford.edu
Department of Mathematics and Statistics
Radford University
Radford, Virginia, USA 24142

Abstract

This work is primarily the product of the first listed author, who completed it as a student under the direction of the second and third listed authors. In this paper we analyze three progressive betting strategies, each applied to three casino games. The betting strategies considered are Martingale, Paroli, and Fibonacci, each applied to the casino games blackjack, craps, and roulette. The aim of this analysis is to try to identify optimal betting strategies for each game with a given or maximum number of bets placed that pay 1:1. The purpose of this work is not to try to discover methods for "beating the house," which are already known to not exist, but rather to search for methods for advancing gameplay through a given or maximum number of bets while retaining the possibility of earning a profit. Programming in the computer algebra system Maple, more specifically through the use of a Maplet, which is like an applet but uses (and requires) Maple's engine, will be used for calculations.

1 Introduction

Casino gamblers have been attempting to "beat the house" ever since organized gambling was introduced during the Chinese Tang dynasty between the 7th and 10th centuries A.D. Players have been attempting to increase their odds of winning through both legal and illegal means, using playing strategies such as choosing when to make a particular decision or how much to wager on a specific outcome. The motivation for this paper came from a run of bad luck by one of the authors at a casino over several months. The hope was that by using some mathematical analysis, we would be able to see how to use betting strategies to skew outcomes in our favor over the short or long term.

Please note that we do not wish to give the impression that anything can be done to change the odds to players or the house. Rather, we only wish to try to identify betting strategies that allow players to limit risk while retaining the potential for success. With a focus on games with around a 50% probability of success, or, as it is known, "1:1 (one-to-one) odds," by applying the betting systems, we propose that players could play a chosen number of bets with only a minimal loss or even a potential profit. The three games we will play through simulation are blackjack, craps, and roulette, to which we will apply the three betting systems Martingale, Paroli, and Fibonacci.

2 The Games

2.1 Blackjack

The most common theory for the origin of blackjack gives credit to early 18th century France with the invention of the game *Vingt-et-Un*, which translates from French as *Twenty-One*. Under the reign of King Louis XV, the game was played at French Royal Court. By the early 19th century it had made its way onto the streets of New Orleans, though it was played with a slight variation on the rules as compared to today. When gambling became legalized in Nevada during the 20th century, the game began being hosted by casinos and gambling halls. Its name was changed to *blackjack* with the hope of growing its popularity, and additional payouts were given to players who won with a black Jack (the Jacks of clubs or spades) or the Ace of spades. These bonus payouts eventually became less common after the game did indeed grow in popularity [3].

A few variations exist for the rules of blackjack, although the odds of winning change only very slightly. The standard rules for blackjack and the parameters for our analysis are:

1. All cards are assigned point values. Cards numbered 2–10 are assigned the number of points of their face value, while Kings, Queens, and Jacks are assigned 10 points. Aces can be assigned either 1 or 11 points, as chosen on each deal by the player.

2. The dealer deals the player two cards, while the dealer receives two cards with one facing up. The player then decides whether to "hit," meaning to take an additional card, or "stand,"

meaning to not take an additional card. If the player hits, then they decide again whether to hit or stand, continuing in this manner until they either stand or "bust," meaning they have more than 21 total points. The player loses if they bust. If the player stands with fewer than 21 points, then the dealer repeatedly draws cards until they either beat the player or bust. In this scenario the house loses only if the dealer busts.

3. For our analysis, we will assume eight full decks of cards are used. Also, if the player's first two cards are a "blackjack," meaning an Ace and any other card worth 10 points for a total of 21 points on the deal, the payoff to the player is 3:2, meaning any bet earns a profit of 50%. Finally, we will assume the player will follow the basic strategy of the betting systems analyzed, which dictate gameplay based on scenarios. Although electronics cannot be used at blackjack tables, basic strategies can be printed and used at tables legally.

Following these rules, the odds are in the dealer's favor, but only by a margin of 0.43096% [5]. That is, the dealer wins on average 50.21548% of the time, while the player wins on average 49.78452% of the time.

2.2 Craps

The most common theory for the origin of the dice game craps is that it was invented during the Crusades, when it was known as *Hazzard*, and grew in popularity during the gambling boom in 17th century France. As with blackjack, craps came to the United States via New Orleans as a street game called *street craps*. The term *craps* comes from the French word *crapaud*, meaning *toad*, which people tended to resemble as they crouched over to play the game on a floor or sidewalk. The American version of craps saw a few minor rule changes over the years, but the game has basically been played in a very similar manner for many years.

Craps consists of 27 bets that can be placed in prediction of the sum of two dice rolled by a *shooter* [4]. A few bets are inverses of each other, so playing both during the same roll would be illogical, but any other combination of bets is reasonable. The parameters for our analysis are:

1. The player only plays the *Field* bet, meaning the sums 3, 4, 9, 10, and 11 are 1:1 winners, while the sums 2 and 12 are 2:1 winners.

The odds for the Field craps bet are in the house's favor by a margin of 5.56% [4].

2.3 Roulette

Roulette is a game played with a small white ball, called the *pellet*, spinning around a horizontal wheel, on which it eventually settles into one of the following 37 or 38 numbered positions: ones

labeled 1–36 and split between red and black with 18 positions for each, one labeled 0, and, sometimes, also one labeled 00. The roulette wheel was invented by the legendary French mathematician Blaise Pascal when he was attempting to create a continuous motion mechanism requiring no outside force to stay in motion [6]. While Pascal's intended experiment failed, he nonetheless accidentally succeeded in creating the roulette wheel.

As with craps, there are many different ways a player can bet on roulette, including on individual numbers, splitting a bet between two or four numbers, and dividing the table into thirds by betting on 1–12, 13–24, or 25–36. The parameters for our analysis are:

1. The player makes the same even-money (1:1) allowed bet on each spin. One allowed bet is "even/odd," in which a player choosing even wins if the pellet lands on a nonzero even number, and a player choosing odd wins if it lands on an odd number. Another allowed bet is "high/low," in which a player choosing high wins if the pellet lands on a number in the range 1–18, and a player choosing low wins if it lands on a number in the range 19–36. The final allowed bet is "black/red," in which a player wins if and only if the pellet lands on their chosen color.
2. The wheel has 38 spaces, including both 0 and 00, since this is the type of wheel most common today. With this wheel, all of our allowed bets have a probability of winning of $\frac{18}{38}$.

The odds for all our allowed bets are in the house's favor by a margin of 5.26% [5].

3 The Betting Systems

3.1 Martingale

The Martingale betting system, which was introduced by French mathematician Paul Pierre Lévy in the 18th century, is likely the most common progressive betting system used today. Legend has it that the system derives its name (with one letter changed, for some reason) from the last name of early 18th century London casino owner John H. Martindale, who encouraged patrons to use it in his own casino, which led, ironically, to its bankruptcy. The system has transcended standard casino gambling, and is now used in many nontraditional forms of gambling, such as investment banking, stock brokering, and sports betting. The rules of Martingale are straightforward—with each loss, one doubles their bet, until they win. Although starting bet sizes of 5% of one's bankroll are more common in practice, we will use 1% in our analysis in order to more clearly see long-term trends [2].

Table 1 shows an example of the Martingale system in practice, with a beginning bankroll of \$100 and initial bet size of \$1. Under Martingale with a beginning bankroll of \$100, after six consecutive losses it would be not possible to make a seventh bet. Nonetheless, even though Martingale is a high risk system, it is also true that for one whose beginning bankroll is sufficient to fund the next bet after n consecutive losses, a win on that next bet would return the beginning bankroll plus the amount of the

initial bet. Exhausting one's bankroll is not the only drawback to the system though. Casinos often have betting limits, so one might reach a point where doubling after a loss would not be allowed.

Table 1: Example of the Martingale betting system.

Round	Bet	Win or Loss	Bankroll
			\$100
1	\$1	Loss	\$ 99
2	\$2	Loss	\$ 97
3	\$4	Loss	\$ 93
4	\$8	Win	\$101
5	\$1	Win	\$102

Table 2 shows the results of applying 1000 trials of the Martingale betting system to each game, stopping if 25, 50, or 100 rounds are reached in each trial, with a beginning bankroll of \$500 and initial bet size of \$5 for each trial. Within each cell of the table, the first number is the average number of rounds played before either the number of rounds indicated in the first column was reached or the next bet could not be made, and the second number is the average final bankroll. As we can see from the table, blackjack shows the highest likelihood of success, with almost 2% in expected profit with at most 25 rounds, and around 0.2% in expected loss with at most 100 rounds.

Table 2: Results from trials of the Martingale betting system.

Rounds	Blackjack	Craps	Roulette
25	23.59 / \$509.10	22.76 / \$482.60	23.33 / \$502.25
50	42.95 / \$504.99	40.96 / \$473.82	40.56 / \$475.34
100	72.56 / \$498.88	65.69 / \$442.77	66.99 / \$441.38

We will now demonstrate a Maplet[1] entitled **Casino** written by the authors which can be used to analyze the three betting systems and three games considered in this paper. This Maplet is available for download at the link labeled [S1] in Section 5. The code that underlies the Maplet is unique to Maple, but could easily be altered for any programming language and any game as long as the player knows the house edge, probability of winning a round, and maximum number of rounds to be played. The **Casino** Maplet allows users to select the betting system and game to be analyzed, and enter the number of rounds, trials, initial bet amount, and beginning bankroll. Clicking the **Compute Parameters and Graph Distribution** button then causes the mean number of turns, mean ending money value, largest ending money value, and smallest ending money value to be displayed, as well as a graph showing the distribution of ending money values.

The screenshots of the **Casino** Maplet in Figures 1–3 show the distribution of ending money values for 1000 trials of the Martingale betting system for all three games with at most 25 rounds, a beginning bankroll of \$500, and an initial bet size of \$5. All show a bimodal distribution with left skewness and a majority of trials ending in profit.

[1] A Maplet is like an applet, but uses the computer algebra system Maple, and is written using Maple functions and syntax.

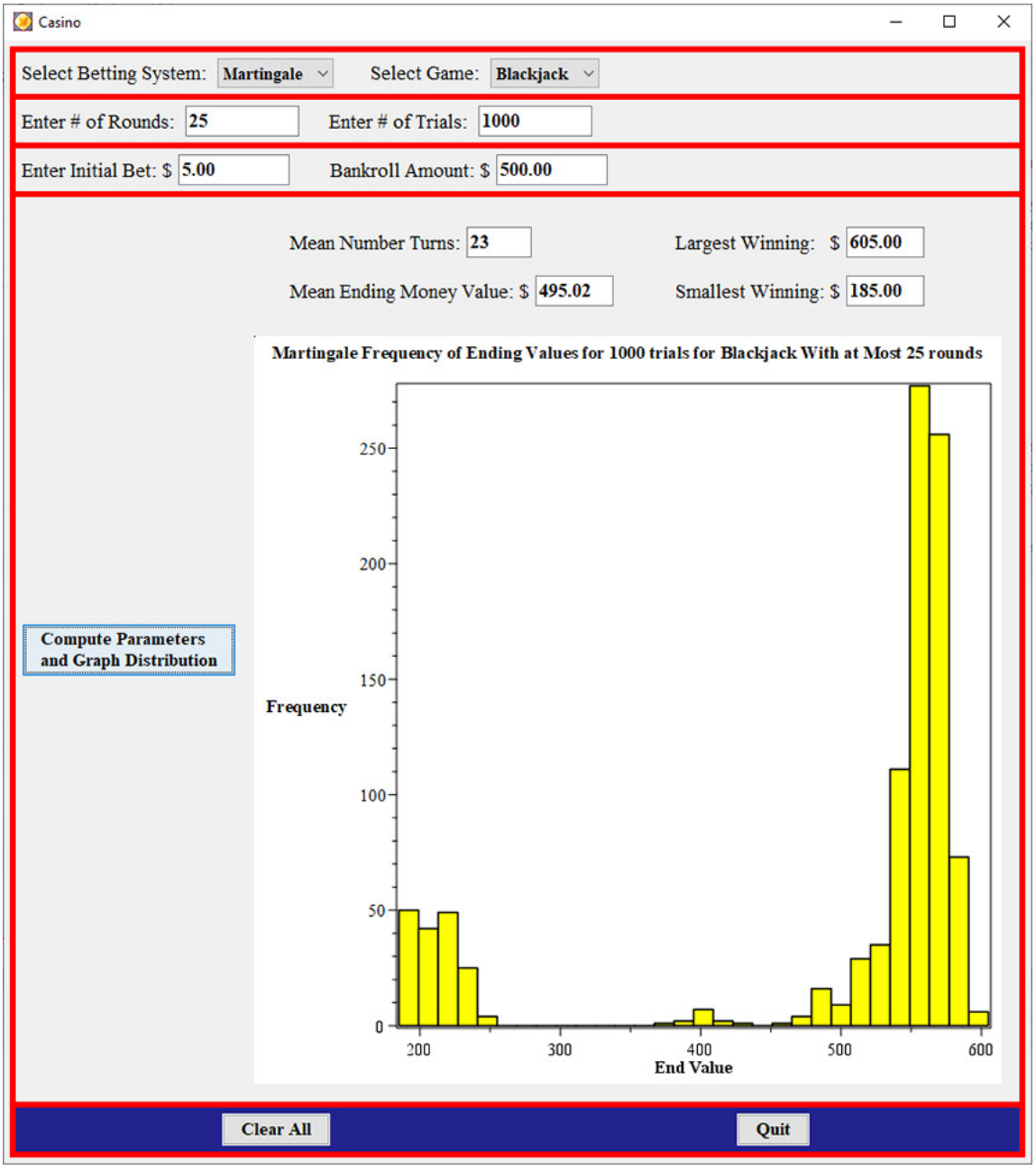

Figure 1: Ending Money Values for Blackjack With at Most 25 Rounds Under Martingale System

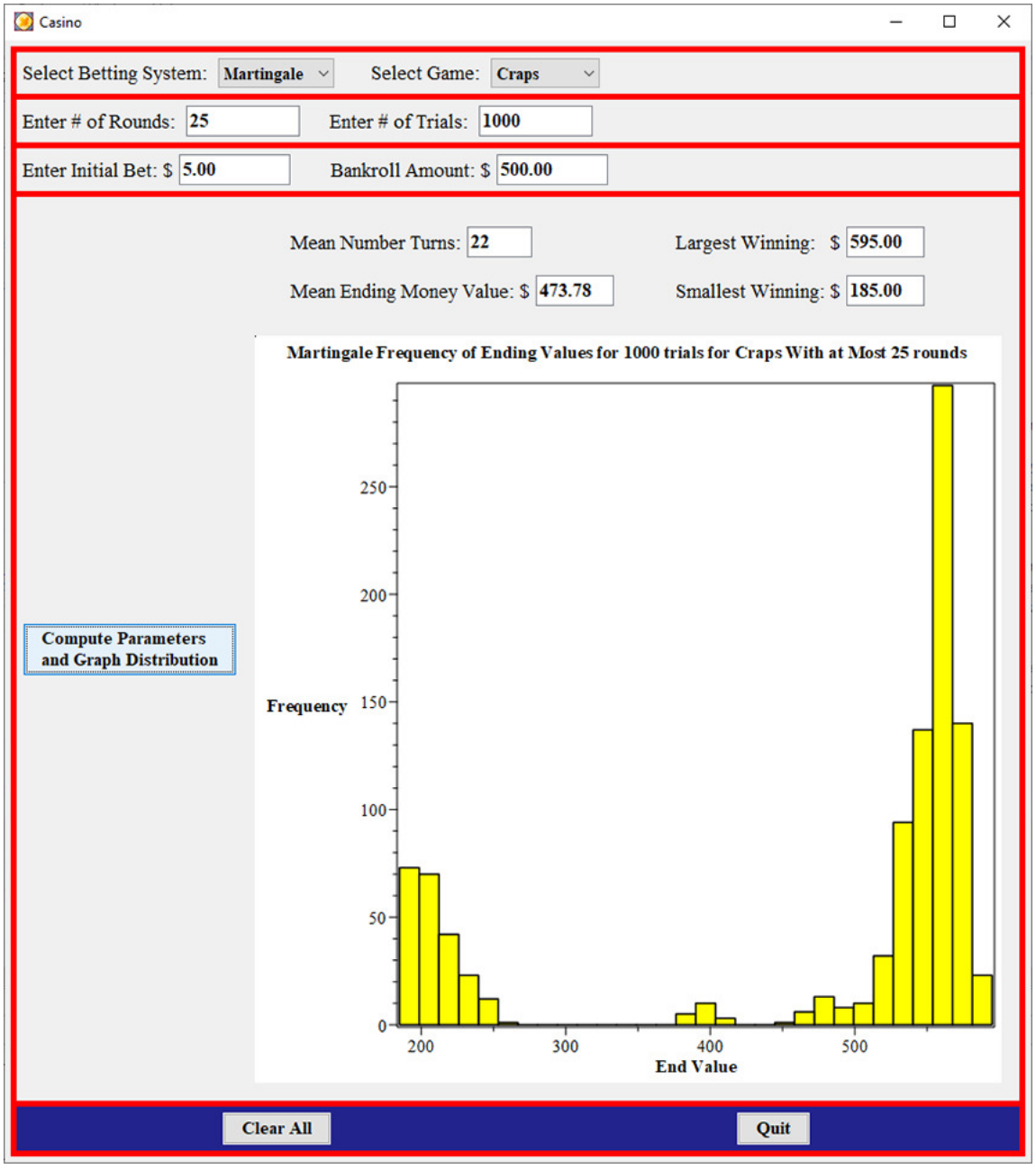

Figure 2: Ending Money Values for Craps With at Most 25 Rounds Under Martingale System

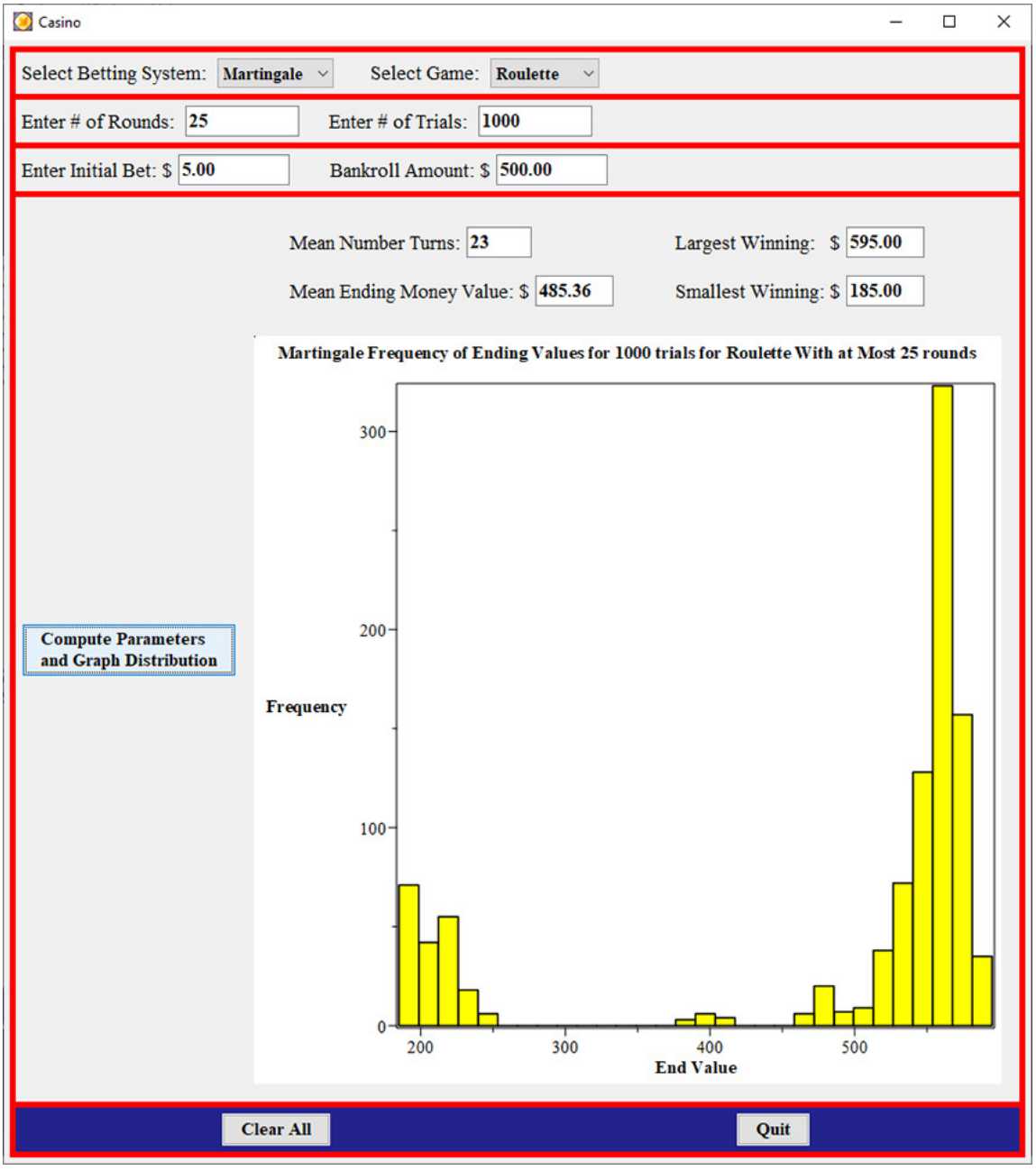

Figure 3: Ending Money Values for Roulette With at Most 25 Rounds Under Martingale System

3.2 Paroli

The Paroli betting system derives its name from the Latin word *par*, which means *to break even*. Like the roulette wheel, the Paroli betting system has been credited as an invention of French mathematician Blaise Pascal. While the Martingale betting system is a high-risk system, Paroli, also known as "anti-Martingale," allows players to set a maximum amount they are willing to lose with each play [1]. Under Paroli, players double their bet after each round until either three consecutive wins or a loss, after which they return to their initial bet amount [5].

Table 3 shows an example of the Paroli system in practice, with a beginning bankroll of \$100 and initial bet size of \$1. Under Paroli with an initial bet size of \$1, three consecutive wins results in a profit of \$7, or, equivalently, "pays 7 to 1." Since each round offers a chance of winning of approximately $\frac{1}{2}$, the probability of winning three consecutive rounds is about $\frac{1}{2^3} = \frac{1}{8}$. That is, under Paroli, players are taking a chance on earning a profit of 7 to 1 against odds of winning of 8 to 1.

Table 3: Example of the Paroli betting system.

Round	Bet	Win or Loss	Bankroll
			\$100
1	\$1	Win	\$101
2	\$2	Win	\$103
3	\$4	Win	\$107
4	\$1	Loss	\$106
5	\$1	Win	\$107

Table 4 shows the results of applying 1000 trials of the Paroli betting system to each game, stopping when 25, 50, or 100 rounds are reached in each trial, with a beginning bankroll of \$500 and initial bet size of \$5 for each trial. The number in each cell of the table is the average final bankroll. In comparison with the Martingale system, the Paroli system rarely returns a large profit. However, under Paroli players can guarantee playing any specified number of rounds, since the most they could lose on any single round would be the value of their initial bet. For example, if a player wanted to guarantee being able to play 25 rounds, they could start by betting 4% of their bankroll, since this would require 25 consecutive losses for their entire bankroll to be lost.

Table 4: Results from trials of the Paroli betting system.

Rounds	Blackjack	Craps	Roulette
25	\$501.79	\$488.11	\$489.81
50	\$500.77	\$476.43	\$478.01
100	\$495.32	\$455.11	\$455.39

The screenshots of the **Casino** Maplet in Figures 4–6 show the distribution of ending money values for 1000 trials of the Paroli betting system for all three games with 100 rounds, a beginning bankroll of \$500, and an initial bet size of \$5. All show a more normal distribution than Martingale, with more predictability and less volatility. In particular, the ending money values rarely dip below \$300.

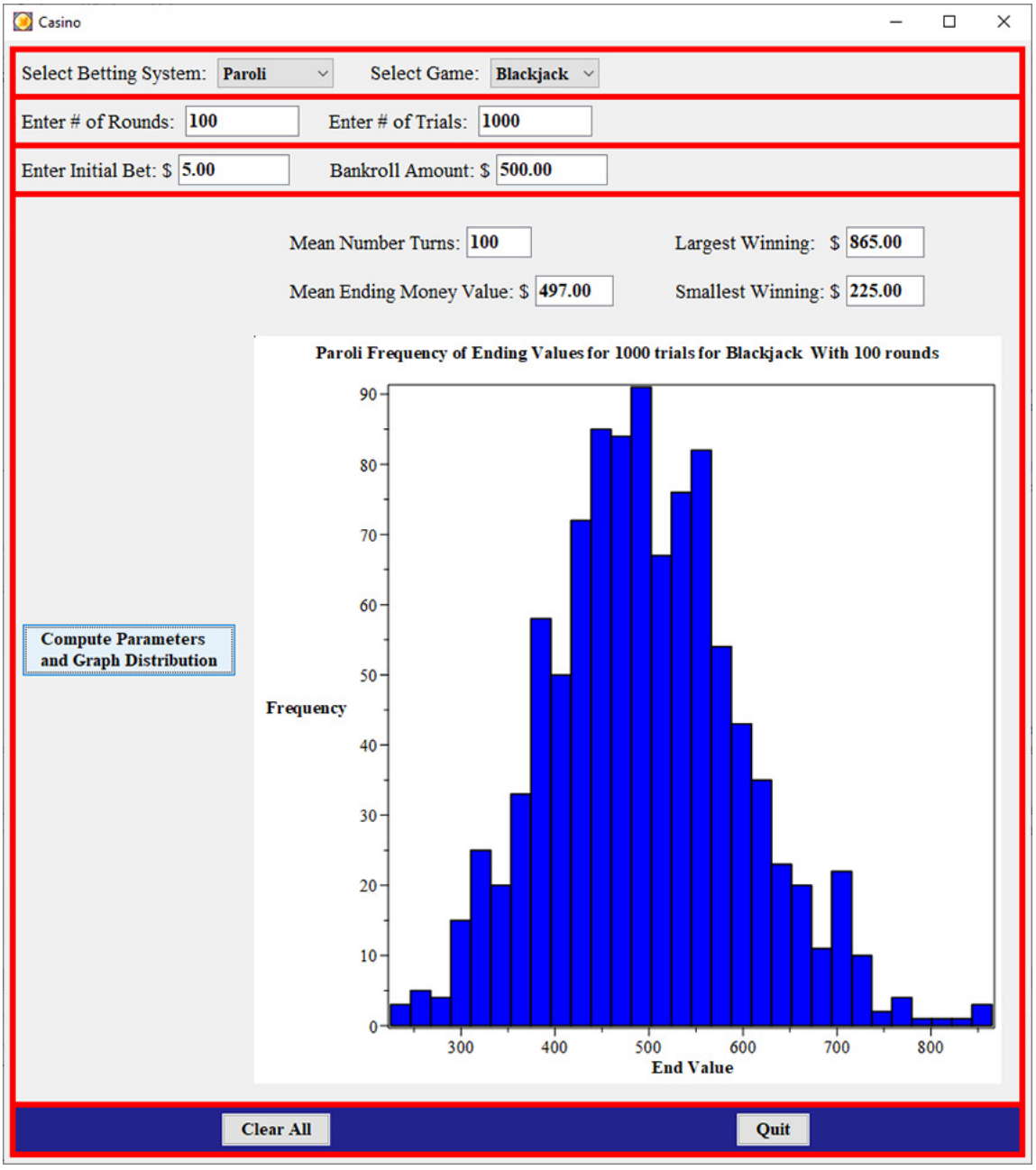

Figure 4: Ending Money Values for Blackjack With at Most 100 Rounds Under Paroli System

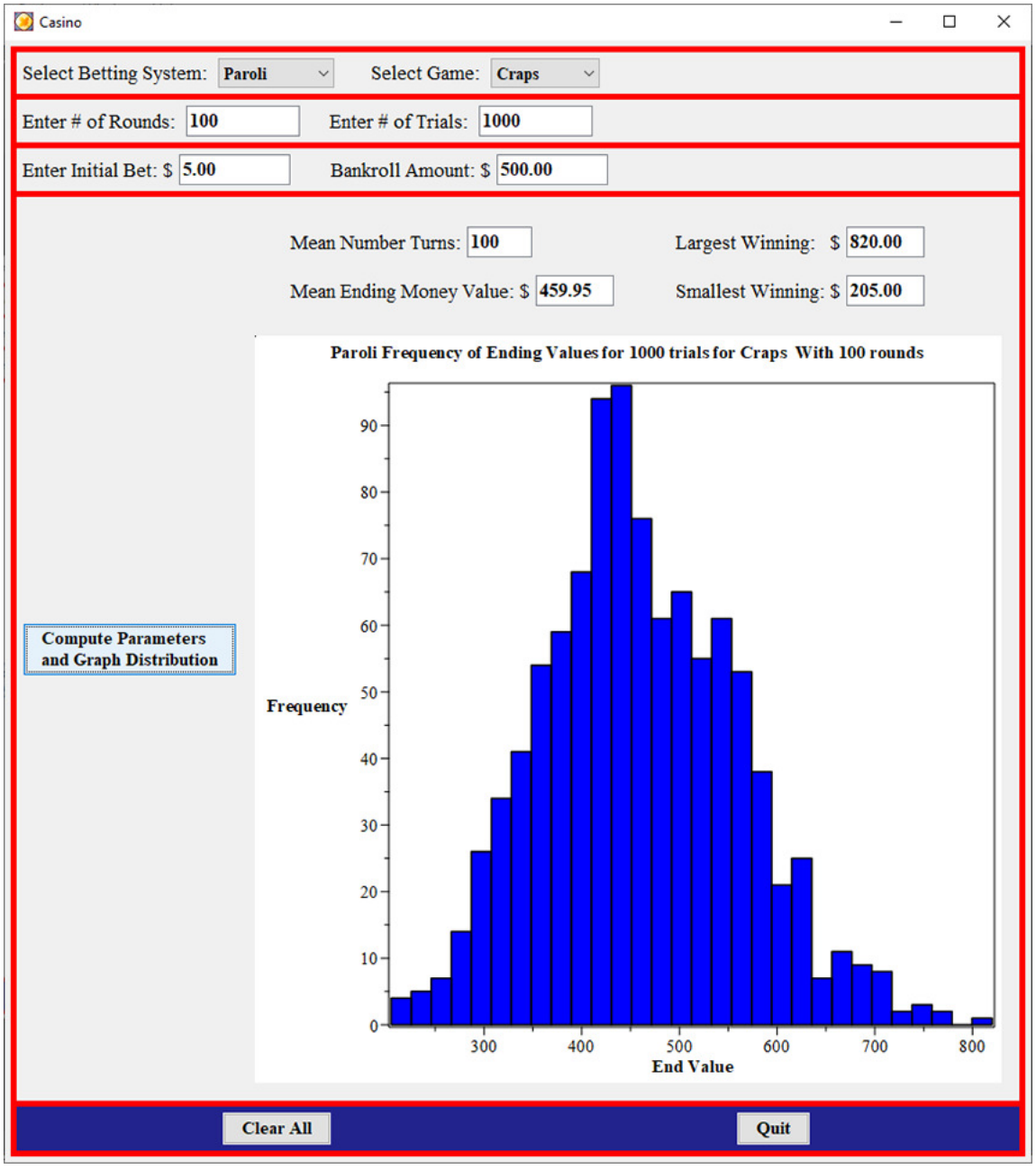

Figure 5: Ending Money Values for Craps With at Most 100 Rounds Under Paroli System

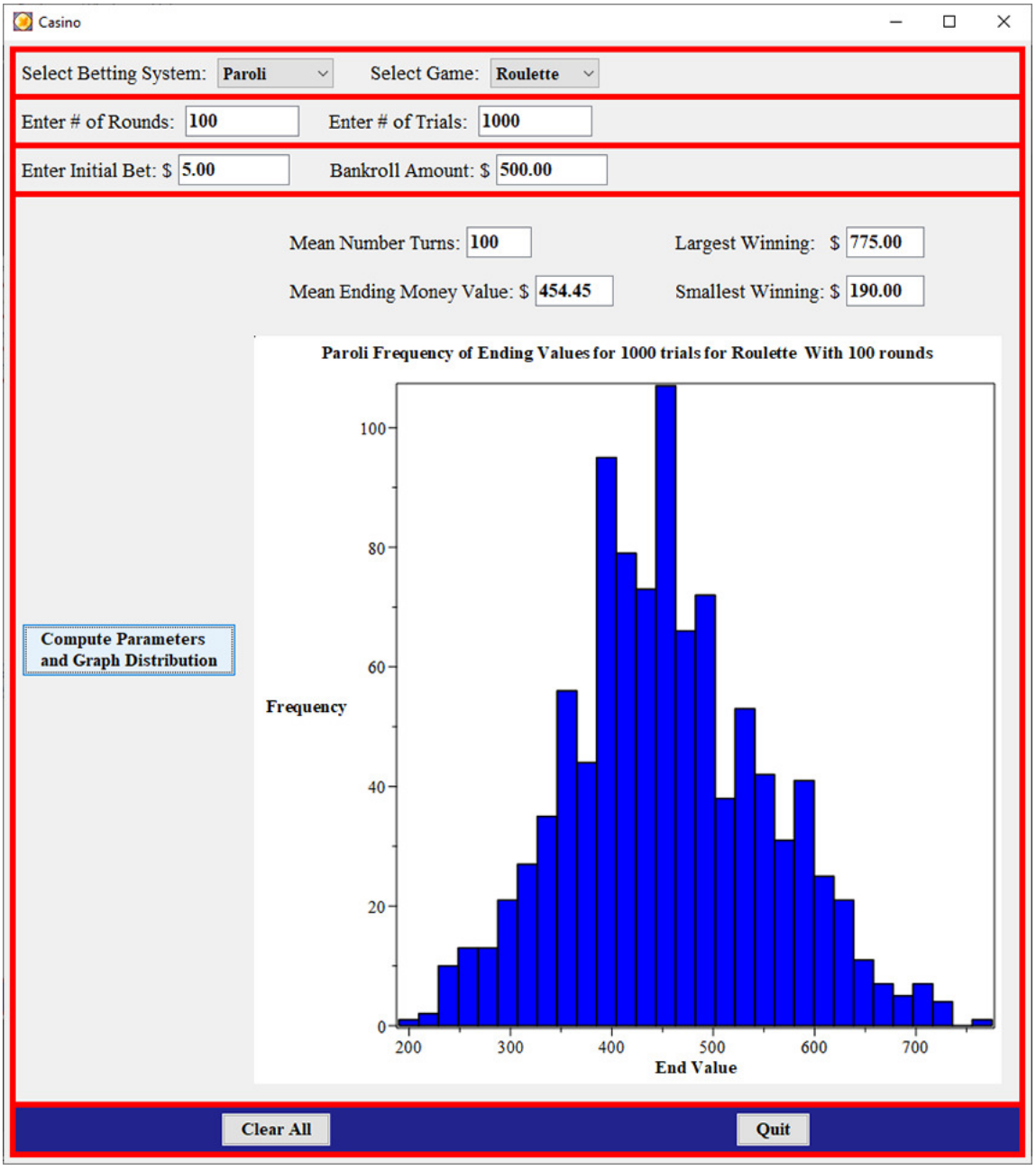

Figure 6: Ending Money Values for Roulette With at Most 100 Rounds Under Paroli System

3.3 Fibonacci

Recall that the Fibonacci number sequence begins with the terms $F_0 = 0$ and $F_1 = 1$, with subsequent terms F_n for $n > 1$ being the sum of the previous two terms: $F_n = F_{n-1} + F_{n-2}$. That is, the Fibonacci sequence is: 0, 1, 1, 2, 3, 5, 8, 13, 21, 34, 55, ... In the Fibonacci betting system, each bet made by a player is their initial bet scaled by a multiplier from this sequence. For the first bet, players multiplying their initial bet by the third number in the sequence, $F_2 = 1$. After each loss, the bet multiplier moves forward one position in the sequence, from F_i to F_{i+1}. After each win, the bet multiplier moves back two positions in the sequence, from F_j to F_{j-2}, though never moving past the third number in the sequence [5].

Table 5 shows an example of the Fibonacci system in practice, with a beginning bankroll of \$100 and initial bet size of \$1. A drawback to the Fibonacci system is that several consecutive losses can quickly lead to very large bets. For this reason, literature on the system often recommends that players use an initial bet size of between only 1% and 5% of their beginning bankroll.

Table 5: Example of the Fibonacci betting system.

Round	Bet	Win or Loss	Bankroll
			\$100
1	\$1	Loss	\$ 99
2	\$2	Loss	\$ 97
3	\$3	Loss	\$ 94
4	\$5	Win	\$ 99
5	\$2	Win	\$101

Table 6 shows the results of applying 1000 trials of the Fibonacci betting system to each game, stopping if 25, 50, or 100 rounds are reached in each trial, with a beginning bankroll of \$500 and initial bet size of \$5 for each trial. Within each cell of the table, the first number is the average number of rounds played before either the number of rounds indicated in the first column was reached or the next bet could not be made, and the second number is the average final bankroll. The results are similar to what we saw for the Martingale and Paroli systems, with even with a better chance of a higher profit. However, unlike Paroli, Fibonacci does not allow players to guarantee being able to play any specified number of rounds, and could also allow bets to become very large.

Table 6: Results from trials of the Fibonacci betting system.

Rounds	Blackjack	Craps	Roulette
25	24.73 / \$504.47	24.54 / \$496.19	24.41 / \$485.67
50	47.49 / \$513.69	46.32 / \$467.82	46.67 / \$479.24
100	90.22 / \$530.51	85.08 / \$450.14	86.13 / \$461.16

The screenshots of the **Casino** Maplet in Figures 7–9 show the distribution of ending money values for 1000 trials of the Fibonacci betting system for all three games with 50 rounds, a beginning bankroll of \$500, and an initial bet size of \$5.

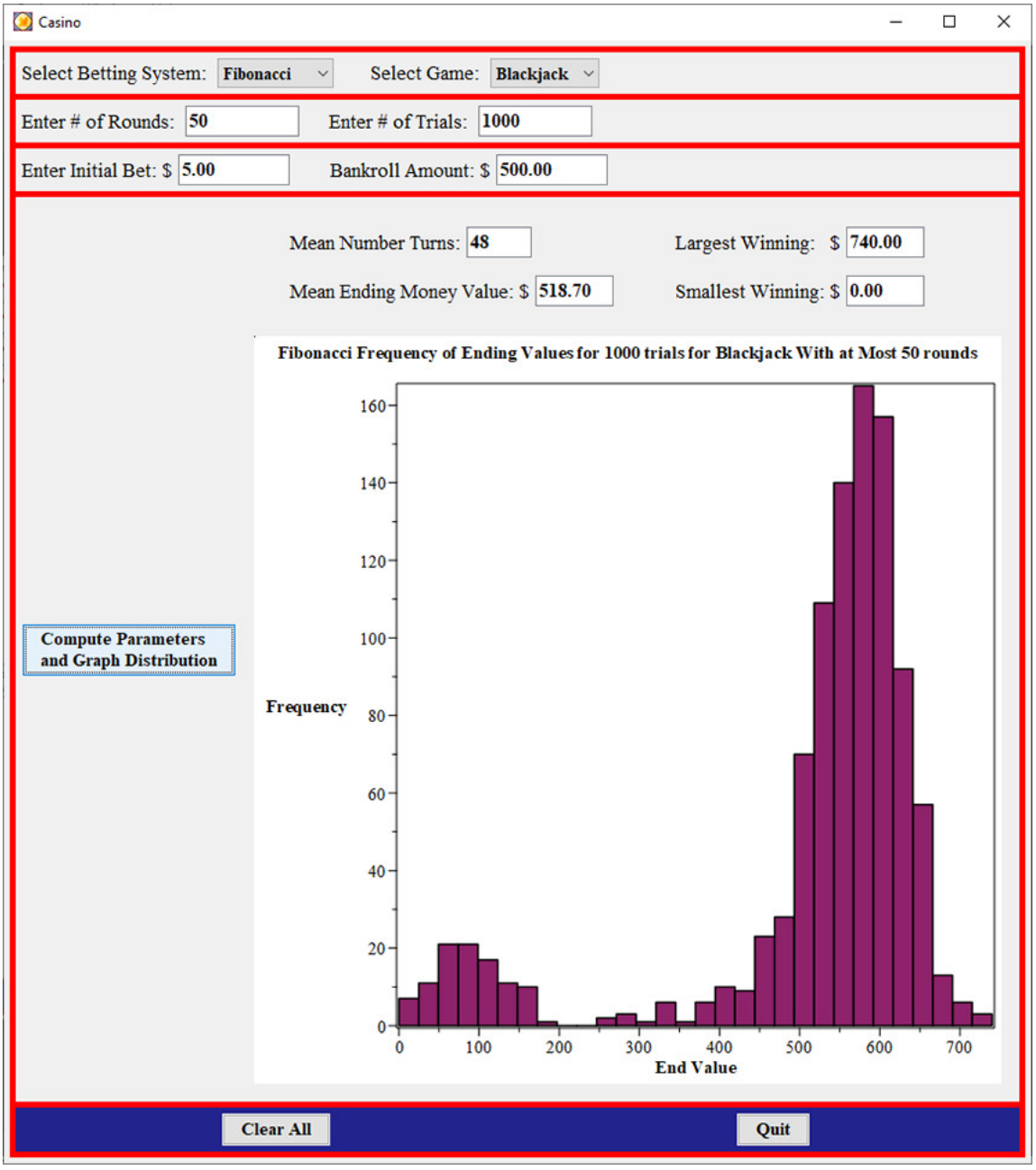

Figure 7: Ending Money Values for Blackjack With at Most 50 Rounds Under Fibonacci System

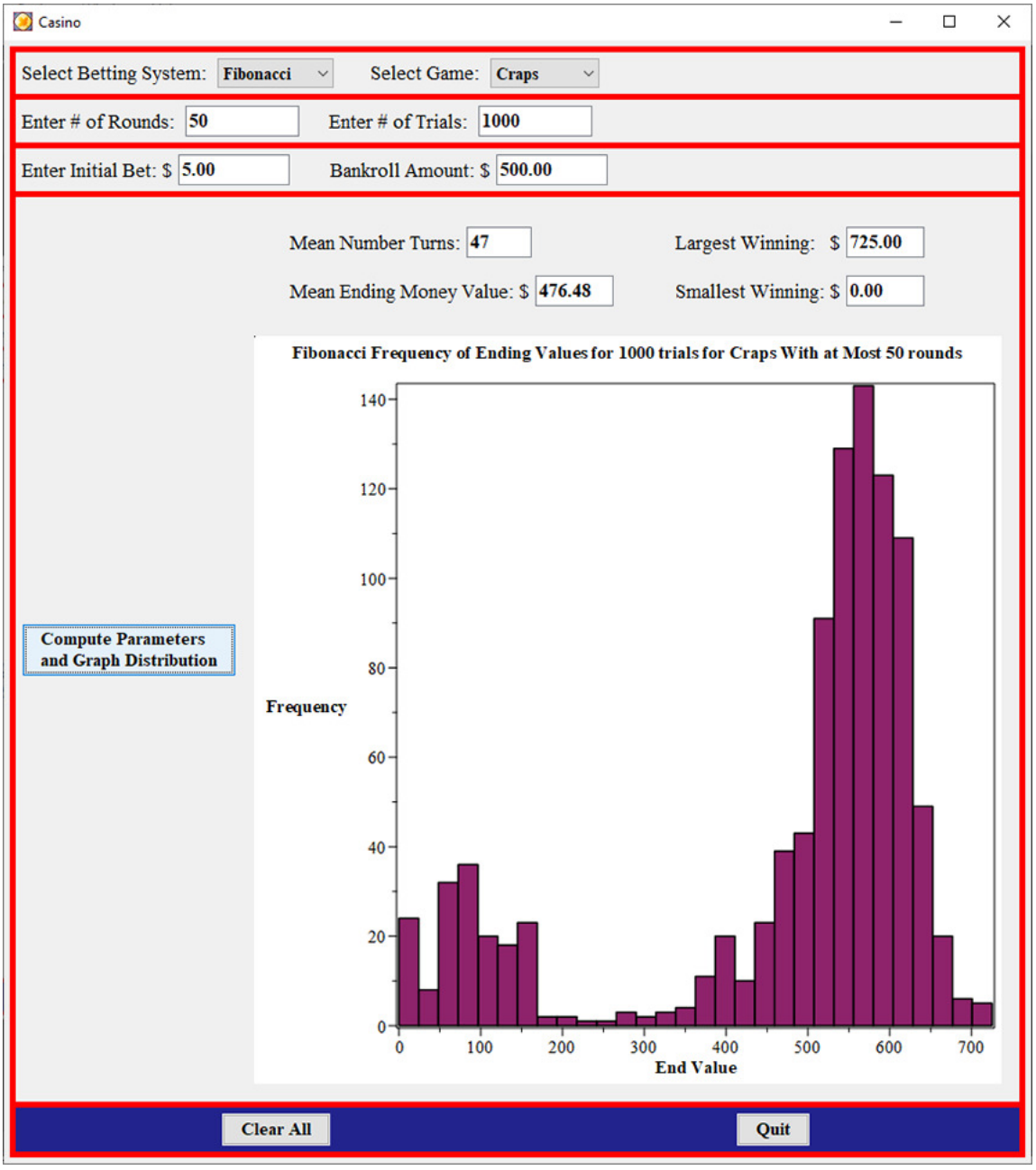

Figure 8: Ending Money Values for Craps With at Most 50 Rounds Under Fibonacci System

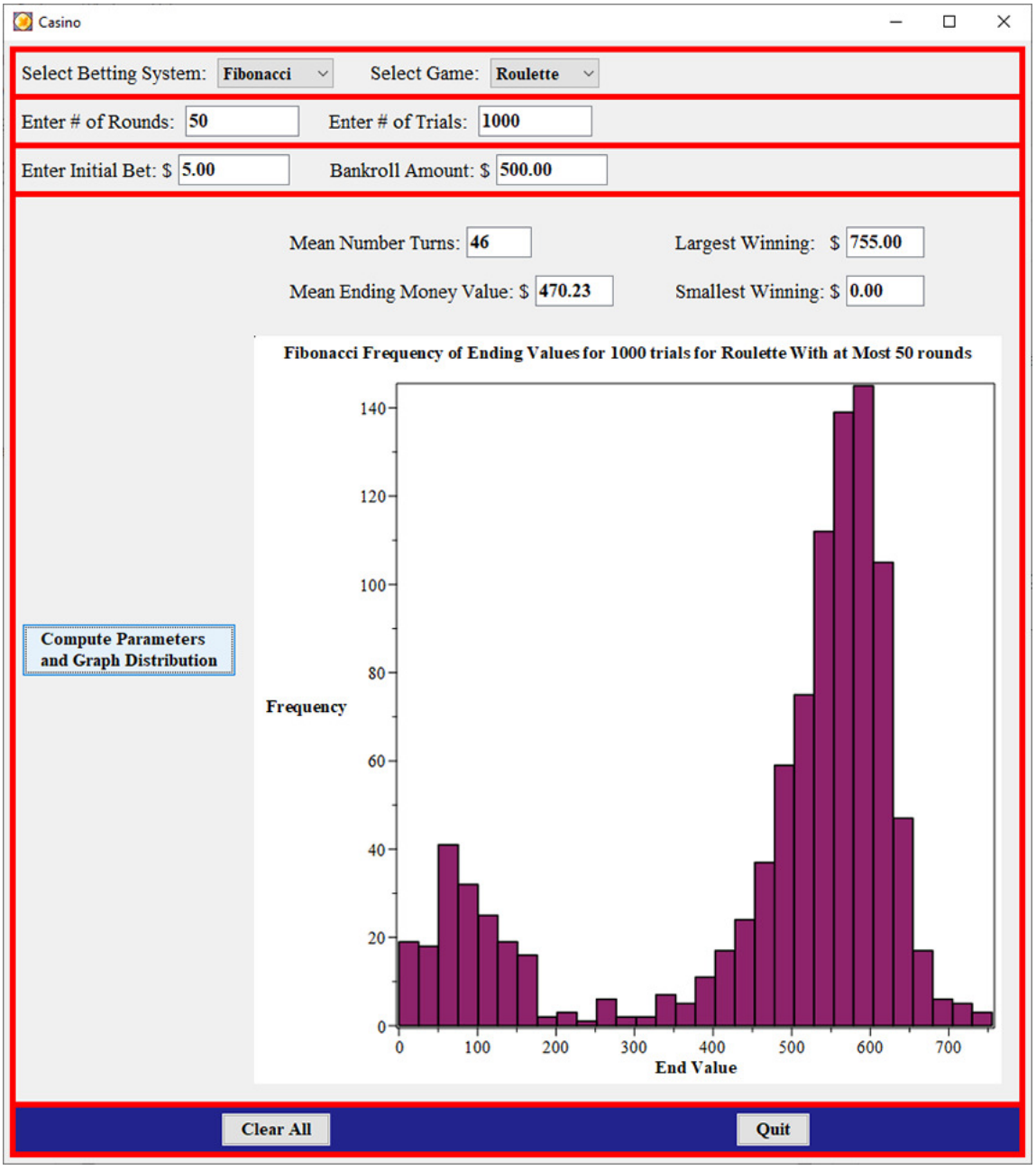

Figure 9: Ending Money Values for Roulette With at Most 50 Rounds Under Fibonacci System

4 Conclusions and Ideas for Future Work

As part of this project, simulations were also done using other number sequences such as Pi and Euler that show more randomness. These systems did not show promise from a gambling perspective though, as the key to a progressive betting system is the ability to regain losses as quickly as possible with a minimal number of wins.

For the analyses described in this paper, the Martingale betting system shows the most promise for potential profit in the short term, unless the probabilities of success on a given round are approximately 50%. However, under the Martingale system, if a player started by betting 1% of their beginning bankroll, then they would only be able to survive six consecutive losses before being unable to place the next bet. Even worse, if a player started by betting 5% of their beginning bankroll, then they would only be able to survive four consecutive losses before being unable to place the next bet. As such, the player would need to decide what it is really worth to them to have a profit potential. An intelligent strategy for the Martingale system would be for a player to identify how much profit they would need before leaving the game. For example, if a player had the goal of earning $25 profit in at most 25 rounds, then it would only take five wins when betting $5, and as soon as the player reached that goal, they could retire.

In contrast to the Martingale betting system, the Paroli betting system allows players to guarantee being able to play any specified number of rounds that they wish. More specifically, if the player chose to start by betting a certain percentage of their beginning bankroll, then they would be able to predict a minimum number of rounds they would be guaranteed of being able to play. For example, if a player started by betting 1% of their beginning bankroll, they would be guaranteed of being able to play a minimum of 100 rounds. Similarly, if they started by betting 5% of their beginning bankroll, they would be guaranteed of being able to play a minimum of 20 rounds. (This assumes the player completes 100 or 20 rounds, respectively, without three consecutive wins.) Another favorable property of the Paroli betting system is that players can double their bets until they earn two wins in a row, or four wins in a row, or any number of wins in a row they want to achieve. Recall though that regardless of however many consecutive wins a player wants to achieve in order to perceive the result as a success, the odds of reaching that number of wins would still need to be higher than the payoff. For example, two consecutive wins would result in a 3 to 1 payout, while the odds of winning two games in a row would be approximately 4 to 1.

Finally, recall that the Fibonacci betting system, like the Martingale betting system, allows bets to potentially become extremely high if players experience a large number of consecutive losses. So, similar to the Martingale system, with the Fibonacci system it would be better for players to start by identifying a profit amount as the goal rather than a number of rounds to be played. The fact though is that all betting systems have benefits and drawbacks, and so it ultimately comes down to the goals of the player. This project only aims to investigate systems with the end goal of allowing players to play for as long as possible and to reach a reasonable number of rounds with the hope of being entertained by a pleasant evening at a gambling table. The system that seems to best fit that criterion is Paroli, given that it is not for high-risk gamblers, and players can guarantee being able to play any specified number of rounds.

Further investigations could include developing an algorithm through which a player could choose a progressive betting system from among the three analyzed in this paper or possibly others, choose a casino game from among the three analyzed in this paper or possibly others, and then have the algorithm return to them the expected outcome of playing their chosen game under their chosen betting system. With the understanding that no system can guarantee a profit, the player could at least make better choices that lead to more pleasurable gambling experiences.

5 Supplementary Electronic Materials

[S1] Maplet that can be used to analyze the three betting systems and the three casino games considered in this paper:
https://www.appstate.edu/~klimare/casino.maplet.

References

[1] Chris Amberly, 2020. The Paroli System – Is It Effective for Sports Betting? Available at: https://www.sportsbetting.com/guides/strategy/paroli-system/.

[2] Black-jack.com, 2023. How Does the Martingale System Work? Available at: https://black-jack.com/strategy/systems/martingale/.

[3] Crescent.edu, 2019. The History of Blackjack. Available at: https://crescent.edu/post/the-history-of-blackjack.

[4] Lolcraps.com, 2023. Field Craps. Available at: https://www.lolcraps.com/craps/bets/field/.

[5] Michael Shackleford, 2023. The Wizard of Odds. Available at: https://wizardofodds.com/site/about/.

[6] Dr. Zar, 2018. The Roulette Wheel: Blaise Pascal's Fortunate Accidental Invention. Available at: https://www.historyandheadlines.com/the-roulette-wheel-blaise-pascals-fortunate-accidental-invention/.

Statistical Inquiry Process and the Use of ICT

Norie AOKI[1], *Hideyo MAKISHITA*[2]
nb22101@shibaura-it.ac.jp, hideyo@shibaura-it.ac.jp

[1]Functional Control Systems, Graduate School, Shibaura Institute of Technology, Japan.

[2]Civil Engineering, Shibaura Institute of Technology, Japan.

Abstract: *In Japan, standards have been established for curricular organization. The latest standards mention the enrichment of inquiry, statistical education, and active use of ICT. We focus on the enrichment of statistical education in inquiry and describe a case study of problem research, one of the educational activities in the SSH project (Super Science High School), a national project to promote science and mathematics education, and problem study in the required course "Mathematics I." Based on this discussion, we propose future directions for statistical education and the use of ICT. Based on this discussion, we propose the future direction of statistics education and the use of ICT.*

1. Introduction

In Japan, there are curriculum standards called "Courses of Study," which have been established by the Ministry of Education, Culture, Sports, Science and Technology (MEXT) to ensure that a particular standard is maintained in all schools throughout Japan. These standards stipulate general curricular considerations, the number of class hours, and each subject area's general goals, contents, and content. Each school determines the textbooks and timetables for its students based on these standards. The Courses of Study are reviewed every ten years to indicate the qualities and abilities necessary for children to live and to consider social changes such as globalization, rapid informatization, and technological innovation. In high schools, education under the new Courses of Study will begin in 2022, and "inquiry" has been identified as a keyword for learning in the overall curriculum.

In addition, in this revision, science and mathematics education is required to enhance learning activities for scientific inquiry through observation, experimentation, and statistical education for analyzing data and solving problems.

Therefore, this paper focuses on "inquiry" learning activities in science and mathematics education and efforts to enhance statistics education. The inquiry process involves problem setting, information gathering, organization and analysis, and summarization and expression. One educational activity that participates in the inquiry process is the Problem Research*[1] conducted at Super Science High Schools (hereafter, SSH*[2]). Based on our experience working at SSH-designated schools from 2008 to 2020, we will summarize the changes in the Courses of Study and the status of the use of ICT and introduce examples of the use of ICT in Problem Research. We want to discuss the case studies from the viewpoint of the statistical inquiry process and propose future statistical education and the use of ICT.

2. The Objectives of Mathematics*[3] and Mathematical Activities in the Courses of Study

The objectives of the mathematics department in the Courses of Study are as follows.

> The goal is to develop the following qualities and abilities to think mathematically through mathematical activities, using mathematical ways of seeing and thinking.

(1) To understand the basic concepts, principles, and rules of quantity and shape and to acquire the skills to mathematize, mathematically interpret, mathematically express, and mathematically process phenomena.
(2) Cultivate the ability to examine events logically using mathematics, find properties of quantities and figures and explore them in an integrated and developed manner, and express events concisely, clearly, and accurately using mathematical expressions.
(3) Cultivate an attitude of persistent thinking and applying mathematics to daily life and learning by realizing the enjoyment of mathematical activities and the value of mathematics and evaluating and improving the problem-solving process in retrospect.

The Courses of Study to date show that "mathematical activities" are of great significance in mathematics education in Japan. Furthermore, ICT is practical and currently indispensable in those activities.

"Mathematical activities" are activities in which the students conduct the learning process of arithmetic and mathematics. The image of this is shown below (see [1]).

It is described as moving between the real world and the world of mathematics. In the real world, the student can perceive everyday life and social events mathematically, process them mathematically, and solve problems. In the world of mathematics, the student can think about mathematical events in an integrated and developed manner and solve problems. These processes are shown to move between the real world and the mathematical world by focusing on the problem expressed mathematically and obtaining results.

Problem research is an activity that can help us realize this learning process, and we have been practicing it. The following is an example of practice with ICT.

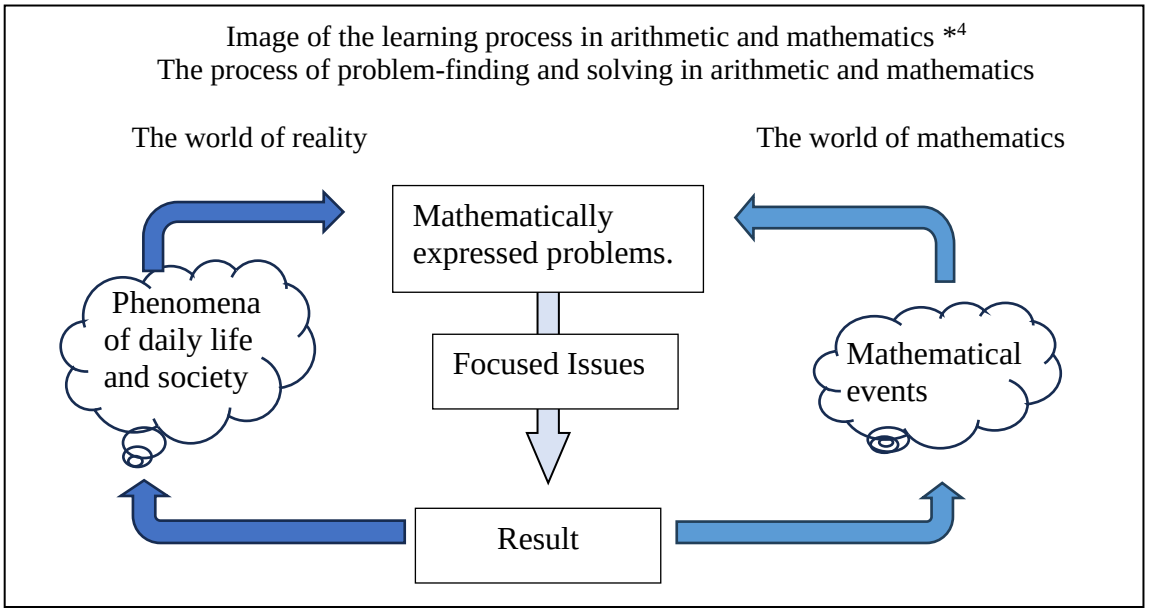

Figure 2.1 Image of the learning process in arithmetic and mathematics*[4]

3. Statistical Inquiry Process and ICT Application

3.1 Students' ICT Environment and Statistical Inquiry Process

Currently, each student is provided with a tablet device. A classroom support application has been installed in the author's prefecture. Each student is given a Google account, and the projector and screen are equipped in each classroom.

The statistical exploration process is a five-step process.

Problem	・Identification of the problem ・Issue setting
Plan	・Data assumptions ・Collection plan
Data	・Collection of data ・Organization into tables
Analysis	・Creation of graphs ・Identification of characteristics and trends
Conclusion	・Conclusion ・Reflection

The process consists of setting up a statistically solvable problem for the original awareness of the situation and what needs to be solved, considering the data to be collected and how to collect them for the set problem, actually collecting the data according to the plan, organizing the data into tables, summarizing the collected data into graphs according to the purpose and type of data, obtaining statistics, identifying characteristics and trends, summarizing and expressing conclusions about the problem from the traits and trends found, and finding further issues and points for improvement for the entire activity. The process is a series of processes to grasp the characteristics and trends of the collected data by summarizing them in graphs and obtaining statistics, etc., according to the purpose and type of data, to express a conclusion about the problem based on the characteristics and trends found, and to see further issues and points for improvement of the entire activity.

3.2 Scenes of ICT use in the statistical inquiry process Class Outline

The use of ICT in the statistical inquiry process is expected to facilitate more concrete imagery in identifying, identifying, and planning issues by recording and storing images and sounds in the steps of problem identification, problem formulation, and planning. In data collection and analysis, data can be obtained, recorded, organized, arranged into tables, and visualized by creating graphs. Students can also be used to summarize conclusions, reflect on, and express or communicate the results. In analyzing data, spreadsheet software such as Excel or R is effective, and in summarizing and describing data, presentation software or Jamboard can be a tool for organizing thoughts. In addition, data collection using the Internet and online conferencing systems may be effective in the inquiry process, such as receiving expert advice. Next, we will discuss examples of ICT applications.

4. Class of the Use of ICT

4.1.1 Problem Research: "Data analysis of photovoltaic power generation and its future use"

Solar panels were installed on the roof of the school building, and temperature, solar radiation, and the amount of electricity generated were measured; these data had been stored on a computer in the school since March 2004. Students learned of the existence of this data and analyzed it. The computer spreadsheet software Excel was used.

Students were interested in energy issues. Since solar power generation has been attracting attention from all over the world as an environmentally friendly method of power generation, and research has been conducted to improve its efficiency, they investigated, based on data accumulated at the school, whether solar radiation is proportional to power generated, whether the temperature is related to power generated, and what can be done to improve the efficiency of power generation, and what should be done to improve the efficiency of power generation. As a method, data on electricity generated by solar panels was imported into a computer and graphed for annual and monthly comparisons. The following data dealt with the data at that time.

date	solar radiation (kwh/m²)	temperature (℃)	the amount of electricity generated (kwh)
1	1.476	23.8	14.41
2	0.893	20.9	7.96
3	4.233	23.8	40.35
4	4.845	23.9	44.77
5	5.471	26.2	50.68
6	4.79	26.8	44.29
7	3.991	28.9	37.06
8	2.191	27	20.76
9	2.408	27.7	22.97
10	1.827	25.4	17.52
11	3.377	25.6	33.16
12	4.457	27.1	41.39
13	2.278	27.6	21.24
14	4.458	30	40.92
15	3.468	28.7	31.61
16	1.888	24.3	17.55
17	2.098	25.6	19.42
18	2.133	26.9	20.36
19	1.975	27.3	18.45
20	4.291	26	39.99
21	1.69	26.3	16.67
22	3.524	26.1	33.68
23	2.18	23.8	20.36
24	3.697	26.8	35.06
25	1.872	27.3	18.03
26	2.594	25.4	24.37
27	2.503	25.3	23.43
28	1.897	25.2	18.58
29	3.774	28.8	35.45
30	2.275	24.9	21.14
31	1.974	24.4	18.91

Figure 4.1 Data of photovoltaic power generation

The data on solar radiation, temperature, and electricity generated were graphed. The graphs were graphed over a day to identify trends. The weather was also used as a reference. There were differences between sunny and rainy days. (See [1] and [2], [3]) On sunny days, the amount of solar radiation and electricity generated were higher than on rainy days.

In addition, a similar graph was also made to grasp the trend and determine the annual change. There were differences depending on the season.

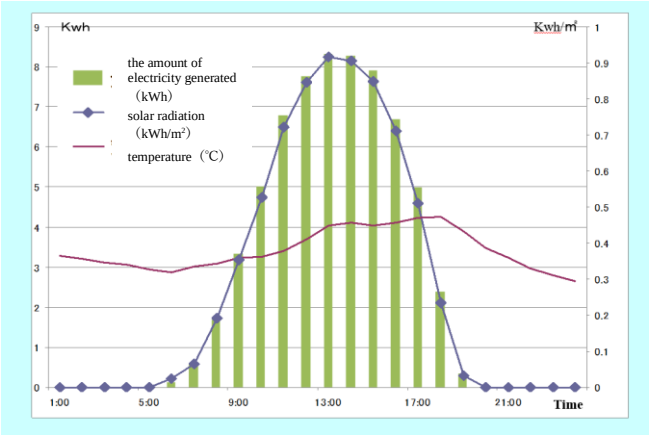

Figure 4.2 Graphs of the amount of electricity generated, solar radiation and temperature (sunny)

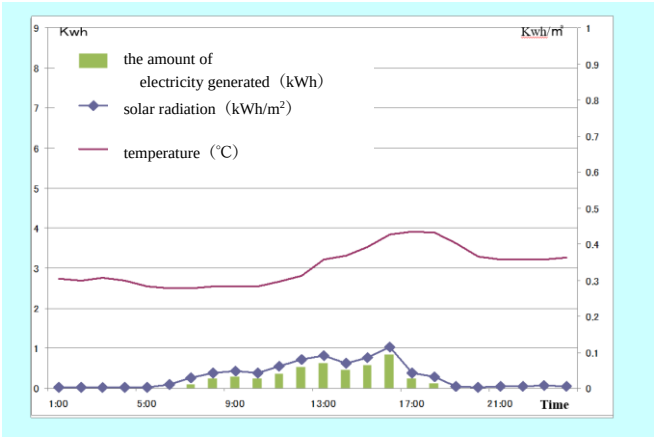

Figure 4.3 Graphs of the amount of electricity generated, solar radiation and temperature (rainy)

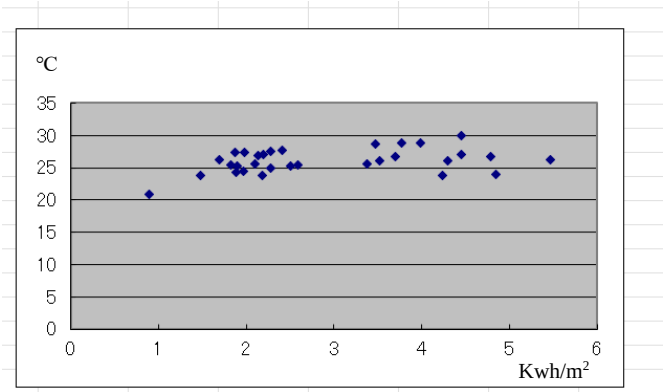

Figure 4.4 Scatter diagram of temperature and solar radiation

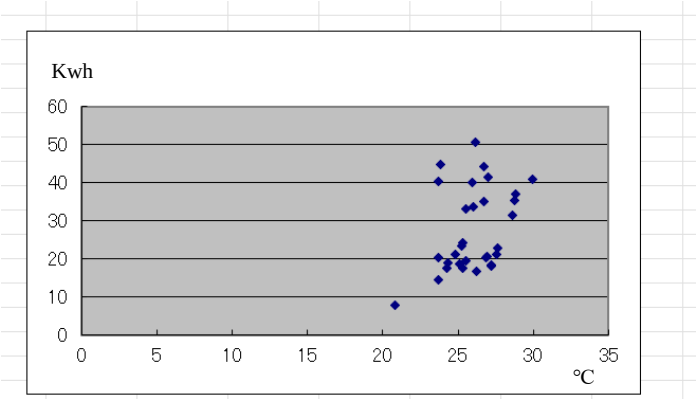

Figure 4.5 Scatter diagram of the amount of electricity generated and temperature

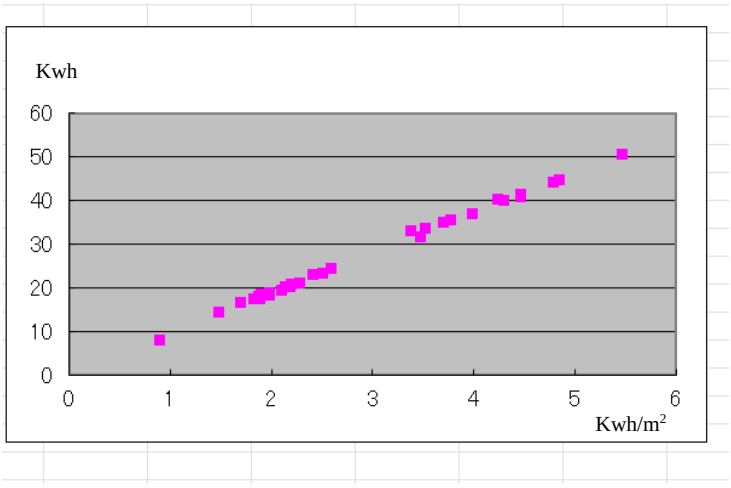

Figure 4.6 Scatter diagram of the amount of electricity generated and solar radiation

Next, Students also examined the correlation between average monthly temperatures, the amount of electricity generated, and solar radiation to determine whether temperature affects them. Scatter plots were created using data from the past five years. It was found that there is no direct relationship between temperature and the amount of electricity generated and between temperature and solar radiation. (See [4] and [5])

Data analysis from the past five years shows that solar radiation and electricity production are proportional. These were compiled throughout the year. (See [6]) This indicates that the amount of solar radiation affects the electricity generated.

As a discussion, the graph shows that the shape of the graph is mountainous in all years, indicating that the summer season tends to have higher temperatures, solar radiation, and electricity generation. The reason for the lower amount of electricity generated from November to February, the winter season, was that geographical factors resulted in fewer sunny days due to higher winter precipitation. A new finding was that electricity generation was higher in the spring months of March through May rather than in the summer when there are more sunny days. They were able to confirm that in some years, this was beyond the summer months. Typhoons and fall rains

influenced the lower amount of electricity generated in September in the fall, while the higher amount in October could be attributed to the influence of clear autumn weather. It was also found that there is a correlation between the amount of solar radiation and the amount of electricity generated, which can be said to be proportional to the amount of electricity generated.
(See [7] and [8])

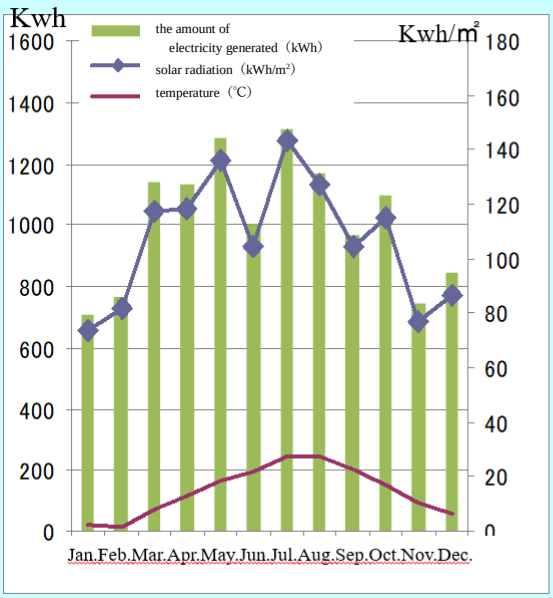

Figure 4.7 Graphs of the amount of electricity generated, solar radiation and temperature (year)

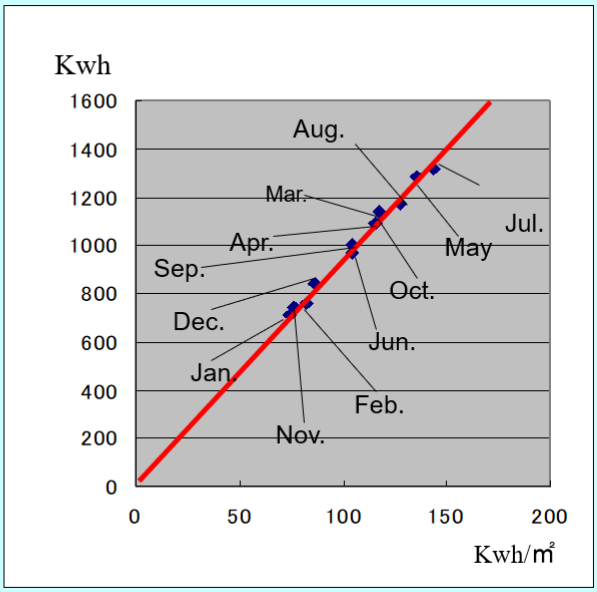

Figure 4.8 Scatter diagram of the amount of electricity generated and solar radiation (year)

For future development issues, Students said that they would like to research the relationship between solar panel temperature and power generation efficiency, the relationship between weather and power generation, and confirm whether there is a relationship between light wavelength and power generation capacity based on measurements of changes in power generation at different light wavelengths and whether it is practical to install solar panels in homes, considering installation costs and electricity costs. The difference in the amount of electricity generated by solar panels and irradiation angles. Since the panels become hot while the sun is shining, they would like to research more effective solar panels, including the use of solar heat.

4.1.2 Course "Fundamentals of Mathematics"

The goal of the course is two points:

1. Acquire knowledge and skills in data processing using a personal computer.
2. Acquire methods to analyze data accurately.
3. Acquired the ability to process and read information accurately and develop an attitude to apply it to real life.

The course aimed to provide students with the basic knowledge and skills necessary to research an issue. To acquire the basic knowledge and skills necessary for research, the students used presentation software and spreadsheet software in data processing to write a report using a PC. The students experienced the hypothesis, verification, and summary process in the computer room.

4.1.3 The problem-based learning of "Mathematics I"

In Japan, Mathematics I is a required course. Required courses are courses that the school's curriculum must take high school students before graduation. The content of Mathematics I includes

numbers and expressions, figures and measurements, quadratic functions, data analysis, and problem-based learning. Problem-based learning encourages students' independent learning and helps them recognize the merits of mathematics by setting tasks that increase students' interest and motivation by relating or developing the content studied or interrelated content with their daily lives. In the Courses of Study, it is stated that the content of Problem-based learning should be implemented at appropriate times and in proper situations to increase the effectiveness of learning based on the relationship with each content, and mathematical activities should be further emphasized when implementing the content. The following is a summary of the contents of the program. The study tasks may be placed at the end of each unit or after every unit, with the latter being the case for content covering multiple fields. The former has the advantage of dealing with the subject immediately after the end of the unit, and the latter has the advantage of allowing students to feel the connection of mathematics.

The author and other research team members conducted a survey on how problem-based learning is described in all 17 Mathematics I textbooks (from five different companies), which the Department of Mathematics approves at upper secondary schools. As a result, they simultaneously investigated whether the problem-based learning in each of the Mathematics I textbooks focused on the world of everyday life and social phenomena or that of mathematics and categorized them as "mathematics" when they dealt with mathematical phenomena and "reality" when they dealt with everyday life and social phenomena.

The results of this survey were as follows.

1. Numbers and expressions (23, reality: 16, math: 7)
2. Quadratic functions (30, reality: 17, mathematics: 13)
3. Trigonometric ratios (25, reality: 13, mathematics: 12)
4. Sets and propositions (10, reality: 7, mathematics: 3)
5. Analysis of data (19, reality: 16, mathematics: 3)

Overall, of the 107 pieces, 73 were "reality "and 34 were "mathematics." In addition, 9 were arranged as content integrating multiple disciplines. Since this paper focuses on the statistical inquiry process, when looking at the field of data analysis, 16 out of 19 dealt with familiar themes.

The themes were as follows.

1. How can we effectively advertise based on the survey results?
2. Using data from national and regional surveys, look for local problems and develop solutions.
3. Analyze the relationship between points won and standings based on data from soccer match results.
4. Investigate the relationship between birds and wing area using data on various birds based on the bird body mass and wing area data.
5. Correlation coefficients from physical fitness data
6. Examine the relationship between winter and summer temperatures.
7. Inferring data from analyzed results.

In this section, we will address the bird body mass and wing area issue. For this assignment, 29 bird species are shown in a scatter plot with weight on the horizontal axis, wing area on the vertical axis, and a box-and-whisker plot of weight along the axis, as shown in the figure below (See [9]).

I created a study plan using this assignment with the following two-hour dividend.

Study Guidance Plan (2 hours dividend 50 minutes x 2 hours)

Hour 1

process	Study Contents and Activities	matters that require attention	Form of study
Introduction (5 minutes)	Confirm the issue currently.		simultaneous
	Data on body mass and wing area for 29 bird species are represented in scatter plots. Box-and-whisker plots were also shown for body mass and wing area, respectively. (See [9]) Consider the following assignment. 1. Let's find out how many grams more than the body mass outlier is from the box-and-whisker diagram of body mass. 2. Let's create a scatter plot again from the remaining data, excluding the outliers obtained in 1. Let's also show a box-and-whisker diagram of body mass and determine how many grams more than the weight outlier is. 3. Summarize the correlation coefficients for each data and summarize what can be said about the bird's weight and wing area from the results.		
		Data will be sent to individual student's terminals after assignment confirmation.	
Deployment (43 minutes)	Group together and work on issues.	The group will discuss and think about it.	Group (about four persons)
	Create scatter plots and box plots using spreadsheet software.	The obtained outlier values, scatter plots, and box plots will be reviewed with the entire class.	
	Calculate the zero-correlation coefficient.	Confirmation of how to obtain correlation coefficients. Assist students as you see fit.	
	Consider the change in the correlation coefficient.	Regarding the change in correlation coefficients, why does this phenomenon occur?	
	Share it with the entire.	How should outliers be handled? What are the criteria for outliers? What statistics are most susceptible to outliers? Conversely, what statistics are less vulnerable? Encourage consideration of data handling by asking questions such as the following.	

Summary (2 minutes)	Reflections on the class	Submit a Google form with your reflections on the current activities.	individual

Hour 2

process	Study Contents and Activities	matters that require attention	Form of study
Introduction (5 minutes)	Confirm the contents at the time before	Reflecting on the activities of the previous period	simultaneous
Deployment (40 minutes)	Understand the statistical exploration process.	Explain the statistical inquiry process, comparing it to the activities of the previous period.	simultaneous
Using the data, let's set up a new issue and analyze it.			
	Set and analyze issues.	We are presenting new data. Assist them in finding more data, working with different data, and other exploration issues.	It should also be possible to discuss the issue in groups.
Summary (5 minutes)	Reflections on the class	Enter your reflections and the issues you set in the Google form and submit.	individual

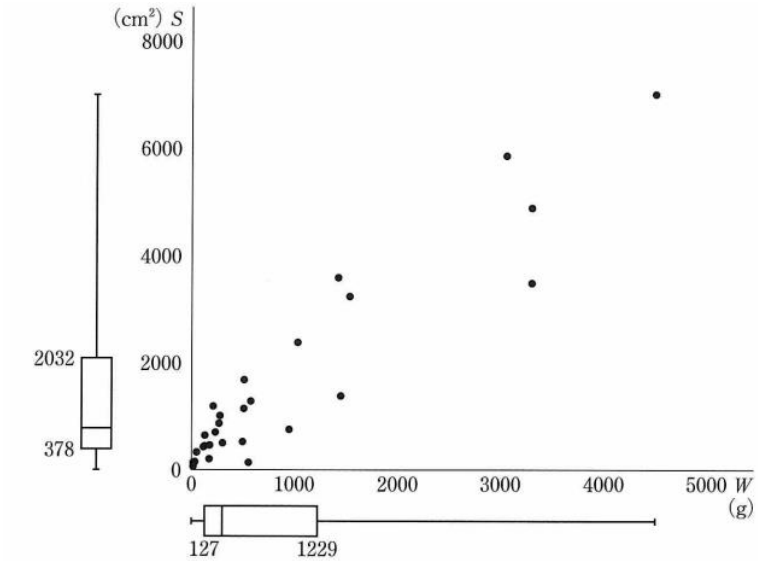

Figure 4.9 Boody mass and Wing area

The author found this issue very interesting and obtained the data[*5]. From that data, the author used 31 data to create scatter plots using Excel and R. The primary tool for analysis is Excel, a computer spreadsheet, but there is also R for statistical analysis software in addition to Excel. R is a simple language that does not require variable declarations, etc.; coding is simple, so it is easy to create. I felt that I would like to introduce it to my students. (See [10] and [11])

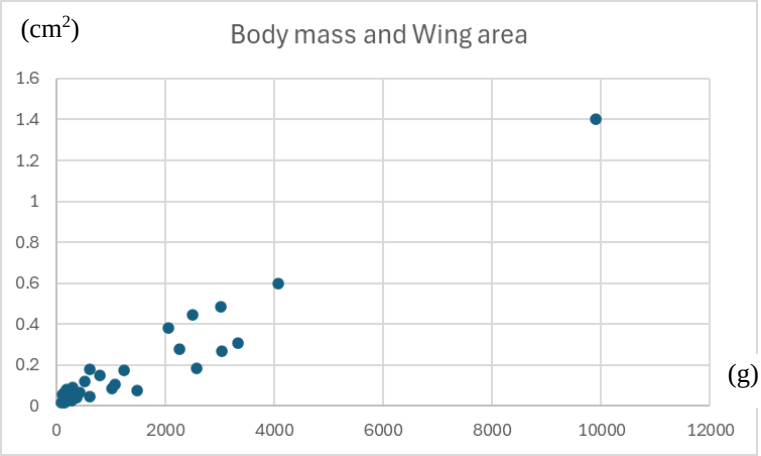

Figure 4.10 Scatter diagram created in Excel

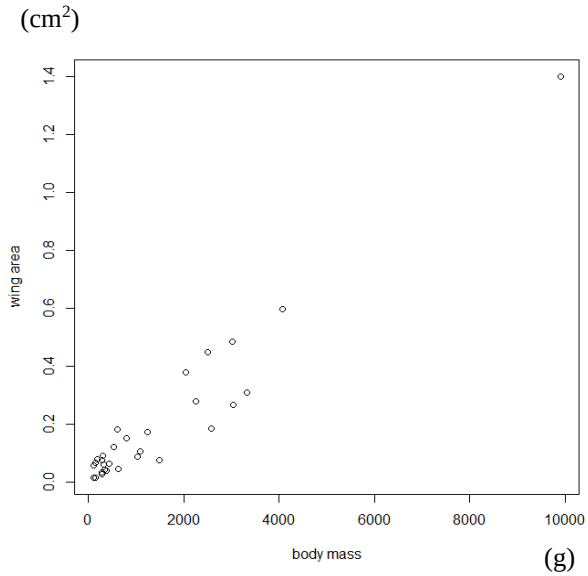

Figure 4.11 Scatter diagram created in R

From this data, students can calculate not only "body mass" and "wing area" but also the correlation coefficient between "body mass" and "wingspan" and between "body mass" and "wing area" for different birds living in southern and northern regions by themselves. By developing such activities, we believe that there is a possibility of developing biological exploration activities from data analysis about the ecology of regions and birds, as well as physical exploration activities from body mass and wing area. It is expected to develop into cross-curricular learning.

4.2 Consideration of Classroom Practice

In the current study guidelines emphasize the enhancement of statistical education. The theme of "analysis of data" as a study content in the statistical field requires students to understand the basic ideas of statistics, organize and analyze data, and identify trends using these ideas. The learning contents are data scattering and data correlation. Let us examine the lessons from the viewpoint of statistical education and ICT utilization.

Problem Research, described in Section 4.1.1, is a practical example in which the mathematical activities described in Chapter 2 of this paper can be practiced through a statistical exploration process. The students have learned to capture trends by creating graphs about the scattering of data and scatter plots about the correlation of data. In junior high school, students learned how to capture trends in data through histograms and representative values under the theme of organizing data, and they handled more data in senior high school. They had the experience of making predictions about the scatter of data and relationships among data, analyzing and verifying them, and finding further issues from them. In addition, they handled data from a solar power generation system installed at the school to deal with concrete data from their immediate surroundings. By using something familiar, the students were more motivated to learn, and they were able to experience the benefits of using ICT. These were effective examples of enhancing statistical education emphasized in the current Courses of Study.

By using ICT to process a large amount of data, they were able to find relationships and confirm the results of previous studies to find out the characteristics of the area in which they live and future issues based on these characteristics. This is also an example of how the real world and the world of mathematics can be perceived as close to each other through analysis of data found in familiar places.

The author believes that ICT is effective in conducting research using data in this way, and Course, described in Section 4.1.2, is a case study aimed at developing a foundation for actively using ICT to use data.

Problem-based learning, described in Section 4.1.3, investigated the theme of problem study positioned as a summary in the "analysis of data" of the field of study related to statistics, which was emphasized in the revision of the Courses of Study and described one instructional example. Each theme deals with a problem close to the students' hearts, and the content allows students to collect multiple types of data according to their objectives, analyze them using statistical methods, and conduct activities to discuss the process and results of the solution. As in Problem Research, described in Section 4.1.1, students can use ICT to organize data into graphs and obtain basic statistics such as variance, standard deviation, and correlation coefficient. Based on these, the students can discuss the conclusions obtained while clarifying the rationale through questions from the teacher and dialogue within the group and develop them into the next exploration topic. They can also critically examine the data by considering the conditions of data collection, etc., or by increasing the number of data further. If a survey was conducted in an inquiry activity, students can use this experience to analyze the data. For example, students may be familiar with surveying and analyzing the time spent using smartphones.

5. Summary and Future tasks

The use of ICT is found to be effective in analyzing data in the statistical inquiry process. As students gain more experience in this process using ICT, they will be able to acquire methods for analyzing real-world problems in the real world in the future. In the problem-solving process, students will be able to review and modify the problem while planning, re-create and analyze graphs, and sometimes re-collect data to reach a conclusion.

This paper introduces examples of ICT applications around data analysis in problem-based research and problem-based learning in "Mathematics I," where exploratory activities are conducted. The theme of problem-based learning listed in the authorized textbooks is the theme of activities in which students use the scatter plots and correlation coefficients they have studied to formulate hypotheses about problem situations, collect data, and test their theories. As shown in the examples of the practical application of the problem study, after analyzing data and deepening consideration

of the hypothesis, students could discover new problems of which they were previously unaware and engage in activities to formulate hypotheses. These experiences also lead to exploring conditions and remedial measures to change from the current distribution of data to the direction considered desirable to solve further or improve the problem.

ICT has the advantage that representative statistics can be easily calculated and visualized for many data types. However, to use ICT to select appropriate statistics, graphs, and methods according to the purpose and type of data in the statistical exploration process, it is necessary to have a solid understanding of statistics such as mean, minimum, maximum, median, mode, range, and interquartile range, as well as bar graphs, line graphs, and scatter plots, It is also necessary to organize the purposes for which graphs, such as bar graphs, line graphs, histograms, box plots, and scatter plots, are often used for what kind of data and for what purposes. These are also important in enhancing statistical education and applying the learning to elementary, middle, and high schools.

On the other hand, in teaching statistical education, the Statistics Bureau of the Ministry of Internal Affairs and Communications website[*6] is a good reference for obtaining information such as data and teaching materials. Along with the deployment of tablet terminals, information on teaching materials and tools related to statistics has also become more common. Data science is also attracting a great deal of attention. The author also wants to utilize them and feels teachers must learn to use data and practice. For this purpose, training, research, and the accumulation of practical examples will become increasingly important in the future.

As for future issues, we would like to conduct further research on the enhancement of statistical education and the use of ICT. We would like to devise practical examples of ICT-enhanced classes on the concept of hypothesis testing, which leads to the content of statistical inference. We would also like to study examples of ICT-enhanced problem-based learning in Math II and Math III.

In this issue, we also discussed the use of ICT in the statistical inquiry process, which focuses on supporting the development of mathematical content such as graph and graphic drawing software, spreadsheet software, and programming languages to deepen mathematical thinking. Other uses of ICT are those focused on setting up problems, using it in the stages of summarizing and concluding, and diversifying summarizing, outputting, and expressing. It is also a future issue to verify what kind of things, how to use them, and what educational effects they can have.

Acknowledgments

This paper introduces the mathematical activities undertaken by the students under the author's guidance. The author would also like to thank all those who assisted in this research.

Appendix

*1 Problem Research is an activity that presents an answer to an issue with a rationale. Students set their assignments. Activities conducted by individuals or groups.

*2 Super Science High School (SSH) is a national project that has been implemented since 2002, with the Japan Science and Technology Agency (JST) as the primary implementing agency, with the objective of "conducting research and development focusing on science and mathematics education to foster future global human resources for science and technology. SSH is an epoch-making initiative in that it allows the promotion of science and technology human resource development in specific schools to begin at the secondary education level and was established as a symbolic project following the birth of the Ministry of Education, Culture, Sports, Science and Technology (MEXT) following the reorganization of central government ministries and agencies. The program was established as a symbolic project that symbolized the birth of the Ministry of

Education, Culture, Sports, Science and Technology (MEXT) after central ministries and agencies.
*3 For the Courses of Study, we referred to the "English Translation of the Courses of Study for Junior High Schools (Provisional Translation)" posted on the website of the Ministry of Education, Culture, Sports, Science, and Technology
(Retrieved July 30, 2023,
https://www.mext.go.jp/a_menu/shotou/new-cs/youryou/eiyaku/1298356.htm).
*4 We translated some image diagrams into English based on p. 26 of Reference [3].
*5 We thank Dr. Kozue Shiomi for providing data on bird weight, wing area, and wing opening length. We thank her very much. The details of the data can be found at the following URL: https://sites.google.com/view/wing-data/home (viewed on May 16, 2023)
*6 The Statistics Bureau of the Ministry of Internal Affairs and Communications website URL: https://www.stat.go.jp/teacher/index.htm (viewed on August 30, 2023).
*7 In the "Problem Study and ICT Use in Mathematics Education" presented at ATCM 2023, we have included a perspective from the statistical inquiry process, and the problem study proposed in the textbook section on enhancing statistical education. We also included a study guidance plan for teaching the class.
*8 The author would like to sincerely thank Dr. Wei-Chi Yang for allowing me to prepare such a paper.

References

[1] Aoki, N. Kanamori, C. Koda, D. Makishita, H. Shibatsuji, T. Takamura, M. (2023): *Survey and Research on Task-Based Learning in High School Mathematics Authorized Textbooks*. Proceedings of the Sixth Japan Society for Science Education.
[2] Araki, H., Ono, M., Kobayashi, Y. (2015): *Overview of Super Science High School Project and Verification of Effectiveness*. DISCUSSION PAPER (National Institute of Science and Technology Policy, Ministry of Education, Culture, Sports, Science and Technology)
[3] Ministry of Education, Culture, Sports, Science, and Technology (2019): *Courses of Study for Senior High Schools (Notification in 2018) Commentary Mathematics Section Science and Mathematics Section*. GAKKOTOSHO.
[4] Okamoto, N. (2022): *New Edition "Mathematics I"*: Ministry of Education, Culture, Sports, Science and Technology Authorized Textbooks. Jikkyo Shuppan
[5] Aoki, N. (2022): *Using ICT in Classroom Practice and Training Teachers*. Proceedings of 2022 Regular Fall Meeting Collection of Submissions, Mathematics Education Society of Japan.
[6] Shimizu, S. (2018): *Education of Arithmetic and Mathematics Subjects in the Future as Aimed for by the New Courses of Study*. Research Bulletin of Mathematics for Learning. The Mathematics Certification Institute of Japan.

Angle trisection as a STEM activity opportunity for mathematics teacher training

Roman Hašek
hasek@pf.jcu.cz
University of South Bohemia
Faculty of Education, Department of Mathematics
Jeronýmova 10, 371 15 České Budějovice
Czech Republic

Abstract

The article is based on the lecture 'Mathematics teacher training from the perspective of STEM – a particular case' given by its author at the ATCM 2023 conference and is an extension of a related paper that was published in the conference proceedings. It further develops the idea that the task of teacher training schools is to create a suitable environment for the provision of education, impulses for the development of the necessary knowledge and skills, as well as to support these. It provides a detailed description of specific creative activities for future teachers, which develop their awareness of the applicability of mathematics in solving real problems and knowledge of its overlap with technology. It is based on historical problems and their context, as presented in the conference paper. Emphasis is placed on the use of computers, especially dynamic geometry software GeoGebra, to model the geometric nature of given problems and for their effective solution.

1 Introduction

The content and methods of teacher training should reflect the requirements of the today. The basic categories of teacher knowledge, subject matter content knowledge, pedagogical content knowledge and curricular knowledge, were identified by Shulman in his well-known study [19]. In addition, at the present time, with expanding opportunities to learn about real-world phenomena from freely available online resources, and in which the boundaries between educational disciplines overlap, the importance of skills that enable a teacher to interpret such phenomena to students through a STEM (Science, Technology, Engineering, and Mathematics) lens, of which creativity and flexibility are key, is becoming more and more important [16]. Recent research has also proved the importance of learning experience for future teachers [11]. In this paper, we present a specific case of a topic that provides opportunities to apply the above principles in mathematics teacher training.

The central topic of the article is the solution of the angle trisection problem. It is used as a supporting medium for illustrating the possibility of creative education of mathematics

teachers. Historical materials devoted to this problem are used as an impetus for the creative and research work of prospective mathematics teachers. Although the problem of trisection is currently perceived as a historical problem that is not the focus of attention in contemporary geometry, the paper brings a new discovery in this field, obtained and proved using tools offered by the GeoGebra software environment [5], and shows its application in a 3D printing project assigned to future mathematics teachers.

As is widely known, the trisection of an angle, i.e. division of an arbitrary angle into three equal parts, together with squaring a circle and doubling a cube, belongs to the classical problems of Greek mathematics, that were proved to be impossible constructions using just a straightedge and compass. The impossibility of this so-called Euclidean construction of a trisection of an angle was proved by French mathematician Pierre Laurent Wantzel in 1873. For more information see [10, 15].

2 The forgotten trisection method

In 1881, Josef Rudolf Vaňaus, a Czech grammar school teacher of mathematics and physics, presented in an article entitled Trisektorie (Czech term for trisectrix), which was published in the Czech *Journal for the Cultivation of Mathematics and Physics* [20], a previously unknown method of using an oblique strophoid [17] for the trisection of an angle. This article offers interesting possibilities to modern researchers.

2.1 Vaňaus' trisectrix

From the text of the article [20] it is apparent that Vaňaus probably did not know that the curve in question is a strophoid. He arrived at it when investigating the properties of algebraic curves given by the equation

$$Ax^3 + By^3 + Cxy^2 + Dx^2y + Ex^2 + Fy^2 + Gxy = 0, \tag{1}$$

which have a double point in the origin of the related Cartesian coordinate system. For a certain class of these curves he identified that they are sets of points equidistant from a circle and some of its secants. As we know today, this feature indicates a strophoid [13, 18]. Since he discovered that such curves were suitable for trisecting an angle due to this property, Vaňaus decided to call them trisektorie.

Besides determining the conditions for the values of the coefficients of equation (1), he defines it as a locus of points as follows (see Fig. 1): *Given a circle c of arbitrary radius r with diameter OA, where O is the origin of the Cartesian coordinate system and A lies on the $x-$axis, draw line l, the secant line of circle c, through A at any direction angle α and place point B on it. Then draw line OB and mark its intersection with circle c as point D. Finally, place M on line OB so that $|MD| = |DB|$. The locus of points M for B moving along line l is the curve in question.* Based on this definition, Vaňaus derives the Cartesian equation of the resulting locus curve, which is

$$a(y^2(2r + x) - x^2(2r - x)) = y(y^2 + x^2 - 4rx), \tag{2}$$

where r is the radius of the circle c and a is the slope of the line l, i.e. $a = \tan\alpha$. Because for him it was a hitherto unknown curve, which he discovered through his research, the author

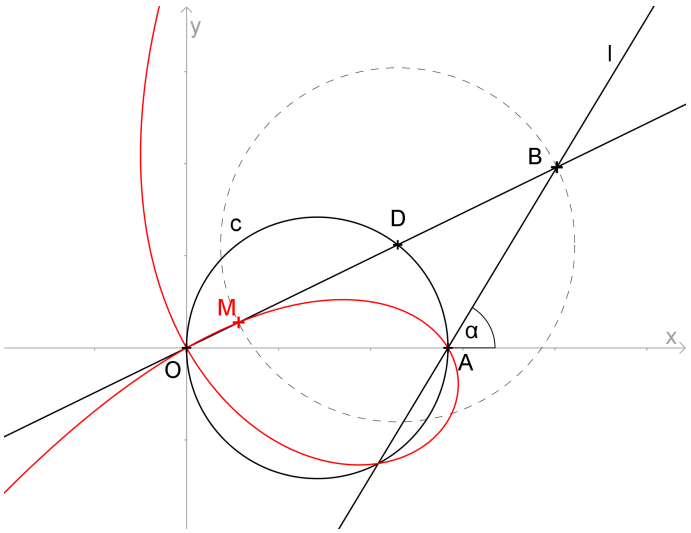

Figure 1: Vaňaus' trisectrix as the locus curve

was looking for analogies with already known curves. For the similarity of the definition as the locus of points he mentions the cissoid of Diocles [2], and for the similarity of the shapes, the folium of Descartes [4].

In the remainder of his article, Vaňaus presents the use of the introduced curve, which we will hereinafter call an oblique strophoid, for trisecting an angle. He proved both his knowledge of the theoretical impossibility of solving this problem with a straightedge and compass alone, as well as his wide overview of other non-Euclidean ways of doing so, adding the confident statement that the method based on the curve introduced by him is the least complex.

2.2 Vaňaus' trisection

Vaňaus' angle trisection method is described in detail in [6], as is proof of its correctness. In addition, the reader is confronted with an interesting problem that needs to be solved through the trisection of an angle. Vaňaus assigned this problem to the readers, grammar school students, of the *Journal for the Cultivation of Mathematics and Physics* in the problem section [21]. The methods of solving this problem are discussed both from the point of view of a student at that time and the present day in [6]. We will therefore present this method only briefly here for the purposes of the further direction of this paper.

In Fig. 2, the same objects are shown as in Fig. 1, but with point B in a different position on line l, it lies on the chord AF, and with the ray OA' and the circle m, with centre O passing through A, added.

Vaňaus proved that for the position of point B on line l, at which point M coincides with the intersection of the strophoid and the circle m, the angle $A'OB$ is a third of the angle $A'OA$ [20, 6]. The proof is not complicated at all. The application of the basic properties of angles in a triangle and a circle is enough, see Fig. 3. A detailed description is given in [6].

The method used by Vaňaus for trisecting angle u is clear, see Fig. 3. The rays OA', OA and OM have a common point O, the vertex of the angle u, while points A', A and M lie on the circle m. The angle $A'OM$ is a third of the angle $A'OA$ if, and only if, point B lies on the perpendicular line from A to OA', D being the midpoint of the segment MB.

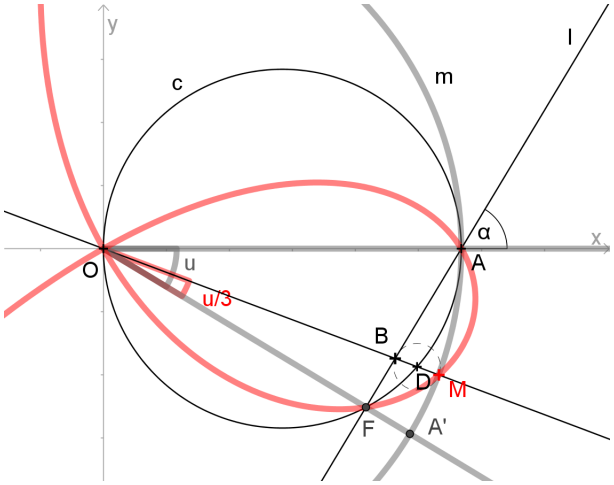

Figure 2: Configuration for trisecting an angle

Although the theoretical basis of the method is therefore well proven and quite understandable, how do we perform this trisection in practice? In this regard, Vaňaus left his successors with a mysterious task, the correct solution of which we will probably never know. At the end of his article, he states: *"In order to correctly draw the part of the trisectrix AMF and, above all, to place the intersection point M precisely, I assembled a very simple device, where the intersection of arc AA' at point M is created by means of a double forced movement."* [20].

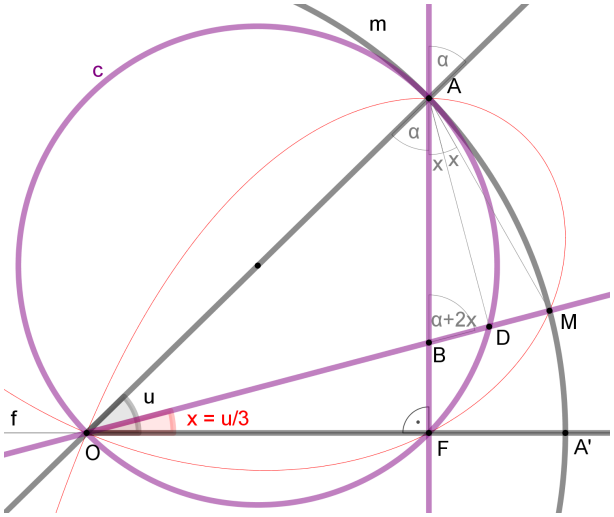

Figure 3: Vaňaus' method of trisection

Unfortunately, the device that Vaňaus mentioned has not survived, as have any written documents or sketches for its construction. One of Vaňaus' legacies, in addition to his written work, is therefore a challenge to us and our students to replace this lost artifact with our own solution. In the following passages of this paper, two intriguing and original results are presented. These arose from attempts to design and build a mechanism that could possibly correspond to the device that Vaňaus mentioned.

The first, is the design and production of a possible Vaňaus trisector by a student teacher

of mathematics and technical education. The process ended with his successful participation in the national Olympiad of Technology 2023 (`http://olympiadatechniky.cz`).

The second, is the discovery of an unsuspected connection between Vaňaus' method and Ceva's trisectrix, a curve described by Tomas Ceva in 1699 [1], which led to the discovery of a new and very simple application of this curve to angle trisection.

3 Possible Vaňaus trisector

The conditions defined by the essence of Vaňaus' method of trisection using an oblique strophoid, which we noted in the comment on Fig. 3 above, must be met by the device that we want to design for the purpose of performing the trisection. We can therefore try to construct a mechanism to comply with these conditions. With this task, student teachers of mathematics, prospective teachers at lower secondary school, were approached. One of them, Tomáš Randa, studying teaching of technical education as a second major, took this task to the stage we see in Fig. 4.

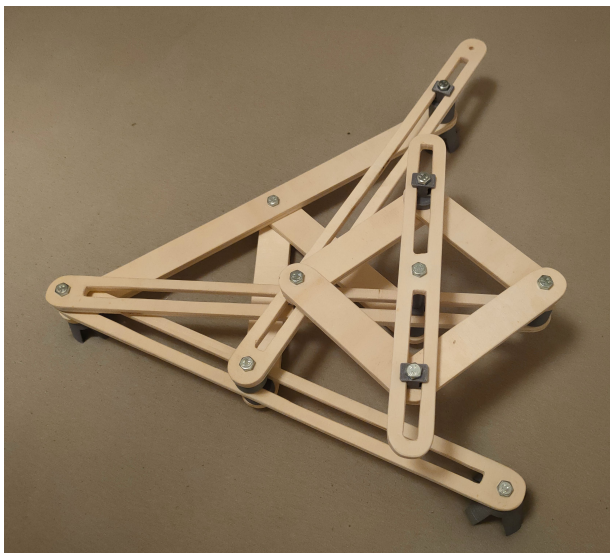

Figure 4: Vaňaus trisector – student work, T. Randa, 2023

It is a mechanism made by hand from poplar wood, with joints printed on a 3D printer. As stated by Vaňaus, the mechanism performs an angle trisection through a double forced movement. The original plan was to print the entire mechanism on a 3D printer, which would have been much easier. However, the student decided to enter the Olympiad of Technology, one of the conditions of which is that a significant part of the submitted object must be made by hand. His efforts paid off in the end, with him taking third place in the category "Didactic technical works" among students from all over the Czech Republic. The work was awarded not only for its technical implementation, but also for its geometric essence and the potential to recall, in a new way, one of the classic problems of geometry and bring the history of efforts to solve it closer to students.

3.1 Geometrical principles of the mechanism

As previously mentioned, the functioning of the mechanism is realised through a double forced movement. For the mechanical implementation of the movement, geometric principles known from the secondary school curriculum were applied. We briefly recall them here.

Thales circle

The Thales circle of a given line segment is the circle which has the line segment as its diameter. Secondary school pupils learn that any triangle, of which two vertices are the end points of the segment in question, and the third vertex, which is different from these two, lies anywhere on the circle, is right-angled [15]. This property is used to ensure that the elements AF and OF are always perpendicular to each other. Point F is therefore connected to the centre C of the segment AC by the segment of length $|AO|/2$ (see the blue segment CF in Fig. 5).

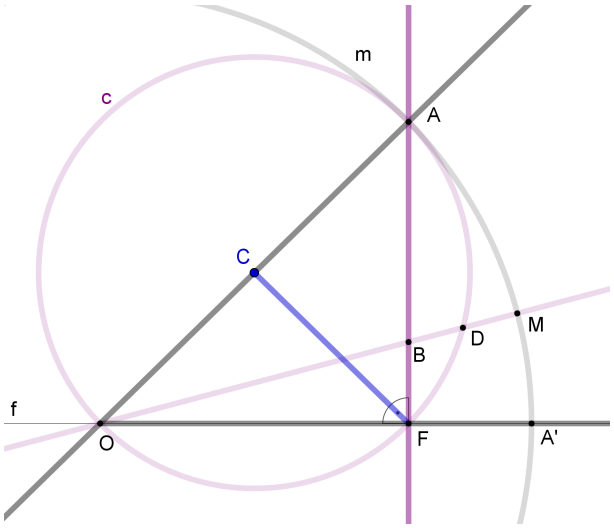

Figure 5: Thales circle

Central symmetry of a rhombus

Any rhombus is centrally symmetric according to the bisector of its diagonals. To keep points B, D and M in such a configuration that point B lies on segment AF, point D is the centre of BM, and, at the same time, moves along circle c, a diamond-shaped linkage with vertices at B, M and centre D is therefore used, with point D additionally connected to C by the segment of length $|AO|/2$ (see the green rhombus and additional line segment in Fig. 6). The rhombus like linkage can be, for example, identified as a part of the Peaucellier-Lipkin linkage [12].

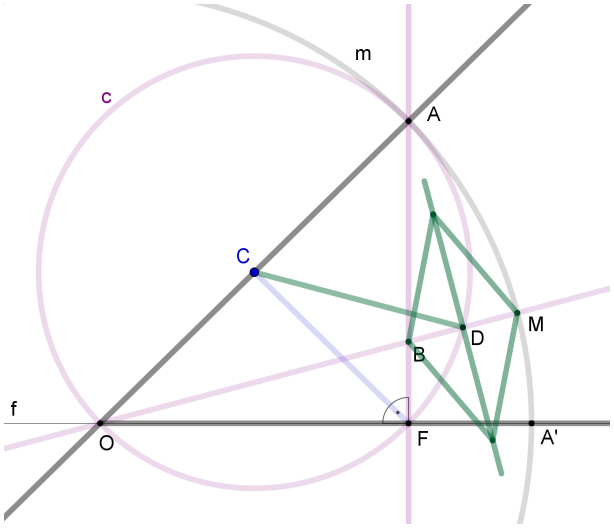

Figure 6: The rhombus like linkage

An authentic mechanical realisation of the aforementioned two geometrical principles can be seen in Fig. 4.

4 New use of Ceva trisectrix

An unexpected consequence of both the analysis of the above mentioned Vaňaus' method of angle trisection and the effort to design the simplest possible device for its implementation, was the discovery of a new and simpler use of the Ceva trisectrix for the trisection of an angle.

4.1 Ceva trisectrix

In 1699, Tommaso Ceva, the younger brother of Giovanni Ceva, published the Latin book *Opuscula mathematica*, in which he presents, among other things, the curve he calls cycloidum anomalarum [1]. Among the properties of this curve, he mentions its suitability for angle trisection.

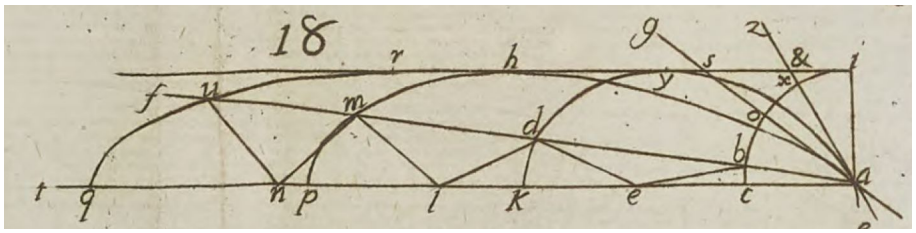

Figure 7: Cycloidas anomalas, T. Ceva, 1699 [1]

Ceva defines his cycloid as a curve that is described by the endpoint of a polyline with an odd number of segments of equal lengths, whose vertices lie alternately on two rays with a common point of origin, which is also the initial vertex of the polyline. In Fig. 7, which is Figure No. 18 from Ceva's book, we can see for example a curve drawn by point d, the endpoint

of polyline *abed* linking rays af and at, when af rotates around a. The other two curves in the figure are those drawn in the same way by points m and u, endpoints of polylines *abedlm* and *abedlmnu*, respectively.

An elementary knowledge of the relations between interior and exterior angles of a triangle is sufficient to prove that if $|\measuredangle cab| = \varphi$, then $|\measuredangle led| = 3\varphi$, $|\measuredangle nlm| = 5\varphi$ and $|\measuredangle qnu| = 7\varphi$, see also Fig. 8, where the relationships between angles essential to the proof are indicated. In what follows, we are only interested in the trisection of an angle, so we will focus mainly on the first of the curves, drawn by point d. This curve is referred to in available sources as the Cycloid of Ceva [22] or Ceva trisectrix [3]. It is a sextic, the algebraic curve of order 6, with the equation

$$(x^2 + y^2)^3 - r^2(3x^2 - y^2)^2 = 0, \tag{3}$$

where r is the length of a segment of the polyline forming it, i.e. the radius of the circle (hereinafter k) along which point b moves in Fig. 7. Under the same definition of r, the polar equation of Ceva trisectrix is

$$\rho(\varphi) = r + 2r\cos 2\varphi. \tag{4}$$

For the sake of completeness, the algebraic equations of the other two cycloids, the parts of which Ceva sketched in his picture are as follows

$$(x^2 + y^2)^5 - r^2(5(x^2 - y^2)^2 - 4y^4)^2 = 0,$$
$$(x^2 + y^2)^7 - r^2(7(x^2 - y^2)^3 - 2y^2(7x^4 - 3y^4))^2 = 0.$$

As is evident, only parts of the curves in question are presented in Fig. 7. The entire Ceva trisectrix is shown in Fig. 8. To verify that the curve is really drawn by a fixed point (point D) on a rolling circle (the green circle), the reader is invited to play the animation in the applet *Ceva trisectrix* [7].

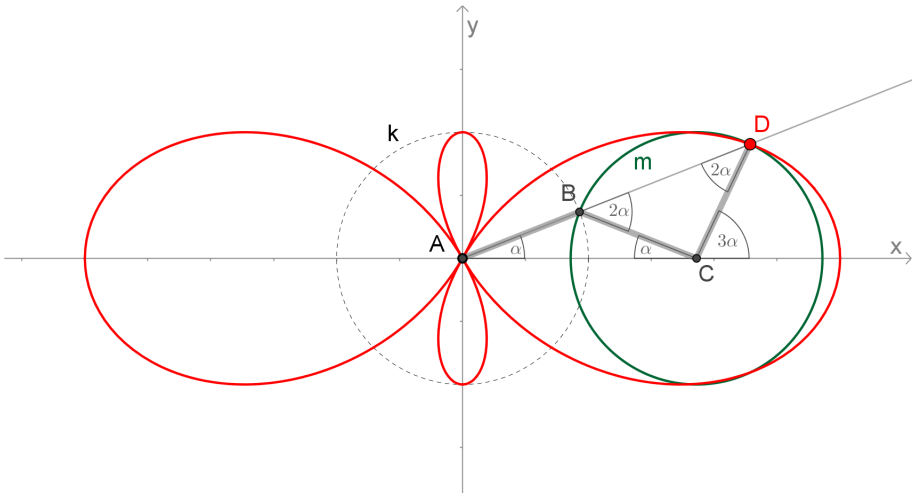

Figure 8: Ceva trisectrix

4.2 New way of use

As we already know, Ceva's curve is the closed curve of the sixth order, with two mutually perpendicular axes of symmetry, having four loops, of which the opposite are always congruent, one pair larger, one pair smaller, pairs not similar to each other, see Fig. 8.

The traditional trisection method based on this curve works with the larger of the loops, as shown in Fig. 8. In contrast, a new method, which we aim to introduce in the following text, works with the smaller of the loops, as shown in Fig. 9.

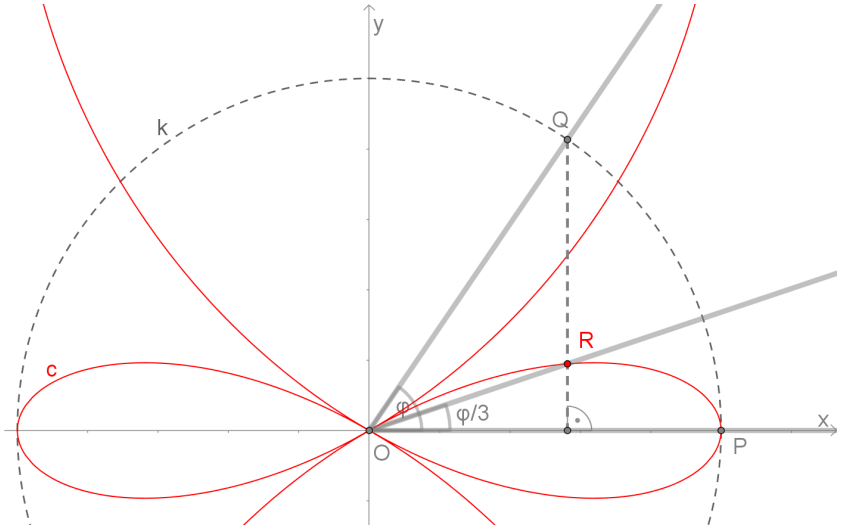

Figure 9: New use of Ceva's curve to trisect an angle

The step-by-step procedure for this new use of the Ceva curve for the trisection of angle φ is as follows:

1. Place the curve in the Cartesian coordinate system, as shown in Fig. 9. Use the polar equation $\rho(\varphi) = r - 2r\cos 2\varphi$.

2. Draw a circle k, the defining circle of the Ceva curve, the radius of r which is equal to the length of the shorter loop.

3. Construct the angle φ, whose third you are interested in, into the first quadrant, so that its first arm merges with the positive semi-axis x, and its second arm intersects k at Q, within this quadrant. From Q, draw a perpendicular line to x, and mark its intersection with Ceva curve c as R. Then the ray OR is the arm of the angle $\measuredangle POR$, the third of $\measuredangle POQ$.

4.3 Genesis of the method

This new method of angle trisection appeared as an unexpected result of the analysis of the trisection method developed by Vaňaus. See section 2.2, or for a more detailed introduction [6]. The main impetus for this was the geometric simplification of the Vaňaus method, which would allow the design of a sufficiently simple device for its implementation.

The basic source of the findings for the analysis was a dynamic geometric model of the Vaňaus method created in GeoGebra [5]. This model is shown in Fig. 10. It is available in interactive form in the applet *Vaňaus' trisection – trace of B* [9]. If we change angle φ by moving point A, the ray SM, where M is the intersection of the corresponding oblique strophoid (it is different for each angle φ) with circle m, is the arm of the angle of size $\varphi/3$. The question arises,

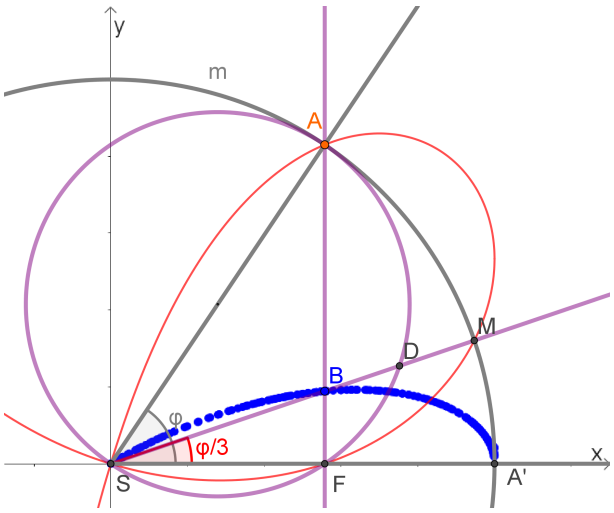

Figure 10: The locus of B when A moves along m

what is the trajectory of point B when A moves along m? The answer to this question could bring about the sought-after simplification. To initially examine the curve of this trajectory, we use the 'Trace on' setting for B in GeoGebra. It draws the blue trace, as can be seen in Fig. 10, or in the corresponding applet [9].

The structure shown in Fig. 10 defines the geometric relationship between A and B such that, for a particular position of A, the position of B can be described by a system of algebraic equations. Using the 'Eliminate' function in GeoGebra CAS, we can then derive the general equation of the locus curve of B. To derive the desired system of equations, we first assign coordinates to the decisive points in Fig. 10 as follows: $A[a_1, a_2]$, $B[x, y]$, $M[m_1, m_2]$. Then, as a preparatory step, we consider the family of Vaňaus' strophoids with parameters a_1, a_2, the coordinates of A, and derive the equations

$$s_1 : \; 2\,R\,r - a_1^2 - a_2^2 = 0, \tag{5}$$

$$\begin{aligned} s_2 : \; & -2\,R\,a\,a_1^2\,m_1^2\,r + 2\,R\,a\,a_1^2\,r\,m_2^2 - 8\,R\,a\,a_1\,m_1\,r\,m_2\,a_2 + 2\,R\,a\,m_1^2\,r\,a_2^2 \\ & - 2\,R\,a\,r\,m_2^2\,a_2^2 + 4\,R\,a_1^2\,m_1\,r\,m_2 - 4\,R\,a_1\,m_1^2\,r\,a_2 + 4\,R\,a_1\,r\,m_2^2\,a_2 \\ & - 4\,R\,m_1\,r\,m_2\,a_2^2 + a\,a_1^3\,m_1^3 + a\,a_1^3\,m_1\,m_2^2 + a\,a_1^2\,m_1^2\,m_2\,a_2 + a\,a_1^2\,m_2^3\,a_2 \\ & + a\,a_1\,m_1^3\,a_2^2 + a\,a_1\,m_1\,m_2^2\,a_2^2 + a\,m_1^2\,m_2\,a_2^3 + a\,m_2^3\,a_2^3 - a_1^3\,m_1^2\,m_2 - a_1^3\,m_2^3 \\ & + a_1^2\,m_1^3\,a_2 + a_1^2\,m_1\,m_2^2\,a_2 - a_1\,m_1^2\,m_2\,a_2^2 - a_1\,m_2^3\,a_2^2 + m_1^3\,a_2^3 + m_1\,m_2^2\,a_2^3 = 0. \end{aligned} \tag{6}$$

defining A and M as the points of intersection of this family of curves with circle m, see lines 2 and 3, respectively, in the GeoGebra CAS code in Fig. 11. Subsequently, we apply the defining relation $a = \tan\alpha = \dfrac{a_1}{a_2}$ for parameter a, which was introduced in (2), together with the fact that A and B lie on the perpendicular to x, and write $a_1 = x$, $a_2 = x/a$, i.e. $A[x, x/a]$. The equations (5), (6) are thereby simplified to the first two equations of the required system

$$e_1 : \; 2\,R\,a^2\,r - a^2\,x^2 - x^2 = 0, \tag{7}$$

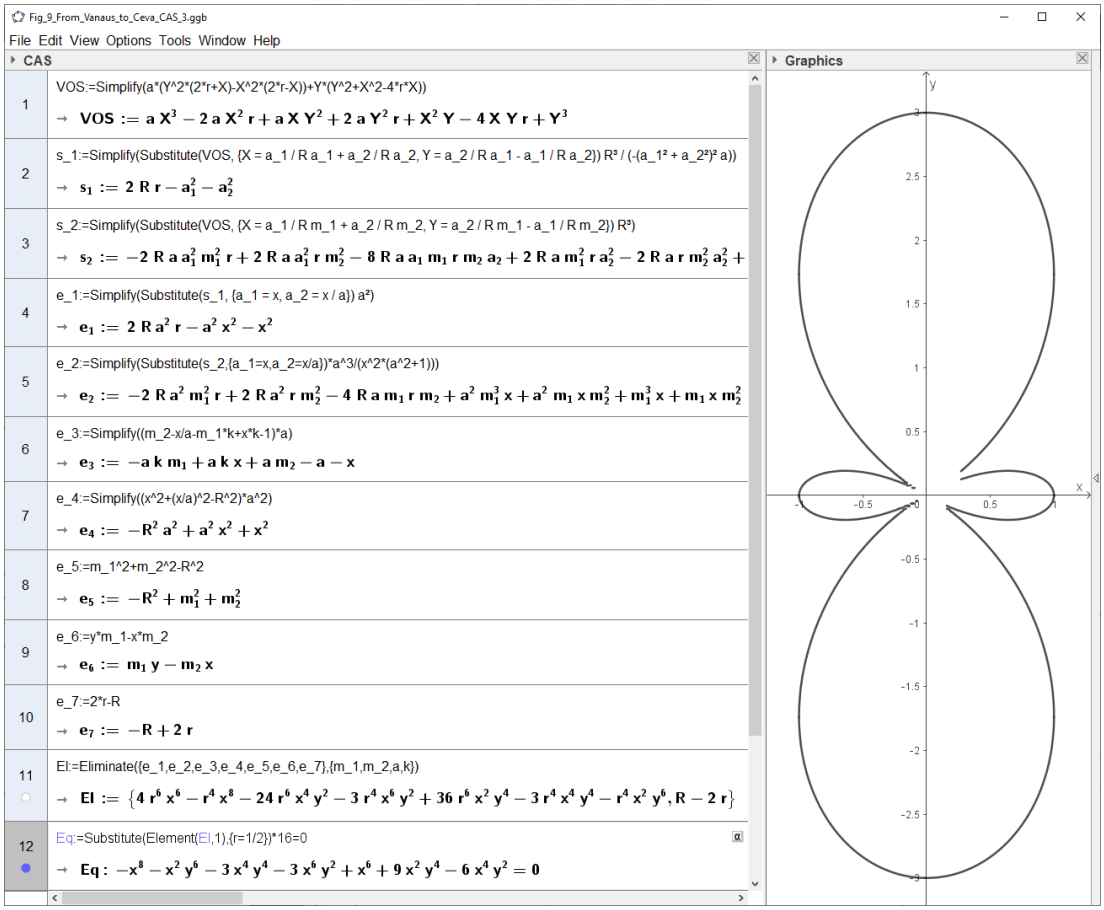

Figure 11: The locus curve of B derived in GeoGebra CAS, plotted for $r = 1/2$

$$e_2 : \ -2\ R\ a^2\ m_1^2\ r + 2\ R\ a^2\ r\ m_2^2 - 4\ R\ a\ m_1\ r\ m_2 + a^2\ m_1^3\ x + a^2\ m_1\ x\ m_2^2 + m_1^3\ x + m_1\ x\ m_2^2 = 0. \quad (8)$$

To avoid the situation where $M[m_1, m_2] \equiv A[a_1, a_2]$, we set the non-degenerate condition $(m_2 - a_2) - k(m_1 - a_1) - 1 = 0$, where k is an additional parameter, which leads to the third equation

$$e_3 : \ -a\ k\ m_1 + a\ k\ x + a\ m_2 - a - x = 0. \quad (9)$$

Then, we add two equations expressing that A and M lie on the same circle m with radius R

$$e_4 : \ -R^2\ a^2 + a^2\ x^2 + x^2 = 0, \quad (10)$$

$$e_5 : \ -R^2 + m_1^2 + m_2^2 = 0. \quad (11)$$

The following equation determines that B is the intersection of SM with the line passing through A perpendicular to the x-axis

$$e_6 : \ m_1\ y - m_2\ x = 0. \quad (12)$$

Finally, the last equation

$$e_7 : \ -R + 2\ r = 0 \quad (13)$$

expresses the relation between the radii r and R.

Then, by eliminating parameters m_1, m_2, a, k from the system of equations $e_1, \ldots, e_7$, utilising the 'Eliminate' function, see line 11 in the GeoGebra CAS code in Fig. 11 (for the complete code from Fig. 11 visit [8]), we obtain

$$4\,r^6\,x^6 - r^4\,x^8 - 24\,r^6\,x^4\,y^2 - 3\,r^4\,x^6\,y^2 + 36\,r^6\,x^2\,y^4 - 3\,r^4\,x^4\,y^4 - r^4\,x^2\,y^6 = 0, \qquad (14)$$

after factorisation

$$-r^4\,x^2\,\left(x^6 - 4\,x^4\,r^2 + 3\,x^4\,y^2 + 24\,x^2\,r^2\,y^2 + 3\,x^2\,y^4 - 36\,r^2\,y^4 + y^6\right) = 0, \qquad (15)$$

where the third factor gives us the final equation of the locus curve of B

$$(x^2 + y^2)^3 - (2r)^2(x^2 - 3y^2)^2 = 0, \qquad (16)$$

which is the equation for Ceva's trisectrix, rotated by ninety degrees compared to (3), except that the value of radius r is now half the value considered in (3).

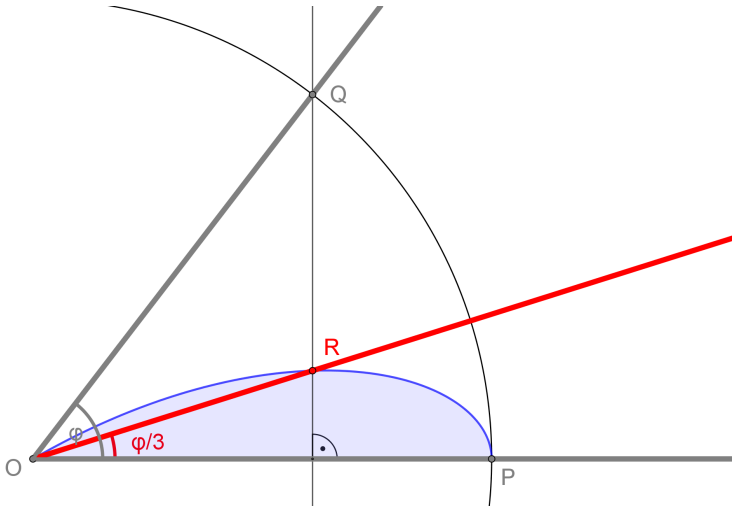

Figure 12: New method of trisection based on Ceva's trisectrix

We can thus take it as proven that the sought-after locus curve of B is a specific part of Ceva's trisectrix with equation (16). On this basis, it is possible to propose a new trisection method, as is clearly presented in Fig. 12.

5 3D printing student project

In addition to a compass and ruler, the idea that having an aid in the shape of the blue area shown in Fig. 12, would complete a set of tools for the construction of the trisection of an angle. This idea subsequently developed into an assignment of a project for students. They were assigned the task of printing the relevant part and describing its production and use as one of the topics of the seminar work of the course 'Computing software' that prospective mathematics teachers attend at our university in their first year of study.

Two students chose to tackle this topic as their joint project. I provided them with the relevant mathematical descriptions of the problem, as presented in this article. To make the trisection aid, they had a Prusa i3 MK3S+ printer (`https://www.prusa3d.com`) at their disposal.

While working on the project, the students made visible progress in their competences and knowledge relevant to the task. At first they were unable to print the required part, as evidenced by a number of failed attempts. A key turning point for their success was finding out the optimal method of geometric representation of the object for 3D printing. After unsuccessful attempts to print a model based directly on the parametric representation in GeoGebra, they concluded that it was more appropriate to replace the area bound by the curve and the segment with a polygon. They used GeoGebra 6 software for its construction and a PrusaSlicer 2.7.4 for model processing. In the end, the quality of the final product was very good (see Fig. 13).

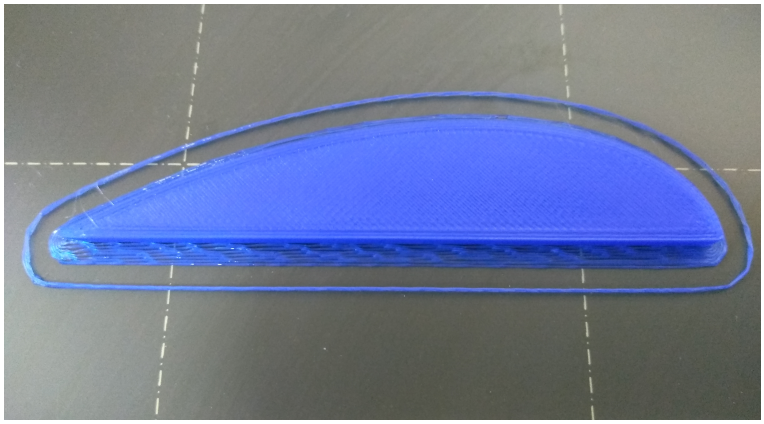

Figure 13: A trisection construction aid printed on a Prusa i3 MK3S+

After debugging the digital model, it was possible to print the aid in larger numbers. The students then distributed these tools among their classmates and demonstrated its use to trisect an angle. For one of results of this workshop see Fig. 14.

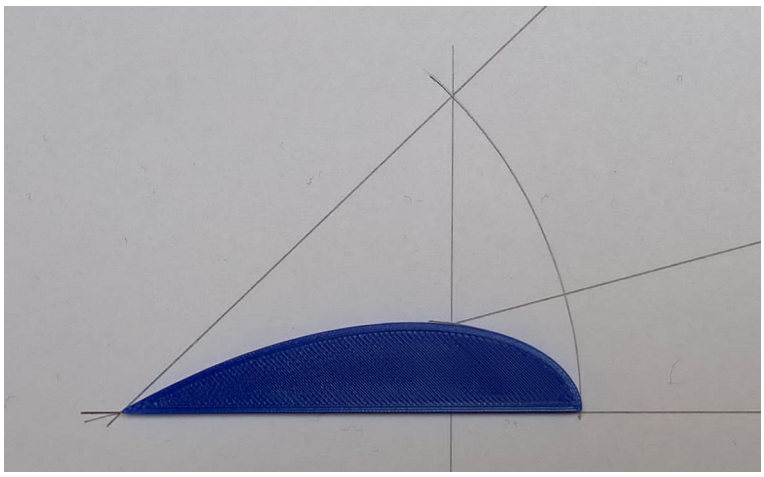

Figure 14: A trisection construction aid in practice

6 Conclusions

As already stated, the skills and abilities that determine the success of a teacher include, among other things, creativity, problem-solving skills, and the ability to acquire new knowledge. We believe that with this paper we have succeeded in showing that this can be achieved through the effective use of suitable digital means, in this particular case, the dynamic mathematics program GeoGebra, PrusaSlicer software and Prusa i3 MK3S+ 3D printer.

Current scientific studies into STEM education as a way of preparing students for an ever-changing world largely concur that concepts such as creativity, the ability to learn and apply new knowledge, problem solving skills, and the carrying out of authentic inquiry, play a significant role in its implementation [14, 16]. Among the ambitions of the paper was to show how these skills can be practiced and developed on the basis of a historical topic, namely solving a specific student project in which the basic mathematical curriculum is applied to solve problems based on appropriately collected and presented historical materials. It was shown that within the framework of such a project, students not only practice and develop the aforementioned skills, in conjunction with their digital competencies, but also carry out the technical design and production of the relevant artifact.

The ambition of the author was also to inspire colleagues to assign the presented problems to their students. Isn't it a captivating idea to collate as many ideas as possible to solve the Vaňaus trisector mystery?

References

[1] Ceva, T., *Opuscula mathematica*, Mediolani, typis Iosephi Pandulfi Malatestae, 1699, https://books.google.cz/books/about/Opuscula_mathematica_Thomae_Ceuae_e_Soc.html?id=2VndoAEACAAJ&redir_esc=y.

[2] "Cissoid of Diocles", In: *Wikipedia*, https://en.wikipedia.org/wiki/Cissoid_of_Diocles, 2023, accessed 29 Jul 2023.

[3] Ferreol, R. "Ceva trisectrix and sectrix", In: *Encyclopédie des formes mathématiques remarquables*, https://mathcurve.com/courbes2d.gb/trisectricedeceva/trisectricedeceva.shtml, accessed 30 Jul 2023.

[4] "Folium of Descartes", In: *Wikipedia*, https://en.wikipedia.org/wiki/Folium_of_Descartes, 2023, accessed 29 Jul 2023.

[5] *GeoGebra, free mathematics software for learning and teaching.* http://www.geogebra.org, accessed 30 Jul 2023.

[6] Hašek, R., "Creative Use of Dynamic Mathematical Environment in Mathematics Teacher Training", In: Richard, P. R., Vélez, M. P. and Van Vaerenbergh, S. (eds) *Mathematics Education in the Age of Artificial Intelligence, Mathematics Education in the Digital Era, vol 17*, Springer, Cham, 2022.

[7] Hašek, R., "Ceva's trisectrix", *GeoGebra*, 2023, https://www.geogebra.org/m/twffkaxt.

[8] Hašek, R., "Locus equation – Ceva's trisectrix", *GeoGebra*, 2023, https://www.geogebra.org/m/wch37fdw.

[9] Hašek, R., "Vaňaus' trisection - trace of B", *GeoGebra*, 2023, https://www.geogebra.org/m/tfpqw8sh.

[10] "Impossible constructions", In: *Wikipedia*, https://en.wikipedia.org/wiki/Straightedge_and_compass_construction#Impossible_constructions, accessed 30 Jul 2023.

[11] Ishii, K., "Active Learning and Teacher Training: Lesson Study and Preofessional Learning Communities", *Scientia in educatione* 8(Special Issue), 2017, 101–118.

[12] Kempe, A. B. *How to Draw a Straight Line – A Lecture on Linkages*. MacMillan and Co., London 1877. The Project Gutenberg EBook, 2008, https://www.gutenberg.org/files/25155/25155-pdf.pdf.

[13] Lawrence, J. D., *A Catalog of Special Plane Curves*, Dover Publications, Inc., New York, 2014.

[14] MacDonald, A., Danaia, L. and Murphy, S. (Editors), *STEM Education Across the Learning Continuum, Early Childhood to Senior Secondary*, Springer Nature Singapore Pte Ltd., 2020.

[15] Ostermann, A. and Wanner, G., *Geometry by its history*, 1st ed. Springer, Berlin, 2012.

[16] Penprase, B. E., "STEM Education for the 21st Century", Springer, Cham, 2020.

[17] Strophoid. In: *Wikipedia*, https://en.wikipedia.org/wiki/Strophoid, 2022, accessed 29 Jul 2023.

[18] Stachel, H., "Strophoids, a Family of Cubic Curves with Remarkable Properties", *Journal of Industrial Design and Engineering Graphics*, 10/1, 2015, 65–72, http://hdl.handle.net/20.500.12708/151841.

[19] Shulman, L. S., "Those Who Understand: Knowledge Growth in Teaching", *Educational Researcher*, Vol. 15, No. 2. (Feb., 1986), pp. 4-14.

[20] Vaňaus, J. R. "Trisektorie", *Časopis pro pěstování mathematiky a fyziky, Vol. 10, No. 3.* JČMF, Praha, 1881, 153–159.

[21] Vaňaus, J. R., "Úloha 36", *Časopis pro pěstování mathematiky a fyziky, Vol. 31, No. 3.* JČMF, Praha, 1902, p. 262, https://dml.cz/handle/10338.dmlcz/122611, accessed 16 Oct 2020.

[22] Weisstein, E. W., "Cycloid of Ceva", From *MathWorld–A Wolfram Web Resource*, https://mathworld.wolfram.com/CycloidofCeva.html, accessed 30 Jul 2023.